Heinrich Heine Universität Düsseldorf

Doctoral Thesis

Functional Role of chloride/proton exchangers ClC-3 and ClC-5 in exocytosis of large dense core vesicles in chromaffin cells

Author:
Maddalena Comini

Supervisor:
Prof. Dr. Christoph Fahlke

A thesis submitted in fulfillment of the requirements for the degree of Doctor Rer. Nat.

in the

Faculty of Mathematics and Natural Sciences (HHU)

Declaration of Authorship

I, Maddalena Comini, declare that this thesis titled "Functional role of ClC-3 and ClC-5 in exocytosis of large dense core vesicles in chromaffin cells" and the work presented in it are my own. I confirm that:

- This work was done wholly or mainly while in candidature for a research degree at this University.
- Where any part of this thesis has previously been submitted for a degree or any other qualification at this University or any other institution, this has been clearly stated.
- Where I have consulted the published work of others, this is always clearly attributed.
- Where I have quoted from the work of others, the source is always given. With the exception of such quotations, this thesis is entirely my own work.
- I have acknowledged all main sources of help.
- Where the thesis is based on work done by myself jointly with others, I have made clear exactly what was done by others and what I have contributed myself.

Signed: _____

Date: _____

Ich versichere an Eides Statt, dass die Dissertation von mir selbständig und ohne unzulässige fremde Hilfe unter Beachtung der Grundsätze zur Sicherung guter wissenschaftlicher Praxis an der Heinrich-Heine-Universität Düsseldorf erstellt worden ist.

Signed: _____

Date: _____

"E quindi uscimmo a riveder le stelle."

Dante Alighieri, (Inferno XXXIV, 139)

HEINRICH HEINE UNIVERSITÄT DÜSSELDORF

Abstract

Faculty of Mathematics and Natural Sciences

Department of Biology

Doctor Rer. Nat.

Functional role of chloride/proton exchangers ClC-3 and ClC-5 in exocytosis of large dense core vesicles in chromaffin cells

The CLC family of chloride channels and transporters is a large and diverse group, which comprises nine members expressed in mammalian cells. Cl^-/H^+ exchangers fulfill several diverse functions, either at the plasma membrane or in intracellular compartments. In this present study we focus on a sub-branch of the CLC family, with particular interest towards two highly similar members: ClC-3 and ClC-5. The physiological relevance of ClC-3 in the central nervous system (CNS) became evident when the *Clcn3*$^{-/-}$ knock-out animal model was generated. ClC-3-deficient mice showed pronounced hippocampal and retinal degeneration[1], starting in the CA1 region of the hippocampus two weeks after birth. Alterations in synaptic neuronal transmission suggest that ClC-3 might play a modulatory role in both excitatory[1][2] as well as inhibitory[3] neurotransmission. Beside its role in neuronal transmission, ClC-3 was more recently proposed as regulator in the neuroendocrinal system, even though its possible role in exocytosis is still under debate[4][5][6][7]. The aim of this project is to characterize the role of ClC-3 in regulated exocytosis of large dense core vesicles (LDCVs) in neuroendocrinal cells. Thus, we elucidated exocytosis in adrenal chromaffin cells through a combined technique of cell membrane capacitance and amperometric recordings. According to previous results[5][6], exocytosis in adult *Clcn3*$^{-/-}$ chromaffin cells (P60) is severely affected ($\sim$70% reduction). We therefore performed amperometric and membrane capacitance measurements in such adult *Clcn3*$^{-/-}$ mice and even though we could detect a similar impairment in exocytosis, we could not observe any significant effect in new born mice lacking of ClC-3. Thus, we investigated whether another chloride/proton exchanger, which share similar functions

to those performed by ClC-3, might compensate for the absence of ClC-3 in early developmental stages (P0). A promising candidate appears to be ClC-5. Quantitative real-time PCR experiments indeed prove that ClC-5 is less abundant (down-regulated) in adrenal glands extracted from adult mice. Intriguingly, ClC-5 was up-regulated in absence of ClC-3 in new born mice, suggesting that it might be compensating for it. To test the effect of ClC-5 in exocytosis, we therefore silenced ClC-5 (via shRNA knock-down strategy) in chromaffin cells isolated from *Clcn3*$^{-/-}$ new born mice. Exocytosis in such double knock-out chromaffin cells was significantly decreased, similarly to the impairment observed in exocytosis measured in *Clcn3*$^{-/-}$ adult mice. Moreover, analysis of single amperometric events did not reveal any difference between DKOs and WT cells, indicating that most probably ClC-3 and ClC-5 do not regulate neurotransmitter loading in LDCVs. Intriguingly, the reduced amperometric spike frequency observed in *Clcn3*$^{-/-}$ adult mice and double KOs new-born mice reflect a decreased LDCV fusion frequency, which suggests a reduced number of primed vesicles. To confirm this hypothesis, we therefore monitored membrane capacitance increase by applying a depolarizing voltage protocol, in order to elucidate the vesicle priming process. In the DKOs we observed a strong reduction in the number of vesicle which are able to reach a fusion-competent state, which indicates that ClC-3 and ClC-5 are able to control vesicle mobilization during neurosecretion. Taken together, our results indicate that ClC-3 and ClC-5 can govern vesicle priming and show for the first time the implication of ClC-5 in LDCV exocytosis. Finally, in order to confirm our hypothesis, we combined laser scan confocal microscopy and immunocytochemistry experiments to prove the substantial comparable subcellular distribution of ClC-3 and ClC-5 and therefore their essential mutual role in neurosecretion.

Zusammenfassung

Funktionelle Rolle der Chlorid/Protonen Austauscher ClC-3 und ClC-5 bei der Exocytose von großen synaptischen Vesikeln in Chromaffin-Zellen

Die CLC-Familie der Chlorid Kanäle und Transporter ist eine große und diverse Gruppe, die aus neun Mitgliedern besteht, die von Säugerzellen exprimiert werden. Cl^-/H^+ Austauscher haben mehrere unterschiedliche Funktionen, sowohl in der Plasmamembran, als auch in intrazellulären Kompartimenten. In der vorliegenden Studie fokussieren wir uns auf eine Untergruppe der CLC-Familie. Im Besonderen gilt dabei unserer Interesse den zwei sehr strukturhnlichen Mitgliedern ClC-3 und ClC-5. Die physiologische Bedeutung von ClC-3 in Zentralen Nervensystem wurde durch das knock-out Tiermodell *Clcn3*$^{-/-}$ nachgewiesen. ClC-3 defiziente Mäuse wiesen eine starke hippokampale und retinale Degeneration auf, die zwei Wochen nach der Geburt in der CA1 Region des Hippokampus begann. Veränderungen bei der synaptischen neuronalen Übertragung lassen vermuten, dass ClC-3 eine modulatorische Rolle sowohl bei der exzitatorischen, als auch bei der inhibitorischen Nervenübertragung spielt. Neben seiner Rolle bei der Nervenübertragung, wird seit kurzem vermutet, dass ClC-3 auch eine regulatorische Rolle im Neuroendokrinen System spielt, auch wenn seine mögliche Rolle bei der Exozytose noch debattiert wird. Das Ziel dieser Studie ist, die Charakterisierung der Rolle von ClC-3 bei der Regulation der Exozytose von großen synaptischen Vesikeln (large dense core vesicles, LDCVs) in neuroendokrinen Zellen. Daher untersuchen wir die Exozytose in adrenalen Chromaffin Zellen mit Hilfe einer kombinierten Technik aus Membrankapazitäts- und amperometrischer Messung. Vorherige Ergebnisse zeigen, dass die Exozytose in Chromaffin Zellen in adulten *Clcn3*$^{-/-}$ Mäusen ernsthaft beeinträchtigt ist (70% Reduktion). Daher untersuchten wir ebenfalls *Clcn3*$^{-/-}$ Mäuse mit Hilfe der Membrankapazitäts- und amperometrischen Messungen, und obwohl wir eine ähnliche Beeinträchtigung der Exozytose bei erwachsenen Mäusen nachwiesen, beobachteten wir keinen signifikanten Effekt bei neugeborenen Mäusen ohne ClC-3. Daher untersuchten wir ob ein anderer Chlorid/Protonen Austauscher, mit ähnlichen funktionellen Eigenschaften wie ClC-3, möglicherweise in der Lage ist den Verlust von ClC-3 in frühen Entwicklungsstadien (P0) zu kompensieren. Ein vielversprechender Kandidat dafür ist ClC-5. Quantitative Real-time PCR hat gezeigt, dass ClC-5 weniger häufig ist, in adrenalen Drüsen aus erwachsenen Mäusen. Um den Beitrag von ClC-5 an der Exozytose zu testen, dämpften wir die Expression von ClC-5 (mit Hilfe der shRNA knock-down Technik) in isolierten Chromaffin Zellen aus neugeborenen *Clcn3*$^{-/-}$ Mäusen. Die Exozytose in solchen

Doppel knock-out Mutanten (DBKOs) war, ähnlich wie bei der beeinträchtigten Exozytose bei erwachsenen *ClCn3* Mäusen, signifikant verringert. Außerdem zeigte die Analyse von amperometrischen Einzelereignissen keinen Unterschied zwischen DBKO und WT Zellen, was daraufhin deutet, dass weder ClC-3 noch ClC-5 eine Rolle bei der Neurotransmitterbeladung von LDCVs spielen. Verblüffenderweise deutet eine verringerte Frequenz der amperometrischen Spikes, die wir bei diesen Experimenten in erwachsenen *Clcn3*$^{-/-}$ beobachteten auf eine verringerte Fusionsfrequenz von LDCVs hin, und weist auf eine geringere Anzahl von vorbereiteten Vesikeln hin. Um diese Hypothese zu bestätigen, kontrollierten wir die Erhöhung der Membrankapazität, über ein depolarisierendes Spannungsprotokoll, um den Vesikel- Vorbereitungsprozess aufzuklären. Bei DBKOs beobachteten wir eine verringerte Anzahl von Vesikeln, die in einen fusionskompetenten Status übergehen konnten, was daraufhin deutet, dass ClC-3 und ClC-5 die Vesikel-Mobilisierung kontrollieren. Es konnte zum ersten Mal die Rolle von ClC-5 in der LDCV Exozytose gezeigt werden. Schließlich kombinierten wir die konfokale Laserscan Mikroskopie und immunohistochemische Experimente um unsere Hypothese der möglichen Beteilung der CLCs an der Neurosekretion, über die subzelluläre Verteilung von ClC-3 und ClC-5 zu bestätigen.

Acknowledgements

I am highly grateful to my scientific adviser Prof. Dr. Christoph Fahlke, who gave me the opportunity to work and learn in his lab. His supportive and scientific guidance has been of great help along my PhD pathway.
I am extremely thankful to my parents, for their immense support, crucial help and unconditioned love. I am lucky to be their daughter.
I would like to thank people and colleagues I had the chance to learn from over these years: very passionate and experienced scientists who not only taught me about science and research but also helped me to deal with frustration that may come from it, when things do not work out as expected. In particular, I thank Steffi and Gabriel very much for their patience and desire to share their scientific knowledge with me. I am very thankful to Verena and Antje who gave me the possibility to perform qRT-PCR experiments at INM-4 (Institute of Neuroscience and Medicine, Fzj). I also have to thank Raul who taught me how to become independent and count on my own strengths.
I am immensely grateful to Thomas, who is the scientist I would be glad to become one day. I also would like to thank his wonderful family, Iulia, Helena and Maria who made me feel less alone during my time in Germany. Many many thanks to Johnny as well, for his helpful suggestions and huge generosity.
I really would like to thank Cristiano, a great professor and wonderful person who had faith and helped me to purse my professional goal and scientific aspirations. Without him probably I would not be doing the job I love.
I am happy to thank my office-mates for their nice company and relaxing office atmosphere that made me start my day with a smile.
I would like to say a big thank you to Safaa, Sarah and Yulia, who have been not only colleagues but overall precious friends during these years.
From the bottom of my hearth, I can say I am very lucky I shared this tough journey with some great brilliant young women, whom I consider dear friends too: Oliveira, Irina and Galyia. I do hope I will spend my time with you in future again.
To my friend Clarita: thanks for making me learn your colorful language and sharing amazing Spanish food.
In the very end, I would like to say thanks for this insane, incredible, tough, painful and amazing experience I will never forget!

Contents

Declaration of Authorship i

Acknowledgements viii

List of Figures xii

List of Tables xiv

Abbreviations xv

1 Introduction 1
1.1 The CLC Family . . . 1
1.2 CLC Biophysical Properties and Transport Functions . . . 3
1.2.1 Physiological Importance of CLCs . . . 5
1.2.2 ClC-3 . . . 6
1.2.3 ClC-5 . . . 9
1.3 Exocytosis . . . 10
1.3.1 Steps of Regulated Exocytosis - SNARE Complex Formation . . . 12
Biogenesis, Docking, Priming and Vesicles Fusion. . . . 13
1.3.2 The Readily and Slow Releasable Pool of vesicles (RRP and SRP) . 15
1.3.3 Exo-endocytosis . . . 15
1.3.4 Neuroendocrine Cells as a Model for Exocytotic Studies . . . 17
1.4 Endosomal System . . . 18
1.4.1 Rab Proteins . . . 18
1.4.2 Vesicles Recycling Process . . . 21

2 Materials and Methods 22
2.1 Materials . . . 22
2.1.1 Reagents . . . 22
2.1.2 Kits . . . 22
2.1.3 Solutions . . . 23
2.1.3.1 PFA 4% . . . 23
2.1.3.2 Locke's Solution . . . 23
2.1.3.3 Poli-D-lysine-hydrobromide in Borate Buffer . . . 23

2.1.3.4 10 cm Petri dish Coating . . . 23
2.1.3.5 4-well dish Coating . . . 24
2.1.4 PC-12 Cell Line . . . 24
2.1.4.1 Thawing procedure for PC-12 Adh cells – ATCC CRL-1721.1 24
2.1.4.2 Complete Growth Medium for PC-12 cells . . . 24
2.1.4.3 PC-12 cells Lipofectamine Transfection . . . 25
2.1.5 Mouse Chromaffin Cells Primary Culture . . . 25
2.1.5.1 Culture Medium for chromaffin cells (Enriched DMEM) . 25
2.1.5.2 Enzymatic Solution . . . 26
2.1.5.3 Inactivating Solution . . . 26
2.1.5.4 Ringer's Solution (Depolarization Protocol) . . . 26
2.1.5.5 Intracellular Solution (Depolarization Protocol) . . . 27
2.1.5.6 Ringer's Solution (Amperometry Recordings) . . . 27
2.1.5.7 Intracellular Solution (Amperometric Recordings) . . . 27
2.2 Methods . . . 28
2.2.1 Genotyping PCR reaction . . . 28
2.2.2 Quantitative real-time PCR (qRT-PCR) . . . 29
2.2.2.1 RNA isolation . . . 29
2.2.2.2 DNAase treatment . . . 30
2.2.2.3 First-Strand cDNA Synthesis . . . 31
2.2.2.4 Standard fragments for qRT-PCR . . . 31
2.2.2.5 Quantitative RT-PCR . . . 32
2.2.2.6 Data Analysis of qRT-PCR . . . 33
2.2.3 Transgenic Mice generation . . . 34
2.2.4 Adrenal Chromaffin Cells Culture . . . 34
2.2.5 Chromaffin cells transient transfection . . . 35
2.2.6 Chromaffin cells Viral infection . . . 35
2.2.7 Chromaffin cells Immunocytochemistry . . . 36
2.2.8 Membrane Capacitance Measurement . . . 36
2.2.8.1 Lindau-Neher Technique or "sine + DC" method . . . 40
2.2.8.2 Exocytotic Stimulation by applying a train of depolarizations 41
2.3 Amperometry Recordings . . . 42
2.3.1 Carbon fiber electrode fabrication . . . 44
2.4 Analysis of single-exocytotic events . . . 47
2.4.1 Spike detection . . . 48
2.4.2 Spike Selection . . . 48
2.4.3 Spike Parameters . . . 48
2.4.4 Spike kinetic properties . . . 50
2.4.5 "Foot" signal . . . 51

3 Results **52**
3.1 Amperometric detection of catecholamines in chromaffin cells . . . 52
3.1.1 Saturating Calcium concentration (20 μM) masks any possible effect on exocytosis in the *Clcn3*$^{-/-}$ mouse model . . . 53
3.1.2 Exocytosis is not impaired in absence of ClC-3 in late post-natal stages at high calcium concentration (20μM) . . . 56

3.2 ClC-5 but not ClC-3 undergoes an age-dependent regulation in adrenal glands . . . 59
3.2.1 Catecholamine release is not affected by the absence of ClC-3 nor ClC-5 in early post-natal stages at saturating calcium concentration (20μM) . . . 62
3.2.2 Spikes frequency is significantly reduced in the absence of ClC-3 in adult stages at low intracellular calcium (3μM) . . . 65
3.2.3 Spikes frequency is significantly reduced in the DKO condition in early post-natal stages at low intracellular calcium (3μM) . . . 68
3.3 LDCV priming is impaired in *Clcn3*$^{-/-}$ adult mice (P60), but not in new-born (P0) . . . 72
3.4 LDCV priming is impaired in the DKOs condition in new born mice (P0) . 74
3.5 Subcellular localization of ClC-3 and ClC-5 in neuroendocrine cells . . . 75
3.5.1 ClC-3 splice variants are located in different subcellular compartments in adrenal chromaffin cells . . . 77
3.5.2 ClC-5 is located in a specific sub-population of recycling vesicles in adrenal chromaffin cells . . . 79
3.5.3 Localization of ClC-3 and ClC-5 in large dense core vesicles (LDCVs) 81

4 Discussion 84
4.1 Membrane capacitance measurements correlated with amperometric recordings permit to monitor exocytosis in real time with high temporal resolution 85
4.1.1 Analysis of amperometric spike's shape reveals information about the cargo content and its release dynamics . . . 85
4.2 Putative role of ClC-3 and ClC-5 in exocytosis . . . 86
4.3 ClC-3 regulates the priming process of LDCVs in adult mice . . . 87
1. ClC-3 might play a direct effect on the priming step. . . . 87
2. ClC-3 might play an indirect effect on the priming step. . 88
4.4 ClC-3 and ClC-5 regulate the priming process in new-born mice . . . 89
4.5 ClC-3 is located in LDCVs, while ClC-5 is mostly expressed in recycling endosomes . . . 90
4.6 Concluding remarks . . . 91

List of Figures

1.1 CLC Family 2
1.2 CLC Structure 4
1.3 Gating Mechanism 5
1.4 The Role of ClC-3 7
1.5 The Role of ClC-3 and ClC-5 9
1.6 Exo-endocytosis 11
1.7 The Priming Process 14
1.8 Different Pools of vesicles 16
1.9 The Mouse Adrenal Gland 17
1.10 Endosomal Pathway 19

2.1 RNA Integrity 30
2.2 qRT-PCR Cycles 33
2.3 RC Circuit 38
2.4 Sine-Wave Stimulus 41
2.5 Depolarization Protocol 42
2.6 Catecholamine Detection 42
2.7 Carbon Fiber Electrode Fabrication 46
2.8 Amperometric Recordings 47
2.9 Spike Parameter Analysis 49
2.10 Algorithm used for Spike Analysis 50

3.1 Exocytosis is not impaired in WT vs KO (P0 mice) at saturating calcium concentration 54
3.2 Amplitude and Charge 55
3.3 Kinetic Parameters 56
3.4 Exocytosis is not impaired in WT vs KO (P60 mice) at saturating calcium concentration 57
3.5 Amplitude and Charge 58
3.6 Kinetic Parameters 59
3.7 qRT-PCR (Reference Genes) 60
3.8 qRT-PCR (P0 vs P60) 61
3.9 qRT-PCR (WT vs KO) 61
3.10 Exocytosis is not impaired in DKOs (P0 mice) at saturating calcium concentration 63
3.11 Amplitude and Charge 64
3.12 Kinetic Parameters 65
3.13 Exocytosis is impaired in WT vs KO (P60 mice) at low calcium concentration 66

3.14 Amplitude and Charge 67
3.15 Kinetic Parameters 68
3.16 Exocytosis is impaired in absence of ClC-3/ClC-5 (P0 mice) at low calcium concentration 69
3.17 Amplitude and Charge 70
3.18 Kinetic Parameters 71
3.19 Membrane Capacitance Measurements (P0) 72
3.20 Membrane Capacitance Measurements (P60) 73
3.21 Membrane Capacitance Measurements (ScrWT, ScrKO, ClC-5kd, and DKOs) 75
3.22 Localization of ClC-3 in PC-12 cells 76
3.23 Localization of ClC-3 and ClC-5 in chromaffin cells 76
3.24 Subcellular Localization of ClC-3b 77
3.25 Subcellular Localization of ClC-3c 78
3.26 Subcellular Localization of ClC-5 80
3.27 Co-localization Analysis 81
3.28 Localization of ClC-3 in LDCVs in PC-12 cells 82
3.29 Localization of ClC-3 and ClC-5 in LDCVs in chromaffin cells 83

List of Tables

2.1 Locke's solution 23
2.2 Complete Growth Medium PC-12 Adh cells 25
2.3 Culture Medium 25
2.4 Enzyme solution 26
2.5 Inactivating solution 26
2.6 Ringer's solution 26
2.7 Depolarization solution 300 nM free $[Ca_i^{2+}]$ 27
2.8 Ringer's solution 27
2.9 Perfusion solution 20 μM $[Ca^{2+}]_i$ 27
2.10 DNA isolation 28
2.11 KAPA Mix reaction 28
2.12 Forward and Reverse Primers 29
2.13 DNAase Treatment 31
2.14 qRT-PCR 33

Abbreviations

aa	**a**amino **a**cids
A	**A**mpere
ATP	**A**denosin **T**ri **P**hosphate
BAPTA	1,2-**B**is (o-**A**mino**P**henoxy)ethane-N,N,N′,N′-**T**etraacetic **A**cid
bp	**b**ase **p**air
°C	**C**elsius
Ca^{2+}	**C**alcium
$[Ca^{2+}]_i$	**I**ntracellular free Calcium Concentration
$CaCl_2$	**C**alcium **C**hloride
cDNA	**C**ircular DNA
C_m	**M**embrane **C**apacitance
CLC	**C**h**L**oride **C**hannel
CO_2	**C**arbon dioxide
C_sOH	**C**esium **H**ydroxide
ΔC_m	**D**elta (change) in membrane capacitance
DIV	**D**ays **I**n **V**itro
DKO	**D**ouble **K**nock-**O**ut
DMEM	**D**ulbecco's **M**odified **E**agle's **M**edium
DMSO	**D**i**M**ethyl**S**ulf**O**xide
DNA	**D**eoxyribo**N**ucleic **A**cid
DPTA	1,3-**D**iamino**P**ropane-N,N,N′,N′,-**T**etraacetic **A**cid
fF	**f**emto **F**arad
Fig	**F**igure
Fw-Primer	**F**orward **P**rimer

g	**g**ram
G_m	**M**embrane Conductance
G_s	**S**eries Conductance
GTP	**G**uanosin **T**ri **P**hosphate
H_2O	Water
HEPES	2-[4-(-**H**ydroxy**E**thyl)**P**iperazin-1-yl]**E**thane**S**ulfonic acid
HCl	**H**ydro**C**hloric acid
Hz	**H**er**z**
Kd	**K**nock-**d**own
KO	**K**nock-**O**ut
LDCV	**L**arge **D**ense **C**ore **V**esicles
μg	**M**icro **g**ram
μm	**M**icro **m**eter
μm	**M**icro **l**iter
Mg^{2+}	**M**agnesium
Mg-ATP	**M**agenisum **A**TP
$Mg^{2+}Cl_2$	**M**agnesium **C**hloride
Min	**M**inute
ml	**M**illi **l**iter
mM	**M**illi **M**olar
mOsm	**M**illi **O**smolar
ms	**M**illi **s**econd
mV	**M**illi **V**olt
MΩ	**M**ega **O**hm
n	**n**umber of the elements (*e.g.*, cells)
Na_2-GTP	**S**odium **G**TP
p-value	**p**robability-value
P0	**P**ost-natal day zero
PCR	**P**olymerase **C**hain **R**eaction
PFA	**P**ara**F**orm**A**ldehyde
Rab	**R**as-**a**ssociated **b**inding protein

Rev-Primer	**R**everse **P**rimer
RNA	**R**ibo **N**ucleic **A**cid
rpm	**r**evolutions **p**er **m**inute
RRP	**R**eadily **R**eleasable **P**ool
SNAP-25	**S**y**N**aptosomal-**A**ssociated **P**rotein of 25kDa
SNARE	**S**oluble (**N**-Ethylmaleimide-Sensitive Factor) **A**ttachment p**R**otein r**E**ceptor
Syb II	**Sy**napto**b**revin II
wt	**w**ild **t**ype

to Cristiano, a teacher and a friend

Chapter 1

Introduction

1.1 The CLC Family

The CLC family is a large and diverse group, which consists of a vast number of chloride channels and transporters, widely present in archaebacteria, eubacteria, yeast, plants and animals. Their large molecular diversity, along with a variety of biophysical properties and biological functions make a clear classification difficult. Chloride channels and transporters may perform their role either at the plasma membrane, to ensure charge transport and control of electrical excitability, or in intracellular compartments, to regulate endosomal acidification and provide electroneutrality. In mammals, the CLC gene family consists of nine known members, which have a differential tissue distribution where they fulfill diverse biological roles. This group can be further divided into three sub-branches, based on their sequence homology (**Fig. 1.1**). Proteins of the first branch (ClC-1, ClC-2 and ClC-K) perform their function at the plasma membrane, where they behave as conventional chloride channels, while the other two branches, (ClC-3 until ClC-5 and ClC-6/ClC-7), fulfill their function in intracellular organelles and vesicular membranes. The latter, in contrast to the previous members, act as Cl^-/H^+ antiporters, as demonstrated for ClC-4 and ClC-5[8][9] and more recently for ClC-3[10], ClC-6[11] and ClC-7[12][13][14].

Depending on their localization and activity, the CLCs have been implicated in several tasks. For instance, anion transport, mediated at the plasma membrane, plays an important role in maintaining the osmotic and salt equilibrium. This is the case of NaCl re-absorption in colonic surface cells, mediated by ClC-2 working in parallel with Cl^-/HCO_3 and Na/H exchangers. A similar role is accomplished by the basolateral ClC-Ka/barttin and ClC-Kb/barttin to guarantee K^+ secretion in the stria vascularis of the

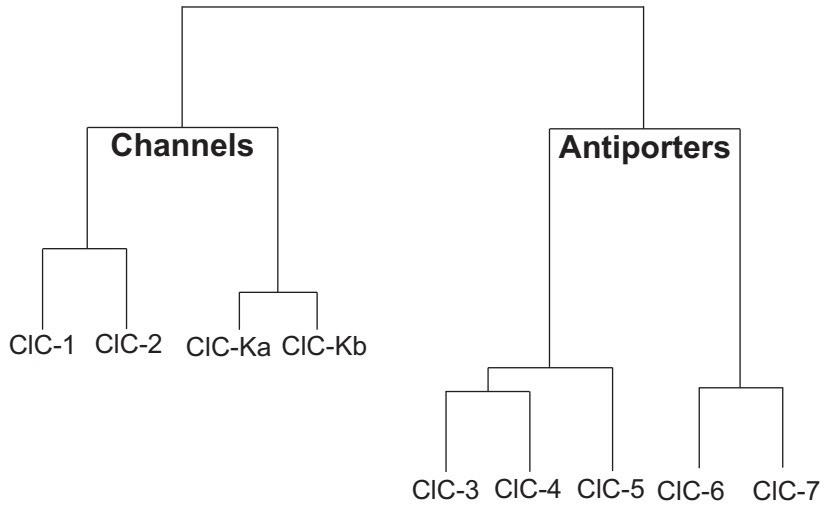

FIGURE 1.1: **Phylogenetic tree of the CLC Family of Cl^- channels based on sequence identity.** The phylogram reports a schematic separation of the main two branches of chloride channels (ClC-1, ClC-2, ClC-Ka and ClC-Kb) and chloride/proton antiporters (ClC-3 through ClC-7).

cochlea or Cl^- recycling in the collecting duct. Chloride movement is also a key function in the modulation of the electrical cell excitability, which is mediated by ClC-1.
Concerning the intracellular Cl^-/H^+ exchangers, they were originally thought to provide an electrical shunt for the vesicular ATPase (V-ATPase), thus regulating the intracellular acidification of endosomes. For instance, in the proximal renal tubule, where ClC-5 co-localizes with the V-ATPase[15], [16], and in synaptic vesicles, where ClC-3 was found[1]. In brief, the intracellular acidification of such organelles is provided by the V-ATPase which, by hydrolyzing ATP, can actively pump protons into the vesicle lumen. This import of protons leads to an increased lumen membrane potential which would prevent the further influx of H^+. Cl^-/H^+ exchangers are supposed to neutralize the positive luminal charge by importing Cl^- anions, therefore acting as counterpart for the V-ATPase, but this hypothesis still needs further investigation.

1.2 CLC Biophysical Properties and Transport Functions

The characteristic structure of all CLC proteins was suggested for the first time in the early eighties, when Miller et all[17][18] pictured the Torpedo chloride channel as a functional dimer. In that study, Miller and colleagues proposed that the dimeric complex was composed of two identical subunits, the so-called protochannels, which had independent opening and closing states. However, the first CLC protein, encoding a voltage-gated chloride channel, was cloned only in 1990 from the electric organ of *Torpedo Marmorata*[19] and permitted an important insight into the chloride channel structure. Finally, about one decade later, in 2002, the X-ray crystallographic structure of the bacterial CLC homologue from *Salmonella Typhimurium* (StClC) became available[20]. This discovery revealed the double-barrel model specific of CLC channels. The EcClC prokaryotic homologue is a dimeric protein, in which each monomer consists of 18 alfa-helices (from A to R), 17 of which are embedded in the plasma membrane, while the N and C termini are located in the cytosol. The main difference with the bacterial homologue, is that the C terminus of the eukaryotic CLCs contain two CBS (cystathionine-beta-synthetase) domains (crystallized in 2006[21]) which are responsible for the ATP binding[22] and the channel trafficking as well[23][24]. The two CBS domains are known to play a role in the gating mechanism,[25],[26], in particular in the slow gating[27], by transducing conformational changes. They also contain a sorting motif necessary for the proper subcellular distribution of the protein[28],[29],[30]. Interestingly, the two CBS domains were shown to be essential for hetero- and homo-dimeric complex formation[30].

CLC eukaryotic proteins are arranged as dimers, with a transmembrane domain and two carboxy termini[33] (**Fig. 1.2**). They can mostly function as homodimers but co-immunoprecipitation studies also revealed that members of the different subfamilies can form heterodimers with the respective subgroup members, that is the case of the hetero-oligomers ClC-1/ClC-2[34][35], ClC-4/ClC-5[36][37] and ClC-3/ClC-4[30]. The two distinct subunits constituting the dimer can work independently and have their own gating pore[38][20].

The dual yet separate gating mechanism is composed of a fast gate, whose opening and closing is proper of each individual subunit, and a slow gate, common to both pores, which function simultaneously, as suggested by Miller and colleagues[17]. The independent fast gating is approximately 10-fold faster than the slow one in mammalian CLCs[17],[45],[46] and is mediated by Glu_{ext}[41],[42],[47]. This peculiar double barrel structure is common to CLC channels, such as ClC-0, ClC-1 and ClC-2[45],[48],[49]. Each subunit of

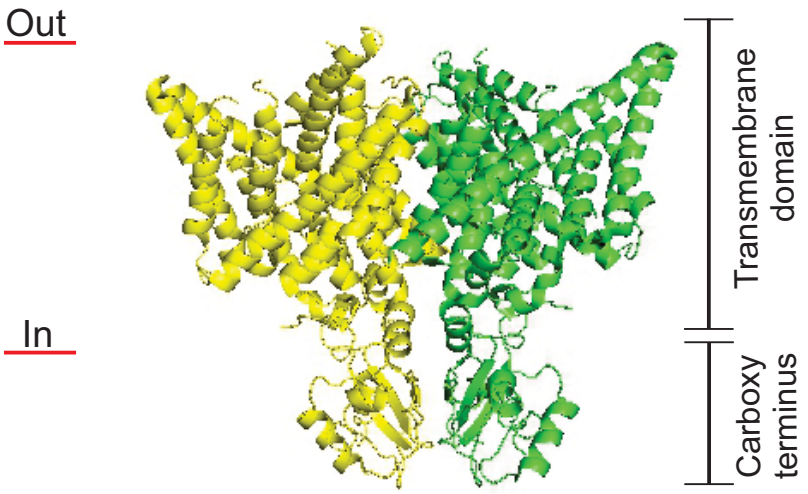

FIGURE 1.2: **Dimeric CmCLC Structure.** The eukaryotic structure was firstly identified from a thermophilic red algae *Cyanidioschyzon merolae*[31] and subsequently characterized[32] PDB ID: 3ORG. This figure was created with Pymol.

the dimer has three distinct chloride binding sites, named S_{in}, S_{cen} and S_{ext} in relation to their inward or outward-facing position in the plasma membrane. S_{ext} (also referred to as Glu_{ext} or E148[42]) can switch between S_{cen} and S_{ext}, depending on the protonation state. In StClC structure, S_{in} and S_{cen} are occupied by Cl^- ions. In S_{cen}, Cl^- ions are coordinated by Y445 (Tyr_{cen}) and S107 (Ser_{cen}) (**Fig. 1.3**). Several mutations have been studied, with particular interest towards the so-called "gating glutamate" (E148), represented in **Fig. 1.3**. The neutralization of the gating glutamate in ClC-ec1 by alanine can eliminate H^+/Cl^- coupling by preventing H^+ transport[39],[40], turning Cl^-/H^+ exchangers into passive conductors and abolishing Cl-dependent gating in CLC channels. This glutamate is also important for fast gating in ClC-0, ClC-1 and ClC-2[41],[42]. An inward-facing glutamate residue in E203 (Glu_{int}) present in EcClC was similarly neutralized after being substituted with an alanine which affected the H^+ transport, but not pH sensitivity. Glu_{int} is proposed to be the proton acceptor which couples Cl^- and H^+ transport in CLC exchangers[43]. Another single point mutation was conducted on Tyr_{cen} which is highly conserved in the CLC family. Substitutions of such residue by alanine, glutamate and histidine lead to mutants with a strong Cl^- transport and reduced H^+ movement[44]. However, a clear picture of the whole structure is still missing and the H^+ movement from Glu_{int} to Glu_{ext} remains a mystery.

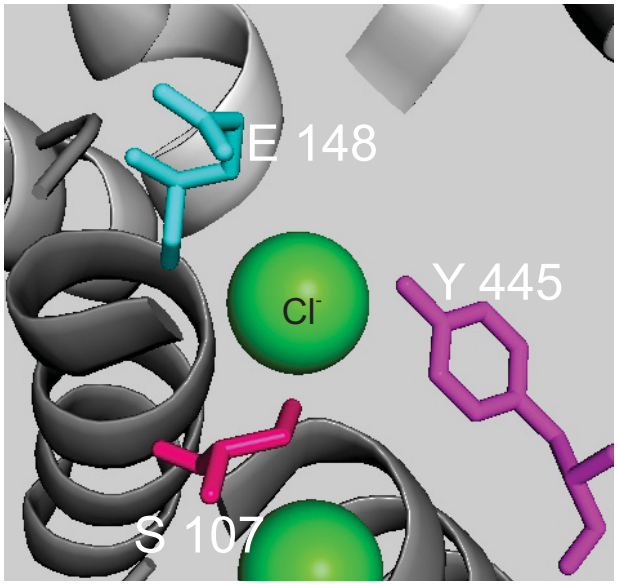

FIGURE 1.3: **Gating Mechanism.** E148 represents the "Gating Glutamate", which is involved in the fast gating of CLC channels. Y445 and S107 are responsible for the chloride binding in S_{cen}, and probably mediate the slow gating of CLCs. This representation refers to the residues involved in the coordination of the chloride ions in EcClC (PDB ID:1OTS) described By Dutzler and colleagues in 2002[20]. This figure was created with Pymol.

1.2.1 Physiological Importance of CLCs

The CLCs are implicated in various pathologies, reflecting the important role they play in several biological processes. For instance, myotonia, a neuromuscular disorder associated with muscle stiffness, is caused by mutations in the chloride channel ClC-1 and was observed both in humans and mice[50],[51]. Bartters syndrome instead, is characterized by severe renal failure and derives from mutations in the kidney-specific channel ClC-Kb[52]. Despite disruption of ClC-4 alters the transferrin receptor recycling in epithelial cells[36], the generation of the ClC-4-deficient mice[53] did not reveal so far any physiological important implications. ClC-6 shares about 45% sequence identity with ClC-7 and has a similar intracellular distribution in the lysosomal compartment where, after disruption, causes a storage disease exclusively observed in neurons[54]. Disruption of ClC-7 leads to a more severe phenotype. Indeed, ClC-7 KO mice show skeletal abnormalities with fragile calcified bones[55]. In humans, mutations of this exchanger were described by Kornak and colleagues in 2001 in osteopetrosis. Several mutations of ClC-7 have been described so far, in particular recessive mutations characterizing the human infantile malignant osteopetrosis, or dominant-negative mutations typical of the Albers-Schoenberg disease[56]. Interestingly, similar to *Clcn*$3^{-/-}$ mice, the ClC-7 KO animal model shows

a progressive retinal degeneration accompanied by neurodegeneration of cortical and hippocampal neurons[57].

1.2.2 ClC-3

This antiporter is broadly expressed in different tissues and organs, such as brain, retina, liver, kidney, pancreas, heart and skeletal muscle[1]. After its cloning in 1994[58][59], it became of great interest when the ClC-3 deficient animal model was generated and showed a severe neuronal and retinal degeneration[1][60][61]. Interestingly, such degeneration initially affects the CA1 region of the hippocampus, starting 2 weeks after birth, and subsequently leads to a complete loss of the hippocampus, accompanied by astrogliosis. *Clcn3*$^{-/-}$ mice are characterized by a high mortality rate, blindness, reduced weight and motor coordination. At the end of the last century, the first putative role suggested for ClC-3 was to mediate the swelling-activated Cl^- current $I_{Cl,\,swell}$. This current has an I^- over Cl^- conductance and it is presents in many mammalian cells, where it regulates electrical activity, cell volume, intracellular pH and cell proliferation[62]. Generation of the *Clcn3*$^{-/-}$ animal model later confirmed that those outwardly rectifying currents were indeed still present and therefore most probably endogenous to the expression system.
Another proposed role for ClC-3 was that of modulating excitatory synaptic transmission in hippocampal neurons. This was suggested by a slight increase in the time course of mEPSC, mediated by NMDA receptors[63]. Since ClC-3 was found to be located on the plasma membrane in post-synaptic sites together with NMDA receptors, a dual combined function of ClC-3 and NMDA receptors was proposed to regulate the long term synaptic plasticity. A lack of ClC-3 would therefore result in an unbalanced synaptic neurotransmission and altered neuronal excitability. The slight increase in the amplitude of mEPSC could be explained as a result of an increased uptake of glutamate in synaptic vesicles where ClC-3 is located. Yoshikawa and colleagues contradicted the fact that ClC-3 itself would be actually present on synaptic vesicles since they observed its presence only in lysosomes and endosomes[61]. Nonetheless, synaptic vesicles derive from endosomes and are even recycled through endosomal compartments[64] which would support the idea that ClC-3 has a broad expression in both vesicles and endosomes. In the central nervous system (SNC), both glutamatergic and GABAergic transmission are severely impaired after disruption of ClC-3[1]. Indeed, in addition to the effect on the membrane potential and the resulting augmented glutamate uptake, the decreased pH gradient would lead to a decreased GABA loading. This would possibly result in neurotoxicity due to the excess of excitatory neurotransmitter, exasperated by a decreased inhibitory effect

caused by lack of GABA. More recently another study suggested a possible implication of ClC-3 in insulin secretion. In 2001, Barg and colleagues[4] proposed that ClC-3 would regulate insulin uptake in secretory granules in β-pancreatic cells by directly controlling their acidification, since they observe the presence of ClC-3 in such vesicles. Once again the lack of a specific antibody was the main issue. This role was further investigated by Jentsch group in 2008[5], who rather postulated an indirect effect of ClC-3 by regulating endosomal acidification and intracellular trafficking. In this study, the presence itself of ClC-3 in large dense core vesicles (the granules which store and release insulin) was questioned, since ClC-3 was rather found in endosomes and synaptic-like microvesicles (SLMVs)[5]. Finally, in 2009 Nelson group[6] confirmed the hypothesis postulated by Barg and colleagues. Despite this recent study, convincing evidence of a potential involvement of ClC-3 in insulin secretion based on a KO animal model is still missing.

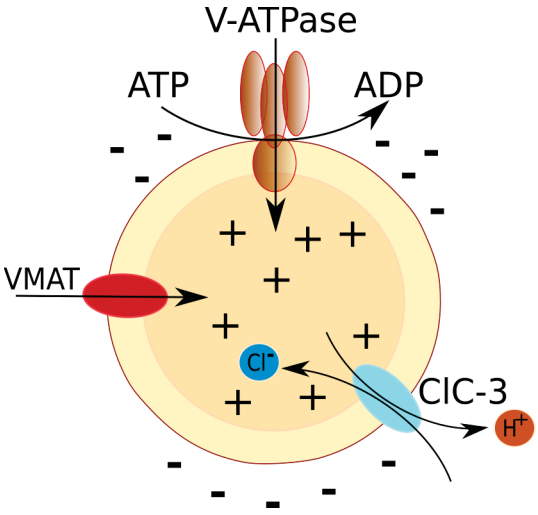

FIGURE 1.4: **Possible role of ClC-3 in intracellular vesicles.** ClC-3 was proposed as mediator in the acidification process of synaptic and large dense core vesicles, where it was postulated to provide an electrogenic shunt for the V-ATPase. Image modified from G. Ahnert-Hilger, 2011[65].

Furthermore, ClC-3 appears to be involved in the acidification of synaptic vesicles[1] as well as endosomes, at least in the hepatic tissue[61]. Interestingly, previous studies proposed that the ion conductance and the electrical shunt for the V-ATPase provided by ClC-3 (**Fig. 1.4**) would play a major role in endosomal acidification. Indeed in the *Clcn3*$^{-/-}$ hepatic vesicles, an elevated (alkaline) pH was observed[61] and later *in vivo* measurements confirmed these results in hepatocites[66]. Similar findings were shown by Nelson group were the pH measured in ClC-3 deficient granules was 1 unit more alkaline than that of WT cells[6]. However, other laboratories have not been able to reproduce a similar difference in granular acidification, as such these results are still questionable[67].

The subcellular localization of ClC-3 indeed revealed an interesting aspect related to the possible physiological role of this exchanger: the alternative splicing in the N-terminal region results in different splice variants which are located in diverse intracellular compartments[68]. In particular, ClC-3a, which is the shortest variant with 760 amino acids, was found in lysosomes, ClC-3b (818aa) was expressed in late endosomes/lysosomes, while ClC-3c (791aa) was the only one to be located in recycling endosomes, probably sorted through an Isoleucine-Prolin motif. On the other hand, ClC-3d, which was recently cloned from mouse liver[69] and ClC-3e, which was identified in 2002[70] and localizes to Golgi[71], are not present in the brain and their functions remain unclear. Interestingly, the different splice variants a, b and c, which were the only ones found in mouse brain, olfactory bulb and spinal cord[68], showed the same biophysical properties but seem to fulfill different functions along the endosomal pathway, at least in the neuronal system[68]. In contrast to their different localization, ClC-3 splice variants mediate large capacitance currents upon depolarization and have identical voltage dependences of the gating charge movement[68]. In 2015, Guzman et al[68] identified the sorting motifs responsible for protein trafficking of the different splice variants of ClC-3. After deletion of one of the three dileucine motifs, called S1 (LLDLLDE), ClC-3a (760aa) could reach the plasma membrane. When over-expressed in an heterologous system, it mediates outward rectifying current at positive potentials (+35mV) upon depolarizing voltage steps, with no inward currents measured at negative potentials. To characterize ClC-3b, all three dileucine motifs S1, S2 (EDDNLL) and S3 (EELL), were deleted. In contrast, ClC-3c is able to independently reach, at least partially, the plasma membrane, where it mediates outward rectifying currents. Once again, a capacitive current was observed at depolarizing voltage steps as well as after stepping back to the holding potential. Once the capacitive currents are integrated, to obtain the "gating charge movement", no differences in the voltage dependence of the three splice variants could be observed. Similarly, when the ionic currents are plotted versus the gating charge movement, ClC-3a, b and c showed a similar transport competence. This leads to the conclusion that despite their different subcellular localization, they share similar biophysical properties and functions, and have identical voltage-dependence and transport-competences. In this puzzling scenario, we seem to be still far away from a deep understanding of the role played by ClC-3. The lack of a specific antibody for ClC-3 has so far prevented its clear and certain localization, contributing to render its characterization more challenging.

1.2.3 ClC-5

The first insight into the role of ClC-5 was obtained in 1994 when it was identified as responsible for Dent's disease[72]. This disorder is characterized by proteinuria, hypercalciuria, kidney stones, nephrocalcinosis, nephrolithiasis and final renal failure. Interestingly, more than 100 mutations of ClC-5 have been associated with Dent's disease and most of them lead to a loss of function of the protein at the plasma membrane[73]. Its subcellular characterization revealed that ClC-5 mainly resides in endosomes together with the V-ATPase[74]. This suggested that ClC-5 might provide an electrical shunt for the protonic pump in the ATPase-mediated endosomal acidification, and might possibly have a similar function to that of ClC-3 (**Fig. 1.5**).

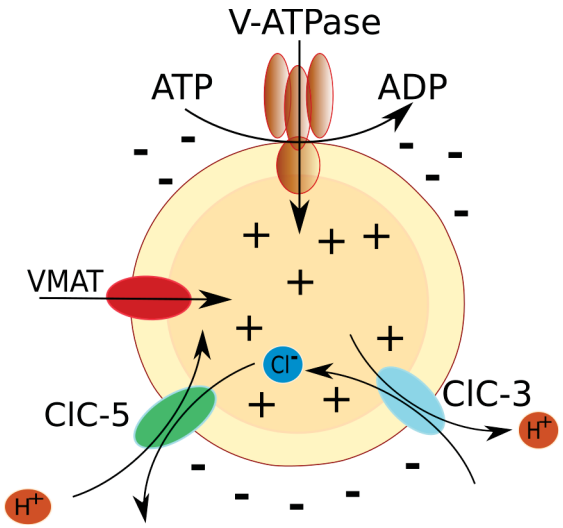

FIGURE 1.5: **Possible role of ClC-5 in intracellular vesicles.** ClC-5 might collaborate with ClC-3 in the regulation of the intracellular endosomal acidification.

Even though ClC-5 shows a broad expression (similarly to ClC-3), it is mainly present in the kidney and is abundant in intestinal and renal epithelia[74],[16]. In particular, it is highly expressed in epithelial cells of the proximal tubule and in β-intercalated cells of the collecting duct, while it is less abundant in the Henle's loop[75]. After the ClC-5 KO animal model was independently generated by two different laboratories[76],[77] focus on study of proximal tubule endocytosis enabled elucidation of the role of this transporter. Indeed, a strong phenotype was observed: the uptake of proteins was reduced by 70% in the proximal tubule[76] and *in vitro* experiments showed a decreased vesicles acidification in cortical endosomes[76],[74]. Lately, *in vivo* pH measurements confirmed an impaired acidification in early endosomes from cultured proximal renal cells[66], similar to that caused by disruption of ClC-3[78]. Accordingly, the Cl^- concentration in early endosomes

was reduced. These findings are coherent with the fact that ClC-5 co-localizes with the V-ATPase in the vesicles below the apical membrane[15]. Astonishingly, when ClC-5 is overexpressed at the plasma membrane in oocytes, it mediates a strongly outward rectifying current, detectable only at positive potential (>+20 mV) and reduced after acidification of the extracellular pH[79], while no currents where measured at negative voltages. In 2010 it was also suggested that ClC-5 might independently regulate the intracellular acidification[80], apart from the ATPase itself, but this still remains an open question. An intriguing hypothesis is that ClC-5 might potentially cooperate or, at least, form heterodimers with the other two members of the same subfamily, that is ClC-3 and ClC-4, with whom it colocalizes after heterologous expression in HEK293 cells[37]. In addition, when the so called "gating-glutamate" is mutated and as a result turns ClC-5 into a pure Cl^- conductor, the endosomal acidification is affected and the endocytosis impaired[81]. While the implication of ClC-5 in those two process have been proved, the link between the two aspects does not appear very clear, considering that the clathrin-mediated endocytosis is regulated in a pH-independent fashion[82]. On the other hand, vesicles recycling appears to be influenced by pH[83], which also plays a major role in the acidification along the whole endocytotic pathway[84]. In addition, studies in ClC-5 KO mice showed that not only endosomal uptake of proteins is impaired, but also recycling of membrane proteins is affected, as shown for the megalin receptor. Indeed, immunofluorescence and Western Blott analysis showed that the amount of megalin on the plasma membrane of proximal tubular cells was reduced[76] and the same was later observed for the other receptor cubilin[85]. Under this new perspective, the role proposed for ClC-5 would indeed appear much more complex than that postulated so far.

1.3 Exocytosis

The exocytotic process allows the cell to release its content in the extracellular space, either into the blood stream or in the synaptic cleft, and is crucial for cellular communication and environmental adaptation. Exocytosis is accompanied by its counterpart, endocytosis, (**Fig. 1.6**) which permits to "phagocyte" and therefore incorporate extracellular material, including released molecules that need to be recycled. This process has been relatively conserved through evolution.

Naturally, given its vital importance, exocytosis needs to be finely and precisely regulated by specific biological sensors and stimuli. It underlies several biological mechanisms, such as the release of glutamatergic or GABAergic neurotransmitters from

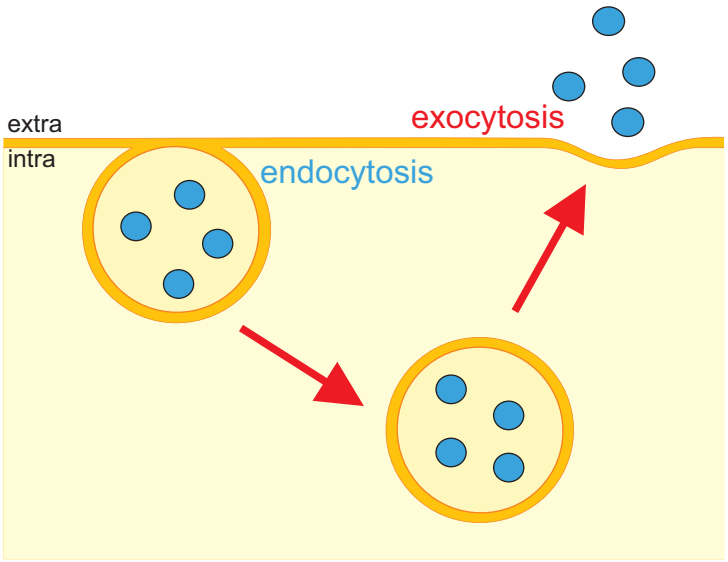

FIGURE 1.6: **Exo-endocytotic process.** A vesicle fuses to the plasma membrane in order to release its cargo outside the cell. The released material can be subsequently endocytosed and recycled.

synaptic vesicles, the secretion of catecholamines such as (Nor)Epinephrine from the neuroendocrinal system, as well as the secretion of insulin from β-pancreatic cells. The exocytotic process has been extensively studied and at least three different modes of release have been characterized so far: (a) full vesicle fusion, followed by endocytosis and vesicle reconstitution, (b) kiss and run fusion, characterized by a rapid alternate of open and re-close state of the fusion pore and (c) kiss and stay release, with partial vesicle fusion[86]. Several methods have been optimized to study this process in neuroendocrinal cells, such as PC-12 cell line[87] and adrenal chromaffin cells[88].

There are two main different exocytotic processes taking place in eukaryotic cells, depending on the nature of the triggering stimulus: one is constitutive and the other is regulated. Those two processes share some similarities but are not identical. Both are, for instance, regulated by SNARE and SNAP proteins, but differ in their released content. While constitutive exocytosis is meant to deliver newly synthesized proteins to the plasma membrane, regulated exocytosis is mainly involved in release of neurotransmitters (Glutamate, GABA, Acetylcholine, Dopamine, *etc*), neuropeptides (NPY, Galanin-like peptide,*etc*) and catecholamines or hormones (epinephrine, insulin and glucagone)[89]. In contrast to constitutive exocytosis, regulated exocytosis relies on a rapid increase of intracellular calcium which triggers the release of the cargo (molecules) stored in the vesicles[90]. In the case of chromaffin cells, several types of voltage-gated Ca^{2+} channels are expressed, such as L, N, P/Q, R and T -type. The rise of cytosolic calcium is critical for the assembly of the exocytotic SNARE machinery and fusion of the vesicle with the

plasma membrane[91],[92].

1.3.1 Steps of Regulated Exocytosis - SNARE Complex Formation

The exocytotic process has to undergo several regulatory steps, which include the formation of a stably assembled exocytotic machinery called SNARE complex. SNARE is an acronym to indicate proteins identified as SNAP receptors[93]. SNAP refers to the soluble NSF attachment protein, while NSF indicates the N-ethylmaleimide-sensitive factor. This complex machinery is formed by the interaction of several proteins which have been extensively studied during the last 20 years. The major players in SNARE complex formation are the *v*-SNARE proteins (or vesicular proteins), located on the vesicle, and the *t*-SNARE proteins (or *trans*-membrane proteins), located on the plasma membrane. The major *t*-SNARE proteins are Sec1/Munc18-1 (mammalian uncoordinated-18 protein), SNAP25 (synaptosomal-associated protein 25), Syntaxin 1 (a multidomain protein with a SNARE domain), the N-ethylmaleimide-sensitive factor (NSF) and the soluble NSF attachment proteins (SNAPs). The most studied *v*-SNARE proteins are Synaptobrevin (or VAMP, vesicle-associated membrane protein) and the Rab3 small GTPases[94]. In order to permit exocytosis, SNARE proteins need to be assembled in a stable complex since individual SNARE proteins are not able to serve as SNAP receptors. Early studies revealed that neuronal SNARE proteins are aligned in parallel, while forming the complex, and are therefore referred to as "zipper" model[95]. The crystal structure of the SNARE complex was resolved in 1998 and revealed a highly twisted four helical bundle, consisted of Synaptobrevin II (Syb), Syntaxin Ia (Syx) and SNAP25B[96]. Syb II and Syx Ia are attached to the vesicle and plasma membrane, respectively, through carboxy-terminal transmembrane domains (TMD). Instead, SNAP25 is anchored to the plasma membrane by palmitoylation of its central region[96]. In regulated exocytosis, Synaptotagmin (Syt) and Complexin (Cpx) proteins play an important function as regulators. Syt is a *v*-SNARE protein composed of a helical transmembrane region anchored to two cytosolic C2 domains (C2A and C2B), which are sensitive to Ca^{2+} influx[97]. First defined as main calcium sensor[98],[99], it does not seem unlikely that Syt also plays a role in completing the *trans* zippering[100], during the SNARE complex formation, as well as in the membrane curvature[101],[102], to promote subsequent fusion[103]. Cpx is a cytosolic protein and its isoform II has been mainly observed in chromaffin cells[104]. While Cpx shows poor direct interaction with Syx, its N-terminal domain is tightly bound to the C-terminus of the SNARE complex (*e.g.*, the TMD of Syx and Syb)[105]. In this context, Cpx binding seems to stabilize

the Syx/Syb interface by therefore maintaining the SNARE complex stably assembled and highly fusogenic[106].
Large dense core vesicles (LDCVs) are responsible for catecholamines release and undergo several maturation steps prior to final fusion.

Biogenesis, Docking, Priming and Vesicles Fusion. Like synaptic vesicles (SVs), LDCVs can store and release their content, such as neurotransmitters, hormones and catecholamines, to the outside of the cell and into the blood stream. Membrane depolarization causes a calcium influx through voltage-gated calcium channels, which then triggers exocytosis. Interestingly, SVs and LDCVs differ in their intracellular trafficking as well as in their biogenesis. Concerning SVs, it is still not clear whether they originate from different machineries and are assembled or coated by different adapter proteins and vesicles precursors from the Golgi apparatus and/or the endosomal system. LDCVs instead, are synthesized *ex novo* from the Golgi, since they need to contain peptides and enzymes.
The presence of different pools of dense-core vesicles reflect different maturation steps through which the vesicles can reach a final fusion-competent state. This subdivision into different populations of vesicles has been challenging and possible only in cellular types that contain large vesicular structures, such as chromaffin cells[107]. In the previous century (1992), Neher and colleagues studied changes in calcium concentration as possible exocytosis trigger. For this purpose, they used calcium-caged compounds to raise the intracellular calcium concentration in a controlled way. With this approach, they were able to distinguish two different populations of LDCVs, which could fuse following different kinetics: the slowly releasable pool of vesicles (SRP) and the readily releasable pool (RRP) (**Fig. 1.7**). In subsequent studies, at least four different types of vesicle pools could be distinguished. The depot pool is the largest one and is composed of around 2000 vesicles in adult mice[108]. From this pool, the vesicles can reach the plasma membrane where they can be docked and anchored. The docking process, which takes place within 100 nm from the plasma membrane, is finely regulated by Munc18-1, the binding partner of Syntaxin I, which was characterized by Voets and colleagues[109]. Once the vesicles are docked, they need to be primed in order to become fusion-competent. The priming process is mainly controlled by the two *t*-SNARE proteins SNAP25 and Syntaxin, and by *v*-SNARE Syb/VAMP. A tight molecular coupling between the TMD of Syb II and the SNARE complex is crucial for LDCVs priming[110].

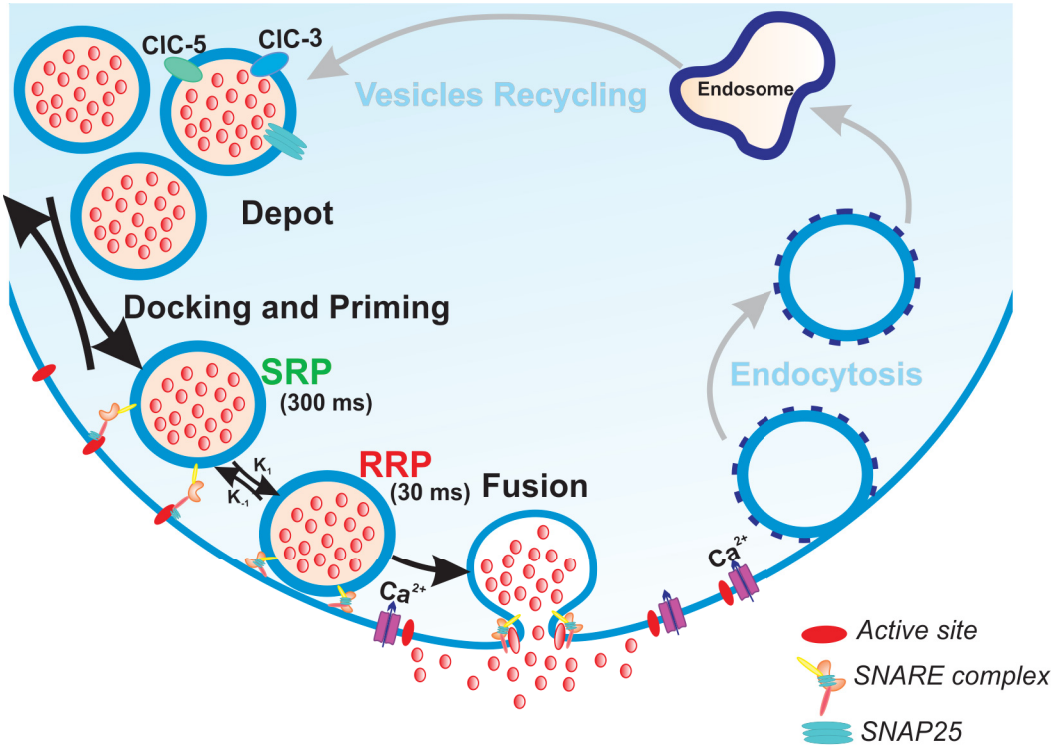

FIGURE 1.7: **Priming process of LDCVs.** Once the vesicles are anchored ("docked") to the plasma membrane, upon calcium stimulus, they get ready ("primed") to fuse to the cell membrane and release their cargo.

The final fusion process is carried out with different release-modes which have been characterized for the LDCVs, while for SVs it is still under debate whether they perform kiss and run or rather undergo an ultra rapid clathrin-independent endocytotis[111].

1.3.2 The Readily and Slow Releasable Pool of vesicles (RRP and SRP)

Once the vesicles are primed, we can distinguish between the slowly releasable pool (SRP), which fuse within hundreds of milliseconds (around 300 ms), and the readily releasable pool (RRP), which is able to fuse within tens of milliseconds (around 30). In reality, several degrees of "priming" are possible and are regulated through different kinetics (**Fig. 1.8**). All these processes are considered reversible reactions and start from the reserve pool of vesicles[112]. When analyzed at high temporal resolution, *e.g.* via the use of flash photolysis of calcium-caged compounds, exocytosis is characterized by a rapid, initial "exocytotic burst" (**Fig. 1.8**) which represents fusion of the readily releasable pool (RRP), fully matured and able to fuse. As soon as these vesicles are depleted, a slower phase of secretion occurs, which reflects the SRP fusion, as reported by Sørensen and colleagues[108]. A possible explanation might be that, before fusion, SRP do not undergo maturation into RRP; indeed, the SRP sensor might be faster than the maturation process itself and therefore hardly detectable. An alternative explanation would be that different degrees in the SNARE complex formation might affect different pools, that means a full and stable complex might be needed for the RRP fusion, while a partially formed SNARE complex might be sufficient for the SRP[108][113]. This model was for the first time described in the neuromuscular junction[114] and eventually characterized in other cell types, such as β-pancreatic and chromaffin cells[115],[116].
Interestingly, a mutation of SNAP25, where the last 9 aminoacids are deleted from its C-terminus, leads to loss of RRP and slows the exocytotic burst[117]. This sequence of 9 aa is essential to permit binding to Synaptotagmin I, a calcium sensor candidate for the regulation of the RRP[118]. SNAP25 exists in two different splice variants, SNAP25a and SNAP25b[119], whose expression level varies in different post-natal stages. In particular, splice variant a is present at embryonic stages, while b is mainly present in adult phases[119]. SNAP25 can regulate both SRP an RRP by possibly influencing their stabilization, either by affecting the SNARE complex formation or by preventing binding to calcium sensors, while Synaptotagmin I would be required for RRP fusion, but not for that of SRP.

1.3.3 Exo-endocytosis

The exo- and endocytotic processes are tightly interwoven and mutually dependent on each other. Endocytosis is needed to ensure vesicle recycling and influence exocytosis as well. Its kinetics can be highly variable depending on the stimulus source and origin.

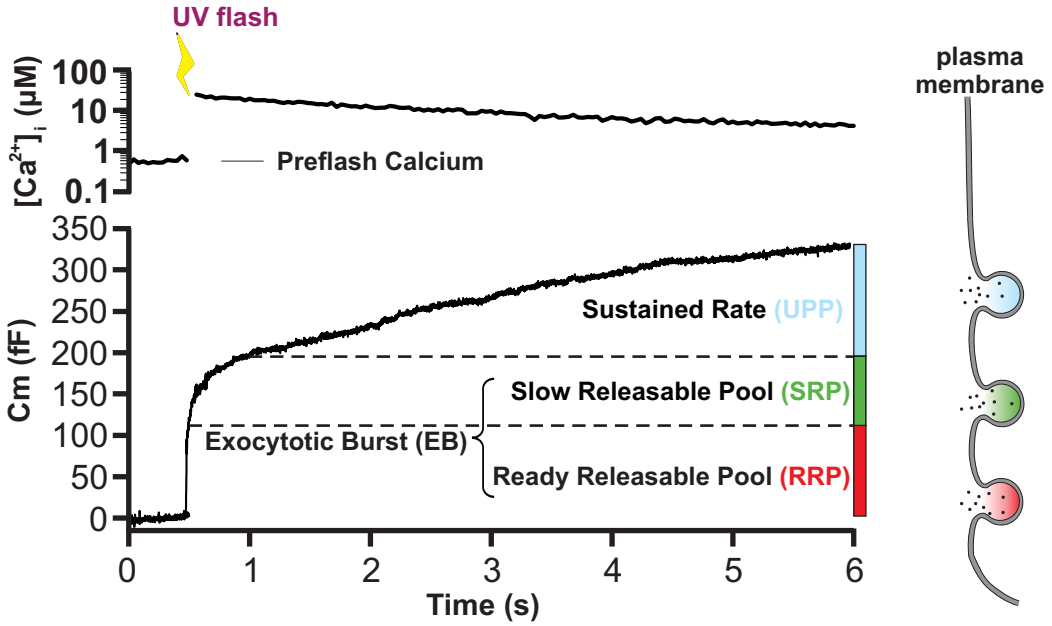

FIGURE 1.8: **Different pools of vesicles in mouse chromaffin cells.** The flash-photolysis technique permits to study in detail the priming process of different populations of vesicles. Image modified from J. Rettig and E. Neher, 2002 [107].

In particular, slow endocytosis is clathrin-dependent and is largely performed by many different cell types (neuroendocrine and neuronal cells, calyx of held, *etc*). Furthermore, both calcium increase and Synaptotagmin activity mediate exocytosis, which in turn impacts endocytosis [120]. The most important SNARE proteins, Synaptobrevin, SNAP25 and Syntaxin, take also part in endocytosis initiation. This process supports not only vesicle recycling but also active-zone clearance and is crucial for vesicle replenishment (and can thus influence the RRP size). On the other hand, rapid exocytosis can occur in only a fraction of individual vesicles and does not describe whole-cell endocytosis [120]. Rapid exocytosis is a candidate to mediate kiss and run/stay processes and would contribute to RRP replenishment, while slow whole-cell endocytosis would preferably follow full fusion [121]. The RRP size therefore depends on both exo- and endocytotic modes. Interestingly, calmodulin inhibitors and calcium influx blockers severely affect endocytosis and RRP replenishment [122]. Since the latter is needed for recovery from short-term depression, appears evident that exo-endocytosis and RRP replenishment play a key role in synaptic plasticity, as shown by analyzing excitatory post-synaptic currents (EPSC) in the calyx of held [120]. Similarly to the effects on exocytosis, the SNARE proteins SNAP25 and Syntaxin, when blocked, can inhibit endocytosis and RRP replenishment as shown in experiments performed at the calyx of held.

1.3.4 Neuroendocrine Cells as a Model for Exocytotic Studies

The exocytotic process has been a popular subject matter since its first description in the Sixties[123]. So far, neuroendocrine cells have been the best characterized model for exocytotic studies. This is due to the many advantages compared to the neuronal network, first of all because of their relatively simple system. Chromaffin cells are a type of neuroendocrine cells, such as β-pancreatic cells and pituitary melanotrophs, which reside in the inner part of the adrenal gland: the medulla. Adrenal glands are located above the kidneys and are composed of the cortex, divided into *Zona Glomerulosa* and *Zona Fasciculata*, and the medulla (in pink), separated by the *Zona Reticularis*, which contains chromaffin cells (**Fig. 1.9**). Adrenal chromaffin cells and sympathetic neurons share a common precursor in the neuronal crest; neuronal crest cells migrate to originate Schwann cells, dorsal root ganglion cells, sympathetic neurons and chromaffin cells (also referred to as adrenal paraneurons)[124]. Chromaffin cells contain secretory granules, such as large dense core vesicles (LDCVs). Upon sympathetic stimulation, they release catecholamines into the blood stream, in order to mediate sympathetic neural responses such as blood pressure regulation, heart rate and glucose level.

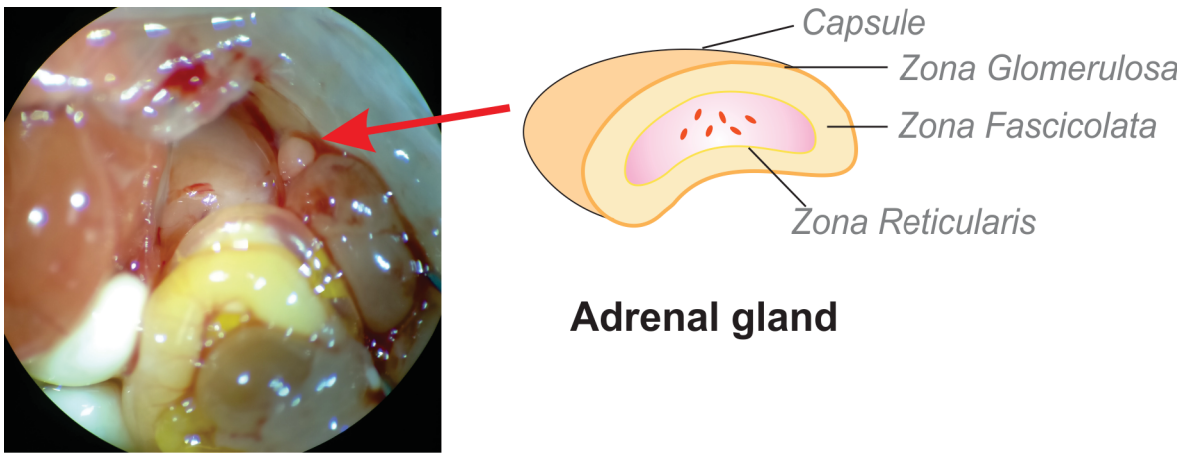

FIGURE 1.9: **Representation of the mouse adrenal gland.** On the left side, a microscopy image of the internal mouse anatomy. The adrenal gland appears as a yellowish sphere located above the right kidney (red arrow). On the right side, the different layers constituting the gland are depicted and chromaffin cells are shown as small red dots.

Due to their round shape, adrenal chromaffin cells allow monitoring of changes in the membrane capacitance, by using the patch clamp technique, which permits to measure exocytotis in real time with a high temporal resolution. Membrane capacitance recordings can also be performed together with amperometric detection. This powerful

combined technique allows to monitor fusion of single secretory vesicles (or "quanta") and therefore to analyze the distinct fusion kinetic properties[125].

1.4 Endosomal System

In cells, vesicles need to be sorted and trafficked to different intracellular compartments, where they perform their biological role. One way to traffic vesicles is through the endosomal pathway, which is composed of a series of organelles and vesicular structures. These structures are in a dynamic state and undergo several biological and morphological changes from the plasma membrane to lysosomal degradation (**Fig. 1.10**). Proteins are normally internalized from the plasma membrane in a clathrin-mediated or clathrin-independent way. Next, cargo proteins, such as SNARE proteins and ion channels, are transported to early endosomes, where they associate with pre-existent early endosomes or other recycled vesicles. This mainly takes place through interaction with Rab5, a GTPase protein[126]. Maturation of vesicles through the different endosomes is accompanied by a progressive acidification of the internal pH. Early endosomes represent the main sorting system, from which the cargo can be transported to the final organelle. From early endosomes, the vesicles arrive to late endosomes which represent the last step before lysosomal degradation. Late endosomes are important for biogenesis of intralumenal vesicles and drive degradation via the ubiquitin system[127]. In the final stage, where late endosomes are fused to lysosomes to concentrate cargo proteins for degradation, more than 50 hydrolases are present and the lumenal pH is as low as 4.5 (in the majority of neuronal cells). The endosomal pH appears to be mainly regulated by the V-ATPase.

1.4.1 Rab Proteins

Rab proteins form a large and diverse family of GTP-binding proteins which regulate endosomal transport and constitute the intracellular pathway. Rab3 (and its different splice variants, 3A, 3B, 3C and 3D[128]), Rab5[129], Rab7[130] and Rab11[131] have been so far extensively studied. These Rab proteins have been associated with specific endosomal organelles, in particular, Rab3 and Rab5 are mainly localized on the surface of early endosomes, Rab7 of late endosomes and Rab11 of recycling endosomes. Rab proteins appear to be involved in both exo- and endocytotic pathways, and Rab3 is a great example of the multiple roles played by these proteins.

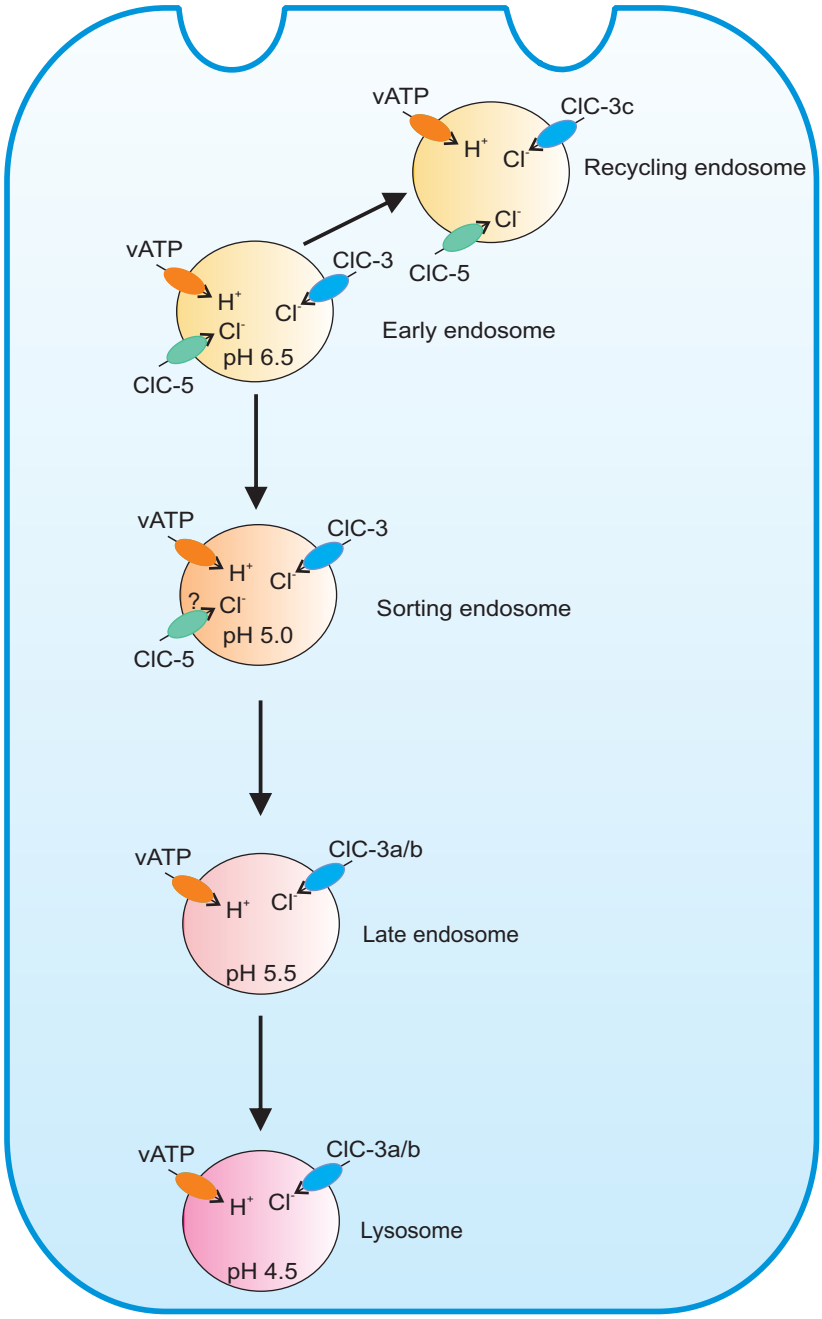

FIGURE 1.10: **Endosomal system representation.** The possible roles of ClC-3 (and its different splice variants) and ClC-5 are depicted along the endosomal pathway, where they are supposed to regulate the intracellular acidification or the chloride concentration. Image modified from T. J. Jentsch, 2012[73].

Rab3 is mainly located on synaptic vesicles where is involved in the docking process. The docking is facilitated by interaction with "scaffolding proteins" such as Piccolo and Bassoon, which move the vesicles close to the RIM molecules. RIM proteins (or Rab-Interacting Molecules) are crucial for the arrangement of the active zone, by interacting not only with Rab proteins but also with calcium channels, which need to be recruited at the plasma membrane[132].

Concerning Rab5, this protein was mainly found in early endosomes, where regulates their biogenesis. It is also expressed on synaptic vesicles and it is implicated in endocytosis, in particular in the clathrin-mediated process. Rab5 counts, among its effectors, PI(3)Kinase[133] which can phosphorilate PI(3)P (abundant on endosomes)[134], suggesting a possible pathway which recycles endocytosed vesicles into endosomal-like structures.

Rab7 is a marker for late endosomal organelles and both ClC-3a and ClC-3b where found in such compartments[68]. In an elegant experiment, siRNA was used to deplete endogenous Rab7 which was proved not to interfere neither with the trafficking through early endosomes nor with the transferrin receptor recycling[130]; in fact, Rab7 appears to be necessary for cargo delivery to lysosomes and for late fusion between late endosomes and lysosomes.

The role of Rab11 appears important in recycling and exocytic processes. Different splice variants of Rab11 exist and show a differential organ and tissue distribution[135][136][131]. Rab11, by interaction with different adaptor proteins, is able to coordinate the movement of the vesicles along actin filaments and microtubules. It was also implicated in exocytosis due to its ability to interact with Sec proteins (subunits of mammalian exocyst complex). In HeLa cells, Rab11 and transferrin receptor (TfR) are concentrated in the perinuclear and pericentriolar regions, corresponding to recycling endosomes. Rab11 is also involved in exocytosis of recycling vesicles at the plasma membrane, as recently demonstrated[137], and, in addition, it is also localized in the trans-Golgi network (TGN) and in post-Golgi vesicles, where it probably mediates intracellular trafficking and sorting to the plasma membrane during exocytosis.

1.4.2 Vesicles Recycling Process

In virtue of energy-saving strategy, after exocytosis the cell prefers to recycle intracellular vesicles, as well as SNARE-proteins, rather than synthesize them *ex novo*. Concerning their recycling process, SVs are recycled and refilled through an uptake process, while neuropeptides are accumulated into LDCVs during their biogenesis in the trans-Golgi network. For this reason, neuropeptides are not available for a rapid release from recycled LDCVs, while catecholamines can be immediately reloaded and secreted from LDCVs after recycling[138] [139]. In general, vesicles are endocytosed and recycled via three possible pathways so far described[140],[139]. The first two pathways are not clathrin-mediated, while the third one makes use of clathrin-coated buds.

1. Vesicles are acidified and refilled with neurotransmitters, while they remain in a readily releasable state and are still docked at the plasma membrane (the so-called "kiss and stay")[141];

2. After "kiss and run", vesicles are locally recycled and refilled[83];

3. After full fusion, vesicles are endocytosed and coated in a clathrin-way manner, and directly refilled or sorted through the endosomal pathway[142].

The first two mechanisms are described by fast kinetics, while the last one is a slow recycling process. The last two pathways are pH-dependent[140] and might be regulated not only by the V-ATPase but also by proton exchangers, such as ClC-3 and/or ClC-5. After recycling, the proteins can be again sorted to the plasma membrane and to vesicle surface, or alternatively be transported to lysosomes for degradation.

Chapter 2

Materials and Methods

2.1 Materials

2.1.1 Reagents

Hereby all the reagents used for the methods are listed.

DMEM	ThermoFisher Sci. Cat No. 61965026
F-12K Medium	ATCC Cat No. 30-2004
Insulin-transferrin-selenium	Gibco Cat No. 51500-056
Penicillin-Streptomycin	Gibco Cat No. 15070-063
Sodium Pyruvate	Gibco Cat No. 11360-034
TRIzol	ThermoFisher Sci. Cat. No. 15596018

All chemicals and reagents were purchased from Sigma - Aldrich unless otherwise stated.

2.1.2 Kits

Kits are listed below.

Hot Start PCR Master Mix	PeqLab
KAPA HotStart Mouse Genotyping Kit	KAPABIOSYSTEMS KK5609
DNase Amplification Grade I	ThermoFisher Scientific Cat No. 18068015
DNA, RNA and protein purification	MACHEREI-NAGEL Cat. No. 740588.250

2.1.3 Solutions

2.1.3.1 PFA 4%

To prepare 1 l of 4% paraformaldehyde, 800 ml of PBS was added to a sterile glass beaker on a stir plate in a ventilate hood. The solution was heated while stirring to approximately 60°C, without reaching the boiling temperature. Subsequently, 40 g of paraformaldehyde powder is added to the heated PBS solution. The pH is slowly adjusted by adding dropwise 1 M NaOH until the solution clears. Once the paraformaldehyde is completely dissolved, the solution is cooled and therefore filtered. Finally the volume of the solution is adjusted to 1 l with PBS. The pH is finally adjusted to approximately 6.9 by adding diluted HCl. The solution is then aliquoted in 50 ml sterile falcon tubes and stored at -20°C.

2.1.3.2 Locke's Solution

Locke's solution is prepared and filtered as following.

Table 2.1: Locke's solution

Component	NaCl	KCl	$NaHCO_3$	HEPES	Glucose
Concentration	154 mM	5.6 mM	3.6 mM	5 mM	5.6 mM

The pH is adjusted to 7.3 using NaOH (osmolality 320 mOsm/kg).

2.1.3.3 Poli-D-lysine-hydrobromide in Borate Buffer

The stock solution of Poli-d-lysine (5 mg/ml) is diluted to 0.25 mg/ml in borate buffer, then batched in 15 ml falcon tubes stored at 4°C.

2.1.3.4 10 cm Petri dish Coating

The 10 cm Petri dishes are coated with 1.5ml of collagen 0.5mg/ml. The collagen is aspired and subsequently the dishes are left semi-open until completely dried. The 10 cm Petri dishes are used for PC-12 cells.

2.1.3.5 4-well dish Coating

Sterile coverslips are placed into 4 well dishes using a sterile forceps. A 100 μg/μl drop of Poly-D-lysine solution is transferred on top of each coverslip and let settled own. After 24 h, the drop is aspired and the coverslip is washed with 1 ml of ddH_20. After 15 minutes incubation, the ddH_20 is aspired. This washing step is repeated 3 times and finally the dishes are left semi - opened until complete drying. The coating procedure is necessary to guarantee good cell adhesion for immunocytochemistry experiments of chromaffin cells.

2.1.4 PC-12 Cell Line

2.1.4.1 Thawing procedure for PC-12 Adh cells – ATCC CRL-1721.1

The thawing procedure is executed following the manufacturer instructions. The vials are removed from liquid N_2 and rapidly thawed by gentle agitation in a 37°C water bath for approximately 2 minutes. Once completely thawed, the cell suspension is transferred drop-wise into a sterile 15 ml falcon tube containing 9 ml of pre-warmed complete growth medium. The cell suspension is therefore centrifuged at 125 x g for 8 minutes, subsequently the supernatant is discarded ant the cell pellet is resuspended in 1 ml of pre-warmed growth medium. The cell suspension is then transferred to a 10 cm Petri dish, previously coated with collagen, containing 10 ml of pre-warmed growth medium, previously placed into the incubator (5% CO_2, at 37°C) for 30 minutes to allow the medium to reach its normal pH (7.0 to 7.6). Cells are then incubated at 37°C in a 5% CO_2 in air atmosphere for optimal conditions. The day after the culture medium is replaced with fresh growth medium.

2.1.4.2 Complete Growth Medium for PC-12 cells

The horse serum was removed from frozen storage and placed overnight in a refrigerator at 4°C. The day after it was transferred to a 37°C water bath with constant gentle agitation until complete thawing. Subsequently it was filtered and dispensed into single-use aliquots in sterile 50 ml falcon tubes and stored at -20°C. Finally, the complete growth medium was prepared as following:

After filtration, the culture medium is batched in sterile 50 ml falcon tubes and stored at 4°C for up to 2 weeks.

Table 2.2: Complete Growth Medium PC-12 Adh cells

Component	Volume
F12K Medium	203.75 ml
Fetal Bovine Serum	6.25 ml
Horse Serum	37.5 ml
Penycillin/streptomycin (25 μg/μl)	2.5 ml

2.1.4.3 PC-12 cells Lipofectamine Transfection

The protocol used for transient Lipofectamine2000® transfection is based on a protocol provided by the manufacturer company. 150 μl of Opti-MEM is added to two 1.5 ml sterile Eppendorf tubes. The DNA is added to one tube, while 2.5x volume/weight of Lipofectamine2000® is added to the other tube. Both mixtures are let sit for 5 minutes, afterwards the content of the DNA tube is mixed with that of the Lipofectamine2000® mixture. The final solution is let sit for 1 h to maximize the transfection efficiency. Finally the mixture is added drop-wise to the Petri dish. The day after the culture medium was replaced with new fresh growth medium and the experiments were performed on DIV 1-3.

2.1.5 Mouse Chromaffin Cells Primary Culture

2.1.5.1 Culture Medium for chromaffin cells (Enriched DMEM)

Mouse chromaffin cells cultures are maintained in enriched culture medium, composed of DMEM (high glucose, GlutaMAX Supplement), 10% Sodium Pyruvate to final concentration 1 mM, 10% Insulin-transferrin-selenium-X (100X) and 4% penicillin/streptomycin (10,000 units). Medium batches are freshly prepared, filtered and kept in the incubator at 37°C, 7.5% CO_2 for equilibration, as following:

Table 2.3: Culture Medium

Component	Volume
DMEM	50 ml
Sodium Pyruvate (100 mM)	500 μl
Insulin-transferrin-selenium-X (100x)	500 μl
Penycillin/streptomycin	200 μl

2.1.5.2 Enzymatic Solution

The enzymatic solution was previously prepared and, after filtration, finally batched (2 ml) in sterile 15 ml falcon tubes and stored at -20°C for up to three months.

Table 2.4: Enzyme solution

Component	Volume	Weight
DMEM	250 ml	
L-Cysteine		50 mg
$CaCl_2$ - $2H_2O$ (100 mM)	2.5 ml	
Na_2-EDTA (50 mM)	2.5 ml	

The pH is adjusted to 7.3 with NaOH and the osmolality is 340 mOsm/kg.

2.1.5.3 Inactivating Solution

Inactivating solution was prepared in advanced, after filtration is batched (2 ml) in sterile 15 ml falcon tubes and stored at -20°C for up to 3 months.

Table 2.5: Inactivating solution

Component	Volume	Weight
DMEM	45 ml	
Fetal Bovine Serum	5 ml	
Albumin		125 mg
Trypsin inhibitor		125 mg

The pH is adjusted to 7.3 with NaOH and the osmolalility is 340 mOsm/kg.

2.1.5.4 Ringer's Solution (Depolarization Protocol)

Table 2.6: Ringer's solution

Component	NaCl	KCl	$CaCl_2$	$MgCl_2$	Hepes	Glucose
Concentration	130 mM	4 mM	2 mM	1 mM	10 mM	30 mM

The pH is adjusted to 7.3 using NaOH. The expected osmolality is around 290 mOsm/kg

2.1.5.5 Intracellular Solution (Depolarization Protocol)

The pH is adjusted to 7.3 using Cs-OH. The expected osmolality is around 300 mOsm/kg. The free $[Ca^{2+}]_i$ is calculated to be 300 nM (via http://maxchelator.stanford.edu/). BAPTA, Mg-ATP and Na_2-GTP are added fresh to the stock solution, which is stored in batches of 100 µl and kept at -20°C.
BAPTA 2.8 mM (10x) stock solution is stored at -20°C, as well as Mg-ATP 20 mM/ Na_2-GTP 5 mM (10x) stock solution.

Table 2.7: Depolarization solution 300 nM free $[Ca_i^{2+}]$

Cs-Glutamate	NaCl	BAPTA	$CaCl_2$	$MgCl_2$	Mg-ATP	Na_2-GTP	Hepes
120 mM	8 mM	0.28 mM	0.18 mM	1 mM	2 mM	0.5 mM	10 mM

2.1.5.6 Ringer's Solution (Amperometry Recordings)

The Ringer's solution used for amperometric measurements is similar to that used for the depolarization protocol.

Table 2.8: Ringer's solution

Component	NaCl	KCl	$CaCl_2$	$MgCl_2$	Hepes	Glucose
Concentration	130 mM	4 mM	2 mM	1 mM	2 0mM	32 mM

The pH is adjusted to 7.3 using NaOH. The expected osmolality is around 310 mOsm/kg.

2.1.5.7 Intracellular Solution (Amperometric Recordings)

Table 2.9: Perfusion solution 20 μM $[Ca^{2+}]_i$

Cs-Glutamate	NaCl	DPTA	$CaCl_2$	Mg-ATP	Na_2-GTP	Hepes
110 mM	8 mM	20 mM	5 mM	2 mM	0.3 mM	40 mM

The pH is adjusted to 7.3 using Cs-OH. The expected osmolality is around 300 mOsm/kg. The free $[Ca^2]_i$ is calculated to be 20 µM. In case of 3 µM of free $[Ca^{2+}]_i$, 1 mM of $CaCl_2$ is used for the perfusion solution.

DPTA, Mg-ATP and Na_2-GTP are added fresh to the stock solution, which is stored in batches of 100 µl and kept at -20°C.

DPTA 200 mM (10x) stock solution is stored at -20 °C, as well as Mg-ATP 20 mM/ Na_2-GTP 3 mM (10x) stock solution.

2.2 Methods

2.2.1 Genotyping PCR reaction

The DNA isolation reaction is prepared in agreement with the instruction reported in Hot Start Kit (KAPABIOSYSTEMS).

In brief, the DNA template used for the genotyping reaction is obtained from a tail biopsy (2 mm) from P0 new born mice. The genomic DNA is extracted using KAPA Express extract buffer and enzyme, according to the manufacturer instruction. Each tail piece is digested at 75°C for 10 minutes and subsequently heat inactivated at 95°C for 5 min. After short vortexing, the samples are centrifuged at 11,000 rpm for 2 minutes at room temperature. Therefore, 1 μl supernatant from each tail piece, containing the genomic DNA, is used for the genotyping PCR reaction.

Table 2.10: DNA isolation

Component	ddH_20	KAPA Buffer 10x	KAPA Enzyme
	88 µl	10 µl	2 µl

The PCR reaction is run as followed, using the specific primers, one for the wt and one for the KO allele, to verify the genotype.

Table 2.11: KAPA Mix reaction

Component	ddH_20	KAPA2G Fast Hot Start	Fw-Primer	Rev-Primer	DNA
	25 µl	12.5 µl	1.25 µl	1.25 µl	1 µl

The PCR genotyping reaction is run under the following conditions: 3 min of heat inactivation at 95°C followed by 35 cycles of denaturation (15 s at 95°C), annealing (15 s at 58°C) and amplification (15 s at 72°C). The last step is then run at 72°C for 2 min.

Hereby a list of primers used for the PCR genotyping reaction:

Table 2.12: Forward and Reverse Primers

Primer Fw ClC-3 wt	gatctaattctgccttcctc
Primer Fw ClC-3 ko	ggaagacaatagcaggcatgc
Primer Rev ClC-3 wt and ko	actctgcccatgttttccact

2.2.2 Quantitative real-time PCR (qRT-PCR)

The expression level of genes of interest was analyzed by quantitative real-time PCR (qRT-PCR) to show a developmental regulation at different post-natal stages.

2.2.2.1 RNA isolation

For the RNA isolation process is of crucial importance to work as much as possible in RNA-free conditions to avoid RNA degradation. Adrenal glands are collected from C57BL/6 mouse strain at different ages, at P0 post-natal day and at P60 to perform developmental studies. The tissue is frozen in liquid N_2 immediately after extraction and stored at -80 °C. For processing, samples are rapidly thawed and then treated with 1 ml TRIzol Reagent® for 20 mg of tissue sample. Samples are subsequently homogenized and transfered into 1.5 ml sterile RNA-ase free tubes. Homogenized tissues are incubated for 5 min at RT to permit complete dissociation of nucleoproteins. Subsequently, 200 µl of chloroform are added to each tube per 1 ml of TRIzol Reagent® and then vigorously shaken by hand for 15 sec. The samples are incubated for 2-3 min at RT and then centrifuged at 12,000 g for 20 min at 4°C. After this step, the appearance of three phases indicates that the RNA has been isolated. In particular, the lower dark red organic phase contains phenol, DNA and proteins. The interphase and a clear upper aqueous phase contain RNA. At this point, it is critical to precipitate the RNA, which has to be carefully separated from the other two phases, with 0.5 ml of 100% isopropanol for ml of TRIzol Reagent® used. The samples are briefly vortexed, then incubated at RT for 10 min, subsequently centrifuged at 12,000 g for 10 min at 4 °C. The supernatant is then removed and the pellet is washed with 1ml of freshly prepared 75% Ethanol in RNAase free water, for ml of TRIzol Reagent® used. The samples are vortexed again and centrifuged at 7,500 g for 5 min at 4 °C. The washing solution can now be removed using a fine tip and the pellet is let dry on air for 15 - 20 min until ethanol is completely vapored. The pellet is then carefully resuspended in 20 μl of RNAase free water, then incubated at 58°C for 15 min, resuspended and incubated again for 10 min. The samples can now be kept on ice and the concentration is measured via a spectrophotometer (Nanodrop 2000, ThermoFisher Scientific). Approximately 1 μl

of sample is loaded (with a 6x loading dye and TE buffer up to 12 μl) and run via gel electrophoresis (agarose 1.5%) for 25 min at 120 V. For a pure RNA sample, the absorbance ratio A280/260 should be > 1.8 and for a good quality RNA sample the 28S band should be as twice as bright compared to 18S and the band at 5S should be visible as well (**Fig. 2.1**).

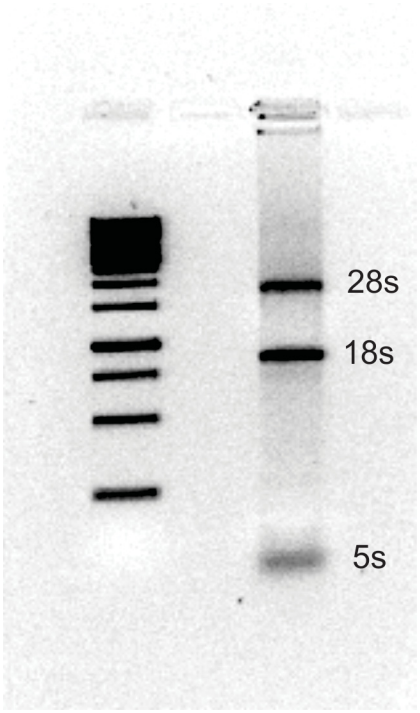

FIGURE 2.1: **RNA integrity.** 1μg of RNA, after being isolated, is run on a 1.5% agarose gel for 35 minutes. The presence of three bands indicates that the RNA quality is acceptable.

A poor quality RNA, contaminated by Phenol or completely degraded would result in a very low molecular weight smear and would therefore be discarded. Good quality RNA samples are treated with DNAase treatment and are the used to synthesize the first strand of cDNA.

2.2.2.2 DNAase treatment

The RNA samples are treated with DNAase in order to eliminate the presence of genomic DNA (gDNA) (using a Thermo Fisher Scientific Kit, DNase 1, Amplification grade Catalog Nr. 18068015) Even though the primers were designed to span introns or in two different exons, gDNA contamination can still be an issue, for example when the target mRNA presents pseudogenes at the level of DNA. A DNase digestion step is therefore necessary and performed using a special kit (Thermo Fisher Scientific, DNase 1, Amplification grade

Catalog Nr. 18068015). For each sample, the following components are added to a 0.5ml micro-centrifuge tube kept on ice:

Table 2.13: DNAase Treatment

Component	Volume
RNA sample	1 μg
10X DNase I Reaction Buffer	1 μl
DNase I (Amplification grade) 1U/μl	1 μl
RNAse free water	up to 10 μl

2.2.2.3 First-Strand cDNA Synthesis

The following RT-PCR reaction is used to synthesize the first-strand cDNA from total RNA. The components are added to a nuclease-free micro-centrifuge tube kept on ice to reach a 20 µl final reaction volume: 1 μl of oligo(dT)20 to a get a final concentration of 2.5 μM, 10 pg - 5 ug total RNA, 1 μl dNTP Mix (10 mM each dATP, dGTP, dCTP and dTTP at neutral pH) to a final concentration of 0.5 mM, ddH_2O to a final volume of 13 μl. This mixture is subsequently heated at 65°C for 5 minutes and incubate on ice for at least 1 minute. After brief centrifugation, the following components are added: 4 μl 5x First strand buffer, 1 μl DTT to a final concentration of 5 mM, 1 μl RNaseOUT Recombinant RNase Inhibitor (Cat. no. 10777-019, 40 units/μl) and 1 μl of SuperScript III RT (200units/µl). The samples are incubated at 50°C for 1 h and subsequently inactivated by heating at 70°C for 15 minutes. The newly synthesized cDNA can now be used as a template for quantitative RT-PCR or stored -80°C.

2.2.2.4 Standard fragments for qRT-PCR

In order to amplify standard fragments up to 500 - 600 bp in length, primer pairs for specific genes were designed according to certain requirements, such as a minimal G/C content of 55% and a melting temperature of 58-62°C. Primer specificity was confirmed by BLAST analysis and tested by PCR on first-strand cDNA. For quantification purposes, a calibration curve is necessary and therefore defined numbers of standard fragments were used as PCR templates to establish it. Standard fragments were subcloned from first-strand cDNA samples, verified by sequencing and purified from gel extraction (DNA purification kit). The molar concentration of purified DNA fragments was determined by spectrophotometer and then the number of molecule was calculated, according to the following equation (2.1), assuming that the average weight of a base pair is 650 Daltons:

$$mol/g * molecules/mol = molecules/g \tag{2.1}$$

This means that one mole of a bp weighs 650 g and thus the molecular weight of a double stranded DNA template can be calculated by multiplying its length (in bp) by 650 D. This gives the number of moles per g, which is the inverse of the molecular weight. Now, considering that 1 mole contains $6.022 * 10^{23}$ (Avogadro's number) molecules, by dividing it by the molecular weight, it is possible to calculate the molecules of template per gram. Finally, the number of copies of template in a given sample can be extrapolated by dividing the number of molecules per gram by $1 * 10^9$, to convert it to ng, and then by multiplying it by the amount of template (in ng). A standard curve was generated using a ten-fold serial dilution for each template and each reaction was run in triplicate.

2.2.2.5 Quantitative RT-PCR

First, known concentration of template are used to generate a standard curve. To obtain a standard curve, a template of the PCR purified fragment of known concentration of 18S, β-Actin, ClC-3 and ClC-5 is used. 1 μl of the purified DNA fragments of the reference genes (18S and β-Actin) and the genes of interest (ClC-3 and ClC-5) is diluted multiple times to get a 10-fold dilution series (of at least 6 dilutions) for each template. All standard dilutions are assayed in triplicate on the Bio-Rad Real-Time PCR detection system . The PCR purified fragment for the standards have been appropriately diluted to reach optimized concentration so that the quantities of target in the experimental samples should fall within the concentration range covered by the standard curve, as recommended in the "Good Practice Guide for the Application of Quantitative PCR"[143] and the MIQE Guidelines. The cDNA samples are measured in triplicate, from three different RNA isolations, where three C57BL/6 adult mice (P60), or five C57BL/6 newborn mice (P0), were used for each isolation. Two samples of cDNA were obtained from each, and finally one cDNA was used to perform quantitative RT-PCR. All reactions were performed in triplicate and run in three independent experiments using CFX96 Touch Real-time PCR Detection System (BIORAD). The qRT-PCR reaction conditions consisted of 15 min heat activation at 95°C followed by 40 cycles of denaturation (5 s at 95°C), annealing (30 s at 52°C), and amplification (30 s at 72°C). Here the list of the forward and reverse primers used for the qRT-PCR reaction:

Table 2.14: qRT-PCR

Gene	Genebank Nr.	Primers 5′-3′	Size
18S	NR 003278.3	Fw CGCCGCTAGAGGTGAAATTCTTG Rev GTGGCTGAACGCCACTTGTCC	522 bp
β-actin	NM 007393.5	Fw CATGAAGTGTGACGTTGACATCCG Rev TGCTCCAACCAACTGCTGTCG	522bp
ClC-3	NM 007711.3	Fw CCTCTTATGGCTGCAGTAATGACC Rev GCACTGCCTCAGACCAAGCTT	525bp
ClC-5	NM 001243762.1	Fw CAGAGGCTTTCATCAGGGGAGTTTTAG Rev CTCAGAATTCCAGCAACAGTGCTCATG	499bp

2.2.2.6 Data Analysis of qRT-PCR

Changes in the fluorescence intensity vs. cycle numbers from a qRT-PCR experiment are represented in a typical sigmoid graph (**Fig. 2.2**).

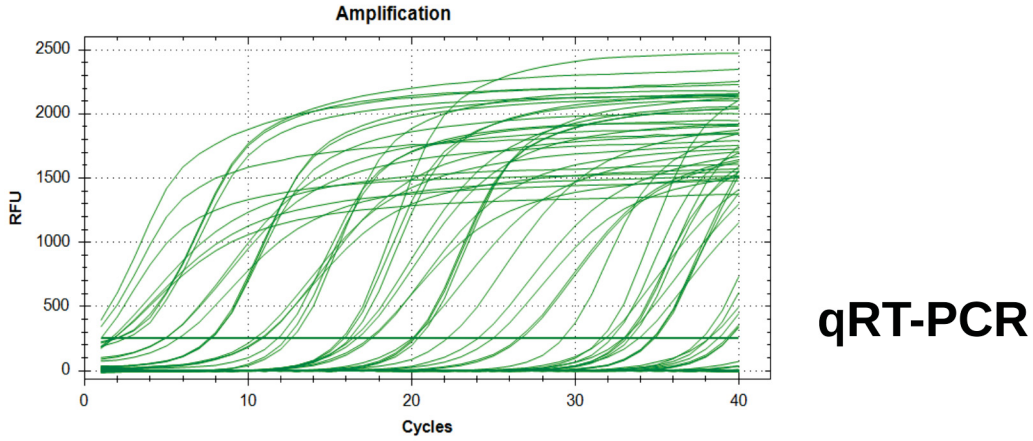

Figure 2.2: **Example of qRT-PCR experiment.**

Changes in fluorescence intensity are depicted from 6 different molar concentrations (dilutions) of defined fragment numbers (e.g 10^4, 10^6, 10^8). The initial phase, exponential phase and final plateau phase represent changes in the fluorescence intensity (**Fig. 2.2**). The calibration curve is calculated by plotting the logarithm of standard fragment molecule numbers [Log Conc] and the corresponding crossing point values [Cycle Number] and fitted applying a linear regression. At the crossing point the same amount of newly synthesized fragment is present in each sample. The amplification efficiency (E) of each qRT-PCR run is calculated form the slope (m) of the calibration curve, applying the following equation (2.2):

$$E = 10^{-1/m} \tag{2.2}$$

m has approximately a value of -3.3, which reflects an efficiency of 2 (for the PCR amplification product). Based on the calibration curve, the initial amount of fragments in each ample can be therefore calculated. The transcription level of ClC-3 and ClC-5 was analyzed and compared to that of reference genes (18S and β-Actin). The data were analyzed using CFX Manager (BIORAD) and the threshold cycle (C_q) value for the gene of interests were normalized to Cq value obtained for the reference gene.

2.2.3 Transgenic Mice generation

The *Clcn3*$^{-/-}$ animal model was kindly provided by T. Jentsch lab and Clcn3 gene disruption was described by Stobrawa et al[1]. In brief, a clone containing the first 6 exons and promoter region was isolated from a mouse genomic library. A first fragment (KpnI-ApaI) from intron and exon 2 and a second fragment (NcoI) from intron 3 and intron 5 were placed in pKO Scrambler V901 vector, containing a pgk promoter-driven neomycin resistance cassette. This deletes a 1kb fragment of CLCN3 (containing exon 3) and results in a frame-shift (splicing from exon 2 to 4). In addition, a pgk promoter-driven diphtheria toxin A cassette was added. Finally, the constructed was electroporated into ES cells (R1). Clones resistant to G418 were chosen and cells from two correct clones were injected into blastocysts (C57BL/6 mice strain). Resulting males were bred with WT females, according to the breeding permission (ATZ 84-02.04.2015.A108). The resulting heterozygous mice (from two different ES clones) were inbred to generate *Clcn3*$^{-/-}$ mutants.

2.2.4 Adrenal Chromaffin Cells Culture

Adrenal chromaffin cells are an ideal native system to characterize and study exocytosis. The following protocol has been modified from one previously published by Sorensen et al. in 2003[144].
Experiments were performed on chromaffin cells prepared from first post-natal day mice (P0) or adult mice (P60), after genotyping was performed. Even though wt and *Clcn3*$^{-/-}$ pups did non exhibit a clear different phenotype, *Clcn3*$^{-/-}$ mice appeared smaller and less vital than the wt litter mates. Animals were sacrificed via decapitation according to the German Law. After being quickly dissected, the adrenal glands were transfered to a 35

mm Petri dish containing 200 µl of cold Locke's solution. Using fine forceps, the glands are cleaned from the adjacent connective tissue and therefore incubated in a 15 ml falcon tube with 400 µl of enzymatic solution for digestion at 37°C for 30 minutes with slight shacking. After careful replacement of the enzymatic solution with 200 µl of inactivating solution, the glands are incubated again at 37°C for 5 minutes. The glands are rinsed out from the latter solution with 450 µl of enriched culture medium, which is then replaced by 200 µl of fresh enriched medium, and mechanically triturated. For optimal trituration, first a 1 ml pipette tip was used and then a 200 µl tip was used until complete dissociation. The final volume is reached by adding 400 µl of enriched medium and finally 50 µl of cell suspension is plated on each 37 mm coverslip in a six-well plate and incubated at 37°C, 7.5% of CO_2. After 30 minutes incubation, the plates are flooded with 3 ml of enriched DMEM per coverslip. Chromaffin cells were used for patch clamp and amperometry experiments after 2-3 DIV (days *in vitro*).

2.2.5 Chromaffin cells transient transfection

Chromaffin cells can be difficult to transfect, therefore a dual, optimized, protocol based on Lipofectamine2000 Reagent® (ThermoFisher Scientific, Cat. 11668-019) transfection and immunostaining has been established to characterize the subcellular localization of ClC-3 and ClC-5. Cell were prepared as previously described, plated on coated 4-well plates, and transfected with Lipofectamine2000 Reagent® the same day (3 - 5 h after preparation). After 45 min of pre-incubation with Opti-MEM medium at 37 °C, 100 μl of Lipofectamine2000 Reagent® and plasmid DNA mixture was added to each 4x well. Cells were then incubated at 37°C for 2 days before Lipofectamine-plasmid DNA mixture was replaced with fresh enriched DMEM growth medium. After 3 - 4 DIV, either cells were prepared for immunostaining, as described below, or used for imaging.

2.2.6 Chromaffin cells Viral infection

WT chromaffin cells were transfected using shRNA to reduce the expression of ClC-5 and generate the ClC-5 knock-down condition or the double KOs one, when *Clcn3*$^{-/-}$ cells were used. shRNA was delivered into the cells 3-5 h after preparation using the Lentiviral Expression System (ViraPower, ThermoFisher Scientific)[145]. Next day the growth medium was replaced with fresh enriched DMEM and cells were used for experiments after 4 DIV.

2.2.7 Chromaffin cells Immunocytochemistry

3-4 DIV after transfection, cells were washed twice with PBS1x, then incubated with 4% PFA at RT for 10 min. The cells were then extensively washed with 50 mm of Glycine, prepared in PBS1x, for 3 times to quench unbound PFA, thus permeabilized with Triton X-100 0.2%, prepared in PBS1x, for 10 min. Afterwards, the cells were incubated with blocking solution (5% goat serum in PBS1x) for 45 min. The primary antibody was prepared at the desired concentration (α Synaptobrevin II mouse and α GFP rabbit diluted 1:500 in blocking sol., Synaptic System 104211 and Abcam ab290, respectively) and then dropwise added to each cover-slip. The cells were then incubated for 2 h at 4°C. After extensive washing steps, at least 3 times with PBS1x (15 min incubation each), the cells were incubated with the secondary antibody (AlexaFluor®488 and AlexaFluor®647 diluted 1:1500 in blocking solution, Invitrogen F(ab')2 A-21237 and A-11008 respectively) for 1 h at 4°C, protected from light sources. Cells were afterwards washed with PBS1x for 4 times (20 min incubation each) and then mounted on microscope glass slides, using Fluoromount Aqueous Mounting medium (Aqua Polymount, Cat. 18606, Polysciences), or incubated overnight at 4°C in PBS1x and imaged the day after. Positive and negative controls were performed to check the specificity of the immunostaining procedure.

2.2.8 Membrane Capacitance Measurement

In 1982, Neher and Marty introduced a new method which permitted to monitor the cell membrane capacitance and therefore measure exocytosis (and endocytosis as well). Whenever exocytosis occurs, that means, every time a vesicle fuses to the plasma membrane, a temporary increase in the cell surface occurs, which can be monitored in real time. Since the cell surface is directly proportional to the membrane capacitance (C_m) (and roughly estimated as $1\mu F/cm^2$) by K.S. Cole in 1968[146]) by measuring changes in the C_m it is possible to monitor the exocytotic process. In particular, the whole-cell patch clamp configuration permits to monitor this process in the whole cell and to achieve a resolution of roughly 40 aF, corresponding to the fusion of a single vesicle with a diameter of 40 nm. In brief, the glass pipette with a resistance or 3.5 - 5.5 MΩ is tightly attached to the cell membrane to generate a constricted electric giga-seal (Giga-Ohm range). This significantly decreases the noise of the recording and allows the so-called cell-attached configuration. When the membrane underneath the pipette is broken, this creates an electrical access to the cell and permits to exchange the intracellular environment with

a known ion concentration (”whole-cell configuration”). In addition, the low access resistance (1 - 12 MΩ) permits to control the cell membrane voltage very precisely. So far several techniques have been established to measure membrane capacitance. Here we focus on the high-resolution measurement of capacitance changes applying a sine-wave stimulus superimposed on an holding potential and employing a lock-in amplifier to analyze the resulting sinusoidal current. In our protocol, we make use of a sinusoidal voltage stimulus with an amplitude of 35 mV, from peak to peak, and a sine-wave frequency of 1 kHz. The resulting current signal I_t can be separated into phase and amplitude, then resolved using a phase-sensitive amplifier set in lock-in configuration[147]. The use of a single sine wave gives only two pieces of information (the amplitude and the phase) whereas the RC circuit in the whole-cell configuration consists of three unknown parameters (C_m, G_m and G_s, **Fig. 2.3**). To overcome this issue, we make use of the ”sine + DC” method, developed by Lindau and Neher in 1988[148], where the DC current provides the third piece of information, together with the two components of the admittance. To calculate the DC current, is necessary to know the reversal potential (E_{rev}) of the G_m. Alternatively, the lock-in amplifier can be used to estimate relative changes in these three parameters (C_m, G_m and G_s) (piece-wise-linear technique[147]). The ”sine wave + DC” method offers several advantages over the above-mentioned technique, because it permits to calculate the actual values of the three parameters.

The basic idea is that the cell acts as a capacitor, since the thin cell membrane (around 5 nm thick with a dielectric constant of 2-3) is made of a phospholipidic bilayer which acts as insulator, while both the intracellular and extracellular spaces are composed of salts in solution and are therefore good conductors. The series conductor-insulator-conductor defines a capacitor. If we now apply an electrical potential (voltage $\boldsymbol{V}$) across the cell membrane, we can separate a charge ($\boldsymbol{Q}$) and, since by definition the membrane has a capacitance $\boldsymbol{C = Q/V}$, the C_m can be roughly estimated as $1\mu F/cm^2$, value probably for the first time estimated by Hodgkin, Huxley and Katz in 1952[149] [150]. When the cell has approximately a spherical shape, as in the case of chromaffin cells, it can be considered as a simple RC (resistor-capacitor) circuit, where a capacitor and a resistor are connected in parallel. When a voltage is applied to the circuit, the resulting current can be described as a sum of the two components: resistive current I_r and capacitive current I_c.
The capacitance of the membrane can be estimated from the phase shift of the resultant sinusoidal current. The time course is defined by the following equation:

$$I_t = (I_c - I_r)e^{(-t/\tau)} + I_r \tag{2.3}$$

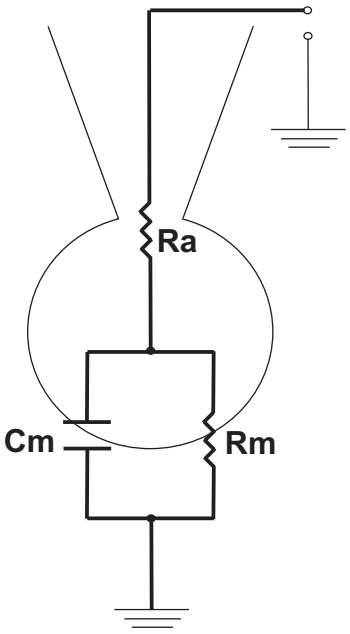

FIGURE 2.3: **RC circuit in the "whole-cell" patch clamp configuration.** A glass pipette is tightly connected to the cell membrane with an access resistance (R_a, synonymous with series resistance R_s) of ∼1 MOhm. A resistor (R_m∼1 GOhm, which is the inverse of the membrane conductance G_m) is coupled in parallel to a (C_m) capacitor, known as RC circuit. Voltage is typically clamped at -70 mV.

where τ describes the time constant of the decay of I_c and t is the time occuring after the volatge stimulus. The equation can be fitted to get approximated values R_s, R_m and C_m showed in **Fig. 2.3**:

$$R_s = \frac{\Delta V}{I_c} \tag{2.4}$$

$$R_m = \frac{\Delta V - R_s I_r}{I_r} \tag{2.5}$$

$$C_m = \Delta(\frac{1}{R_s} + \frac{1}{R_m}) \tag{2.6}$$

This method however presents some disadvantages, that is the lack of a precise way to calculate I_c due to the filtering of the current and the voltage signal, together with the current peak amplitude estimation which cannot be fully compensated by the pipette capacitance. In addition, the temporal resolution of the C_m recording is limited by the time interval between the voltage steps, which can lead to membrane recharging. To overcome

this issue, the use of a sine wave stimulus (sinusoidal excitation) has been extensively used to achieve a high temporal resolution. When applying a sine wave voltage, an ideal resistor does not introduce any phase shift to the measured sinusoidal current. However, a capacitor induces a 90° shift to the measured current and therefore the measured phase needs to be corrected by 90° [151]. In the whole-cell configuration, a sine wave frequency of 1 kHz is used and would result in low noise recordings, (usually a range of 500-3000 Hz gives the lowest noise level). Eq 2.3 can be written as:

$$I_t = I_r + I_c \tag{2.7}$$

where I_r represents the ionic current deriving from the ion flux through the ion channels located on the plasma membrane, while I_c results from the amount of charge separated by the membrane. The sine wave voltage stimulus is applied to measure the C_m and, in a circuit consisting of an AC source and a resistor, is given by:

$$V = V_0 \cdot cos(\omega t) \tag{2.8}$$

where ω represents the angular frequency of the sine voltage. The sine wave voltage results in a sinusoidal current which can be described by Ohm's law, when it is applied to an ideal resistor (R):

$$IR_t = \frac{V_t}{R} = (\frac{V_0}{R})cos(\omega t) \tag{2.9}$$

Therefore, the sine wave amplitude of the resulting current is inversely proportional to the applied voltage. In the case of a linear circuit, the resulting sinusoidal current has the same frequency as the voltage and, in the case of a resistor, the current and the voltage are in phase and R describes the ratio of peak voltage to current. However, there is a 90° phase shift between the current and the voltage and the final I_r can be written as:

$$I_t = \frac{V_0 sin(\omega t)}{R_m} + C_m V_0 \omega cos(\omega t) \tag{2.10}$$

where R_m is used for the membrane resistance and C_m for the membrane capacitance.

2.2.8.1 Lindau-Neher Technique or "sine + DC" method

In order to determine R_m and C_m, Lindau and Neher established a technique to calculate those unknown parameters from eq 2.10. In case of a circuit with R_m and C_m in parallel, the total admittance can be written as:

$$|Y| = Y_{C_M} + Y_{R_M} = j(\omega)C_M + \frac{1}{R_M} \tag{2.11}$$

The measured sinusoidal current I_t is analyzed and distinguished into two sinusoidal components by using a lock-in amplifier. One component is in phase with the voltage stimulus (real component or output Y_1) and one is 90° shifted with respect to the voltage (imaginary component or Y_2). These two components, divided by the stimulus voltage amplitude, give the real (A, corresponding to Y_1) and imaginary (B, corresponding to Y_2) absolute values of the complex admittance (Y), or in other words:

$$Y(\omega) = A + jB \tag{2.12}$$

Y is the admittance, measured in Siemens, and it is a complex value composed of A which is the conductance and B which is the susceptance, where j signifies a phase of 90°, and $\omega = 2\pi f$ where f is the frequency of the sinusoidal stimulus.

In particular,

$$A = \frac{1 + \omega^2 R_m R_p C_m^2}{R_t(1 + \omega^2 R_p^2 C_m^2)} \tag{2.13}$$

and

$$B = \frac{\omega R_m^2 C_m}{R_t^2(1 + \omega^2 R_p^2 C_m^2)} \tag{2.14}$$

C_m is measured in the whole-cell configuration, which can be described as an RC circuit, as reported in **Fig. 2.3**. The electrical admittance (Y) is a parameter used to measure how easily the current can flow through the circuit and it is calculated using a lock-in amplifier as described by Lindau and Neher in 1998. In brief, Y is measured at 1 kHz frequency by superimposing a sinusoidal voltage (**Fig. 2.4**) on the holding potential.

The resulting sinusoidal current is analyzed at two mutual orthogonal phase angles using a 2 phase-sensitive detector.

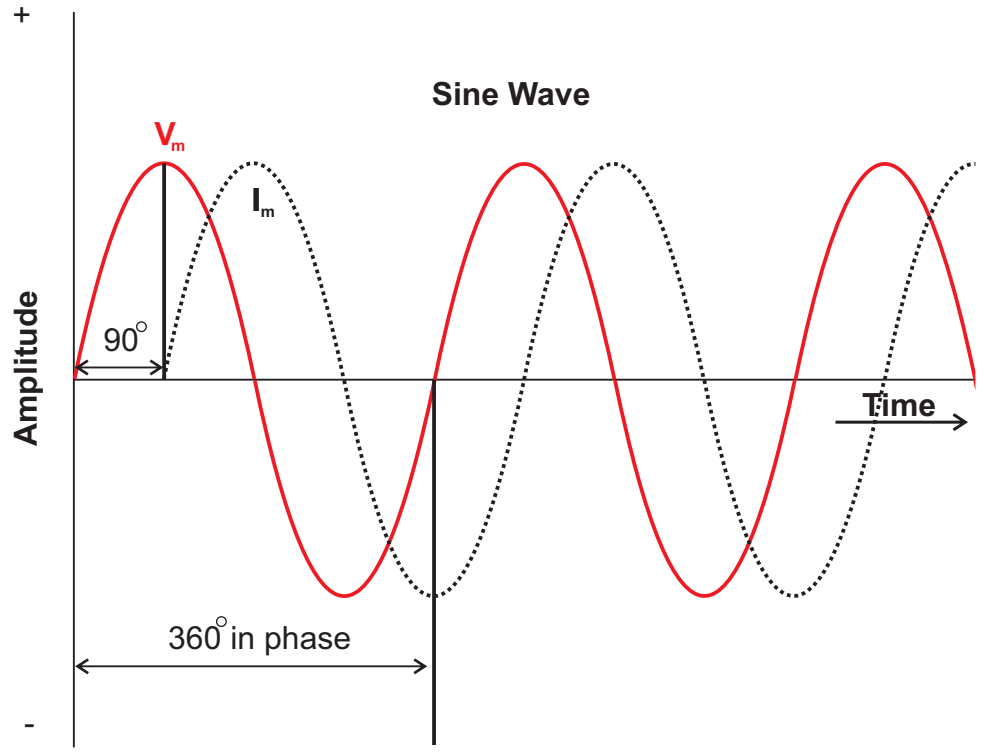

FIGURE 2.4: **Sinusoidal stimulus.** Sine wave voltage stimulus is represented in phase with the current.

2.2.8.2 Exocytotic Stimulation by applying a train of depolarizations

In the protocol (**Fig. 2.5**) we are using when we apply a depolarizing stimulus, the applied voltage is a sine wave stimulus which is superimposed on an DC - holding potential of - 70 mV (which lasts 300 ms), with a frequency of 1 kHz and 35 mV amplitude, and it is repeated several times. Each sinusoidal stimulus is interrupted by a depolarizing step which goes to + 10 mV for 100 ms and which allows the opening of the voltage-gated calcium channels. Each cycle, composed of a 300 ms step where we apply the sine-wave stimulus and 3 constant steps (first step of 10 ms at - 70 mV, second step + 10 mV for 100 ms and third step to - 70 mV for 10 ms), is repeated for 19 times to get a final measurement of approximately 8 sec. A patch pipette (borosilicate glass, Harvard Apparatus, UK) of 3 - 5 MΩ resistance and an ECP - 10 amplifier (HEKA Electronik, Lambrecht, Germany) are used to perform whole-cell patch clamp recordings. Current signals are digitized at 25 kHz and R_s, R_m and C_m are acquired with the use of a lock-in amplifier and the "Pulse"

Software package (HEKA), which is utilized to control the sine-wave stimulus and the data acquisition.

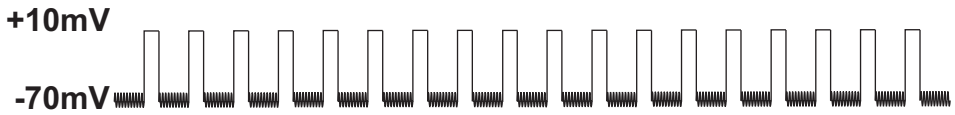

FIGURE 2.5: **Depolarization Protocol.** A train of depolarizing steps is applied to measure the cell membrane capacitance.

2.3 Amperometry Recordings

Fusion of individual vesicles can be electrochemically detected by placing a carbon fiber electrode in close proximity to the cell membrane, applying gently pressure and a positive voltage (+ 800 mV). The applied voltage should exceed the redox potential of the substance to detect, in order to oxidize it. Such chemical reaction transfers electrons to the electrode, permitting to monitor exocytosis of single vesicles in real time.

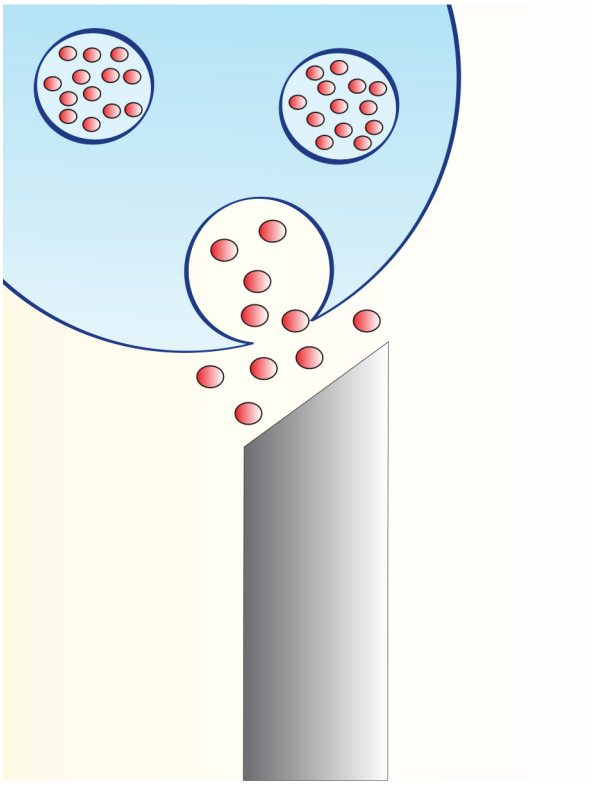

FIGURE 2.6: **Electrochemical detection.**
Catecholamines, such as (Nor)Epinephrine, are detected via a carbon-fiber microelectrode.

An elegant combination of amperometry with capacitance recordings offers the advantage of monitoring exocytosis as increase in the C_m (roughly estimated to be 1 fF per single granule[152]), and the relative amount of released catecholamines (**Fig. 2.6**). The concentration of oxidized catecholamines, released as single "quanta", can be calculated as following, since the integral of the current over time represents the spike charge:

$$Q = \int Idt = Men \tag{2.15}$$

Where M is the number of molecules and e is the elementary charge of an electron ($1.6x10^{19}$ Coulomb) and n is number of moles of electrons transferred per mole of catecholamine, which by convention is considered to be 2. It appears therefore convenient to calculate the number of released molecules (N), which depends on the electric charge (Q) as:

$$N = \frac{Q}{nF} \tag{2.16}$$

Where F is the Faraday's constant and n is the nr of e^- donated by each mole of catecholamine:

$$N = Q[pC]x10^{-12}[\frac{C}{pC}]x\frac{6.023x10^{23}\frac{electrons}{mole}}{2x\frac{electrons}{molecule}x96,485\frac{C}{mole}} = Q[pC]x3.121x10^{6}\frac{molecule}{pC} \tag{2.17}$$

The carbon fiber electrode, with a diameter of 5 μm, can cover approximately 300 μm^2 of the cell surface[153] and for distances $\lesssim 3$ μm the electrode can oxidize and detect more than 90% of the released transmitters, as calculated by Schroeder and colleagues[154]. The vesicle fusion occurs in the whole cell and has an uniform distribution over the whole cell surface. The molecules will be released and diffuse in the extracellular space with a diffusional coefficient of 5.4 X $10^{-6}cm^2\ cm^{-1}$ [155]. Bruns and colleagues[153] calculated the transmitters collection efficiency since the proximity of the electrode can be variable and the fiber tip might be irregular. The issue comes along with the fact that some events, occurring far from the electrode, might still be detectable outside of the detecting area and the diffusional space would therefore affect the spike parameters. Monte-Carlo simulations were performed assuming the electrode-distance would be below 300 nm, on average. Once released, the molecules can diffuse with a coefficient of 5.4 X $10^{-6}cm^2$

cm^{-1} and are assumed to be absorbed at the disk-like tip of the electrode (diameter 5 μm). Different event types, characterized by different peak amplitudes and kinetic properties are compared and finally amplitude and charge are scaled to the volume of the vesicle. Under these conditions, they concluded that LDCV (large dense core vesicles) events can be detected at distances up to 1 μm from the center of the carbon fiber, while for SLMVs (synaptic-like microvesicles) the threshold is less than 250 nm and are therefore more commonly affected by diffusional distortion. In order to reduce the loss of detectable molecules the due to the diffusional space, it is fundamental to place the electrode in thigh contact with the cell surface and consider for analysis only those spikes (events) which show fast kinetics (half width < 2 ms, rise time < 700 μs) because they were most likely released from sites close to the electrode.

2.3.1 Carbon fiber electrode fabrication

The electrodes are prepared following a protocol first described by Schulte and Chow[156], using anodic electrophoretic deposition of paint, modified by D. Bruns[125] and subsequently adapted in our lab. In brief, the following steps are necessary to prepare a good quality carbon fiber microelectrode:

- Removal of the fiber sizing,
- Establish electrical connection between the fiber and the wire,
- Thread the carbon fiber into a capillary tube,
- Pull the pipette-fiber,
- Make epoxy-glass seal,
- Bake the electrodes at 192.5 °C for 2.5h,
- Coat the fiber tip with Sylgard®.

1. **Removal of the fiber sizing**.

Preliminary, the bundle of carbon fibers (5 μm diameter, Amoco, Greenville, SC, USA) is boiled in 100 ml of boiling Acetone for 30 min or longer, in order to remove the sizing. The fibers are then remove and transfer to a beaker containing 50 - 100 ml of fresh acetone. Finally the fibers are let air-dry overnight on an open 10 cm Petri dish. Next day the fibers can be more easily separated and ready for manipulation. The fibers are cut to lengths of about 5 cm using a surgical blade and are placed onto a clean glass plate to

be separated. In this step is crucial to maneuver the fibers as less as possible, with the help of fine forceps (Dumont Nr. 5, FineScience) under a dissecting microscope in bright illumination.

2. **Establish electrical connection between the fiber and the wire**.

A single strand of carbon fiber is positioned so that one end of the fiber protrudes beyond the edge of the plate by about 0.5 cm and is therefore free to be electrically connected to a copper wire (length 15 cm, diameter 0.4 mm), using a small drop of conductive carbon paste (kindly provided by Prof. Dr. D. Bruns). The carbon paste has to be kept fluid by adding an appropriate volume of N-t-butil Acetate.

3. **Thread the carbon fiber into a capillary tube**.

After several fibers are prepared in this was, they are let air-dried completely for 10min and subsequently cannulated into a glass capillary tube (GC150-10, Harvard Apparatus, USA) and the free end of the wire is then glued to the tube by adding a drop of two-component epoxy glue.

4. **Pull the pipette-fiber**.

When the glue is finally dry, the glass capillary which contains the copper wire connected to the carbon fiber, is then pulled using a micro-pipette puller (Sutter Instrument, CA, USA) after adjusting an appropriate pulling program.

5. **Make epoxy-glass seal**.

After the pulling step, the carbon fiber is appropriately cut with clean scissors in such a way that the tip of the fiber protrudes out of the capillary by a few millimeters. The protruding tip is then insulated by electro-deposition of paint. The electro-deposition paint (EDP) solution is previously diluted with dd H_2O 1:3 and throughly mixed by pipetting up and down. An U-shaped platinum foil is filled with EDP solution and is used as cathode. Anodic paint (Electrocoating ZQ84-3225, BASF, Muenster, Germany) is composed of negatively charged polymers which precipitate when applying a constant voltage (6 V) to the cathode to induce acidic conditions in the electrochemical cell, formed by the cathode (platinum foil) and the anode (tip of the carbon fiber). Here, water hydrolysis occurs and leads to protons production and formation of a precipitate on the fiber.

6. **Bake the electrodes at 192.5°C for 2.5 h**.

This electrically insulating layer now fully covers the surface of the carbon fiber and has to be cured at high temperature (192.5 °C) in an initially cold oven whose initial temperature should not be greater than 30°C. The protocol has been adjusted to reach a uniform and

homogeneous thickness of the insulating layer (approx. 0.5 - 1 μm), by applying 6 V for 10 sec.

7. **Coat the fiber tip with Sylgard®.**

To ensure a perfect seal between the glass tip and the carbon fiber, in order to perform low-noise experiments, a drop of Sylgard® is applied at the junction tip and let air-dried for 24 h or alternatively baked at 65 °C for 30 minutes.

Before each experiment, is critical to cut the fiber tip with a clean surgical blade to expose the active surface of the carbon fiber which should show a clean, perpendicular and straight cut not to damage the cell or partially expose a reduced active area of the fiber.

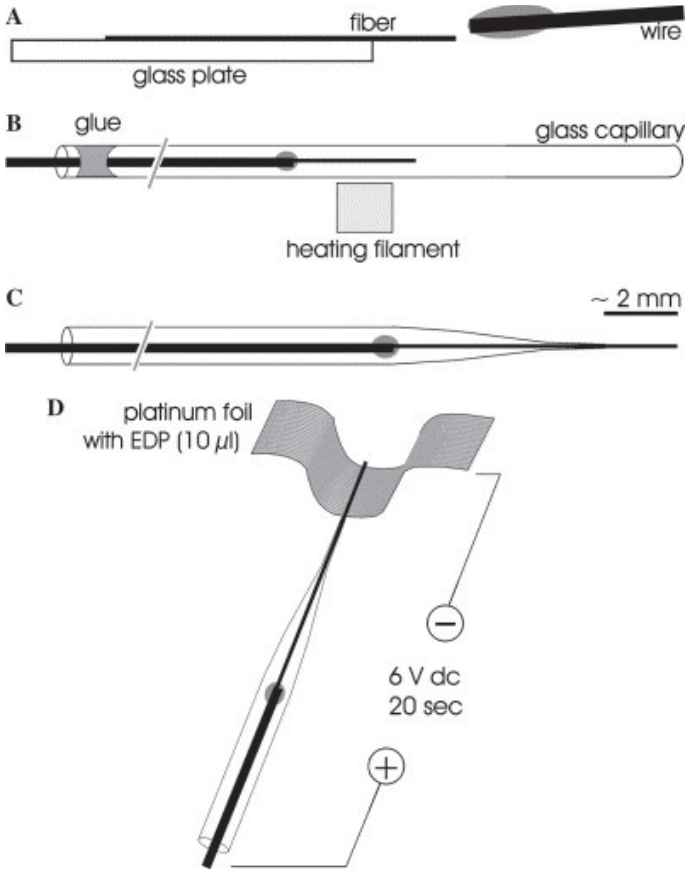

FIGURE 2.7: **Carbon Fiber Electrode Fabrication.** The different steps illustrate how to produce amperometric carbon fiber electrodes. The image is taken from Bruns et al.[125]

2.4 Analysis of single-exocytotic events

IgorPro 7.01 Software (Wavematrics) was used to evaluate the five different parameters which characterize the fusion process. Each amperometric spike was analyzed (**Fig. 2.8**) using the full-automatic analysis of amperometric recordings provided by a Macro installed in IgorPro, as described below.

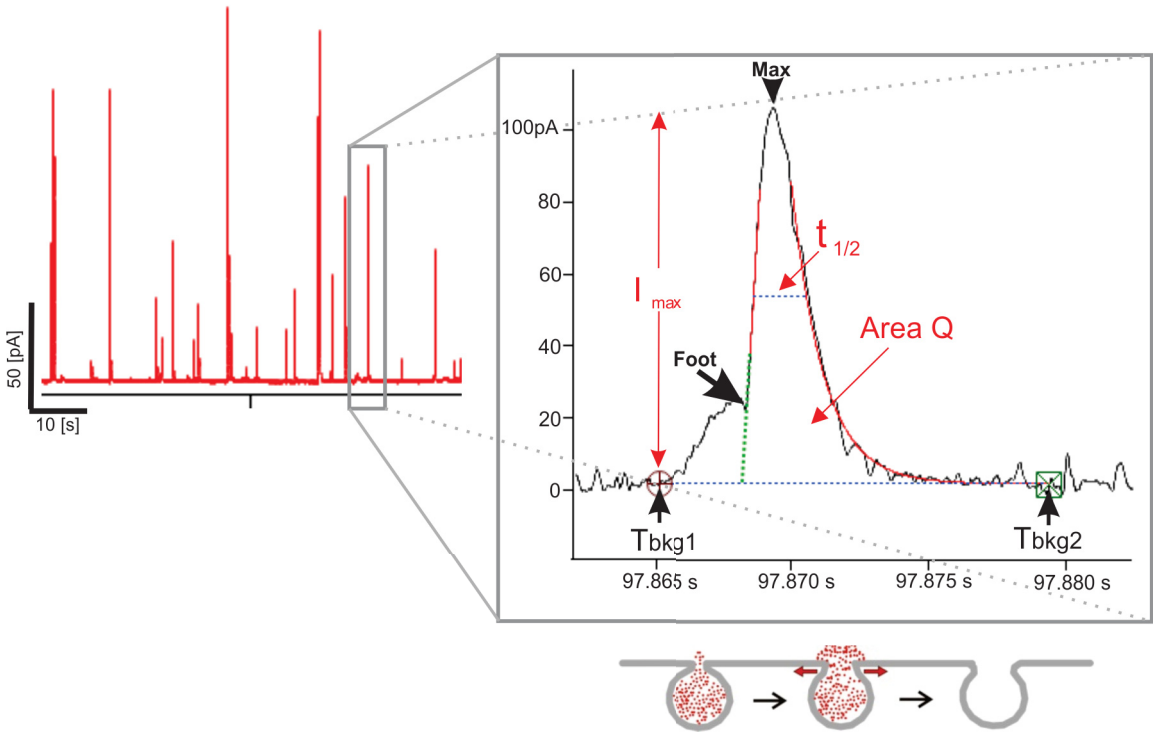

FIGURE 2.8: **Representative amperometric recording.** A zoom in highlights a single spike and the parameters (I_{max} or ampltiude, Q or charge, as well as kinetic properties, such as $Rise_{time}$, $t_{1/2}$ and $Decay_{time}$) considered for spike analysis.

The software and the macro used for this purpose permit digital filtering, noise analysis, spike identification and kinetic evaluation. Therefore, it is of clear importance the criteria settings for the data analysis. An Igor-based macro ("Prepare for Quanta Analysis") used for quanta analysis was developed in Sulzer lab and freely available online (sulzerlab.org/download.html). During data acquisition, amperometric traces are digitally filtered with a low-pass Bessel filter set at 2 kHz to reduce high-frequency noise. The measurements are then sampled at 25 kHz frequency. From each amperometric recording, the median value is calculated for each parameter ($Rise_{time}$, $Decay_{time}$, $T_{1/2}$, Q) apart for the I_{Max} in which case the mean value is considered. Finally, the average of the mean (or median) values is considered for statistical analysis.

2.4.1 Spike detection

The spike detection threshold is set at 7 pA, and a spike is identified when either the current (I) or its time derivative (dI/dt) exceeds a defined threshold. The threshold is usually a multiple of the standard deviation of the noise (SD_I) or its derivative ($SD_{dI/dt}$). The program (Macro "Prepare for Quanta Analysis) will then search for the local maximum which exceed the threshold; once the maximum for each spike has been localized, then single spikes can be analyzed in terms of half width, rise and decay time, amplitude (I_{max}) and charge (Q). Since the noise level affects the number of detected spikes, the setup has also been properly grounded.

2.4.2 Spike Selection

Spikes with half width < 2ms and rise time < half width are considered for analysis. Measurements with at least 20 spikes are considered for statistical analysis. Because spike distribution may contain different populations of vesicles, the median value is calculated for each spike parameter. It is crucial an appropriate selection for the spike beginning and end, since this affects all the other spike parameters. The spike beginning and end are determined using a protocol originally designed in the Wightman laboratory[157], that means using (SD_I) threshold.

2.4.3 Spike Parameters

In addition to quantitative information (*e.g.* the amount of released catecholamines), spike analysis provides information about the kinetics which characterize the fusion and release process (**Fig. 2.9**). The half width ($T_{1/2}$), which represent th spike duration and is the width of the peak measured at half of its maximum amplitude, is a kinetic indicator of the whole release process. The rise time (T_{rise}) reflects the rate of the pore expansion and the decay time (T_{decay}) indicates the rate of diffusion along with the closing of the fusion pore. The maximum current (I_{max}) provides information about the maximum flux of catecholamines and represents the maximum peak of the spike. After the baseline and the time at spike maximum (T_{max}) are determined, the other characteristics can be calculated via the first multipass algorithm described by Whitman and colleagues[157]. Several steps are considered during the data analysis of single amperometric events, as described by Mosharov et al[158].

1. in **Fig. 2.10 A**, T_{max} (time at spike maximum) is found between $T(dI/dt)_{max}$ and the time point which shows the same current value on the descending segment of the spike, as highlighted by the circles.

2. T_{bkg1} is located where the steady-state current precedes the spike (from $T(dI/dt)_{max}$ towards the beginning of the trace) and persist for a defined duration ΔT_{min}. The trace is divided into equal ΔT_{min} segments and the average current is compared between adjacent segments (**Fig. 2.10 B**). The steady state I_SS is found when two segments have a certain current within one SD_I of each other. T_{bkg1} is then set to the first time-point at the defined I_{SS} value.

3. Note that, when determining T_{bkg2} (spike end), high-frequency noise contribution increases and might therefore affect a proper assessment of the time point when it is close to background levels. Therefore, T_{bkg2} is determined starting from T_{max} of the current spike until $T(dI/dt)_{max}$ of the following spike. If unsuccessful, T_{bkg2} is set at the minimum of the current within ΔT_{bkg2}

4. Spike amplitude I_{max} (pA) is measured between the current at T_{max} and the baseline current under the spike maximum.

5. Spike half-width $t_{1/2}$ms is evaluated at 50% of I_{max}.

6. The amount Q (charge) of catecholamines released during each single exocytotic event is the area under the spike curve, above the baseline.

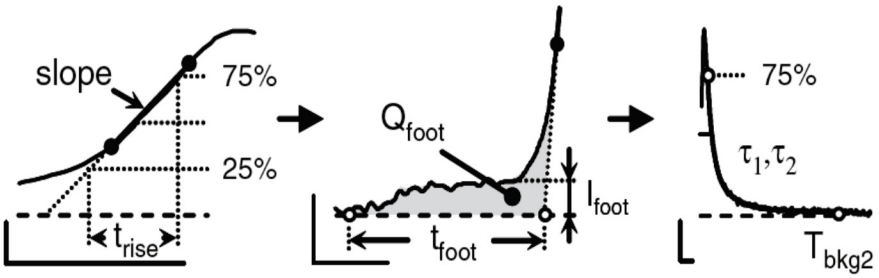

FIGURE 2.9: **Kinetic parameters of amperometric spikes.** Kinetic parameters, such as rise time, half width and decay time, are illustrated by Masharov et al[159].

The algorithm for finding T_{max} is shown in figure **2.10**. The upper panel shows the amperometric current and the lower panel its time derivative, in **Fig. 2.10 A**. In **Fig. 2.10 B** the program searches for the steady-state current that precedes the spike.

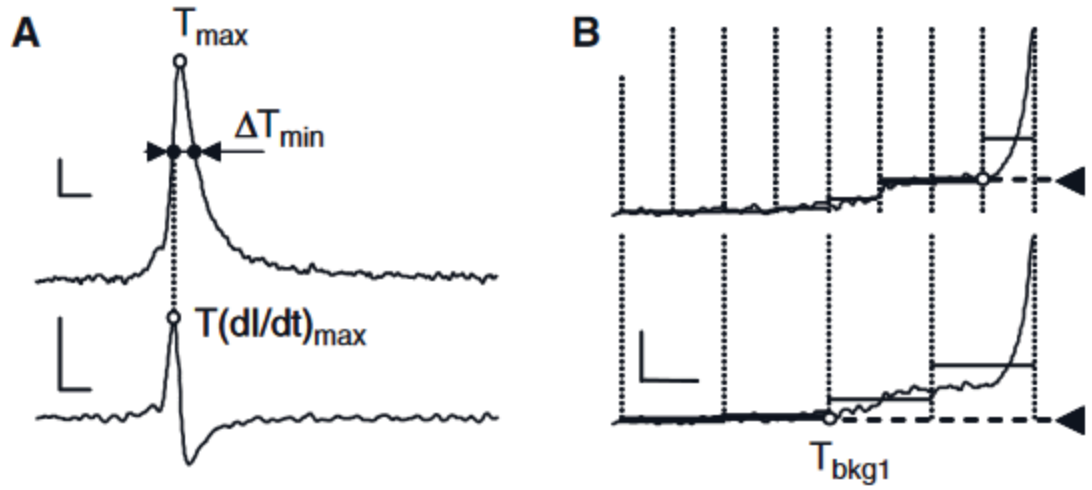

FIGURE 2.10: **Algorithms used for spike detection.** (**A**) Algorithm to find T_{max}. Upper panel represents amperometric current, while lower panel shows its time derivative. (**B**) Search for the steady-state current, preceding a spike. Image taken from Mosharov et al[159].

2.4.4 Spike kinetic properties

The rising phase, as well as the pre-spike signal, are derived from the linear fit of the current between two points on the ascending segment of the spike. The middle of the linear segment is at $T(dI/dt)_{max}$, while the two time-points are found at current at $T(dI/dt)_{max}$ +- 1/2 of ΔI between currents at T_{max} and $T(dI/dt)_{max}$. When the spikes have no foot signal, then these points are approximated at 25% and 75% of I_{max}. The B coefficient of the slope (or the linear regression tangent) represents the slope of the spike's rising phase (pA/ms). The spike beginning, excluding the foot, is found by extrapolating the linear fit onto the spike's baseline. Spike rise time t_{rise} is calculated on the extrapolated rising phase of the spike and represents the spike duration or the time necessary for a spike to reach a certain percentage of the I_{max}, *e.g.* from 25% to 75%. In detail, the lower point ($T_{25\%}$) is calculated at (T_x + 0.25)/slope, while the upper point ($T_{75\%}$) is found at (I_{max} x 0.75) current within the trace segment between T_{max} and T_X. Time to peak tP (ms) is the Δ time between T_{max} and T_X and it is equal to t_{rise} from 0 to 100% of I_{max}. The foot signal beginning coincides with T_{bkg1} and end at T_X. The foot duration t_{foot} represent the Δ between the two points. Q_{foot} is the area of the region which precedes the linear rising phase of tghe spike. Finally, I_{foot} can be calculated as average current within the t_{foot}. If analysis considers individual events that have foot signal with steady states, then the steady state is calculated within t_{foot}, using the same algorithm used to define T_{bkg1} and half of a minimal foot duration

is used as ΔT_{min}. The falling phase can be described by two time constants, τ_1 and τ_2, of the double-exponential fit of the current between 75% of I_{max} on the falling phase and T_{bkg2}[158].

2.4.5 "Foot" signal

The pre-spike signal, the so-called "foot" signal, can be detected via amperometry and represents the fusion pore formation. The initial flux of catecholamines through the narrow pore was for the first time described by Chow and colleagues[160]. The majority of catecholamines are stored and embedded into a polyelectrolytes matrix and are released only during complete fusion, while some "free" monoamines can be released during the pore formation[138]. Interestingly not all spikes show the presence of a foot signal and a correlation between the presence of the foot and the total amount of released catecholamines suggests that the foot is correlated to the vesicle size[138][161], where the vesicle matrix volume might influence physical and kinetic properties of the release process.

Chapter 3

Results

Granule exocytosis of large dense core vesicles (LDCVs) was studied by using a combination of capacitance measurements and amperometric detection, as previously described. Single chromaffin cells were dialyzed using a pipette solution containing 20 or 3 μM of free calcium. Increase of intracellular calcium is the major stimulus which leads to exocytosis, monitored as step-like increases in the cell membrane capacitance together with the amount of catecholamines (Nor- and Epinephrine) released by each single vesicle, characterized in terms of spike amplitude (I_{max}) and charge (Q). The fusion process can also be kinetically described as spike half width ($T_{1/2}$), rise ($Rise_{time}$) and decay time ($Decay_{time}$). In the second set of experiments, by applying a depolarizing voltage protocol via the patch clamp technique, it was possible to "mimic" the physiological response occurring after a depolarizing stimulus. Our goal was to elucidate the priming step and therefore distinguish among different populations of vesicles, reflecting different steps of the priming mechanism. Finally, amperometry and capacitance measurements allowed us to characterize the impact of ClC-3 and ClC-5 antiporters on exocytosis in chromaffin cells.

3.1 Amperometric detection of catecholamines in chromaffin cells

Amperometry allows the detection of catecholamines through the use of a carbon fiber electrode, which is gently placed in contact with the cell membrane. The electrode is held

at a positive potential (+ 800 mV) sufficient to oxidize the catecholamines released by single vesicles fusing to the plasma membrane.

3.1.1 Saturating Calcium concentration (20 μM) masks any possible effect on exocytosis in the *Clcn3*$^{-/-}$ mouse model

Before starting the recording, the cell is dialyzed for around 30 seconds with 20 μM of $[Ca^{2+}]_i$ to enable the fusion of secretory granules. In this manner, the priming process is exasperated by such spontaneous and saturating raise in intracellular calcium concentration and therefore permits to measure exocytosis. The aim of this set of experiments was to characterize the fusion process comparing WT and *Clcn3*$^{-/-}$ conditions. We compared the wild type (WT) response versus *Clcn3*$^{-/-}$ (KO) in early post-natal stages (P0 - P1 new born mice) as well as in late stages (P60 adult mice). Under this condition, we could not detect any significant impairment in exocytosis mediated by *Clcn3*$^{-/-}$ cells in any of the two different post-natal stages (P0 and P60, **Fig. 3.1** and **Fig. 3.4**, respectively).

When characterizing exocytosis, it is essential to monitor increase in the membrane capacitance simultaneously with the frequency of amperometric spikes (or the number of vesicles fusing during exocytosis), since the two values should be consistent with one another. Recordings with at least 30 events/cell were considered for analysis. Since the cell membrane capacitance (C_m) increase is directly proportional to the cell surface, it is also important to analyze cells with comparable initial size when comparing different conditions. For this purpose, the bar graph reports the averaged cell surface for each condition, which is approximately 4 pF, corresponding to a diameter of ca. 9 μm (since $C_m = 1\mu F/cm^2$) (**Fig. 3.1 D**). In **Fig. 3.1 C**, the number of exocytotic events (also referred to as spike frequency) shows a high correlation with the increase in the cell membrane capacitance (C_m). When comparing the WT and the *Clcn3*$^{-/-}$ condition, spike frequency and ΔC_m are not affected by the absence of ClC-3 (**Fig. 3.1 C**).

When single amperometric events are analyzed, amplitude and charge parameters reveal that the amount of released catecholamines during exocytosis is not reduced in *Clcn3*$^{-/-}$ cells. Indeed, amplitude and charge are correlated to each other and represent the vesicle cargo. The bar graphs (**Fig. 3.2 A, B**) report WT condition in black (n = 20) vs KO in red (n = 18). Values are given as means of the median value for spike amplitude and means of the mean values for the other parameters (charge and kinetic properties). Frequency distribution graphs (**Fig. 3.2 C, D**) depict cumulative events/bin and show that

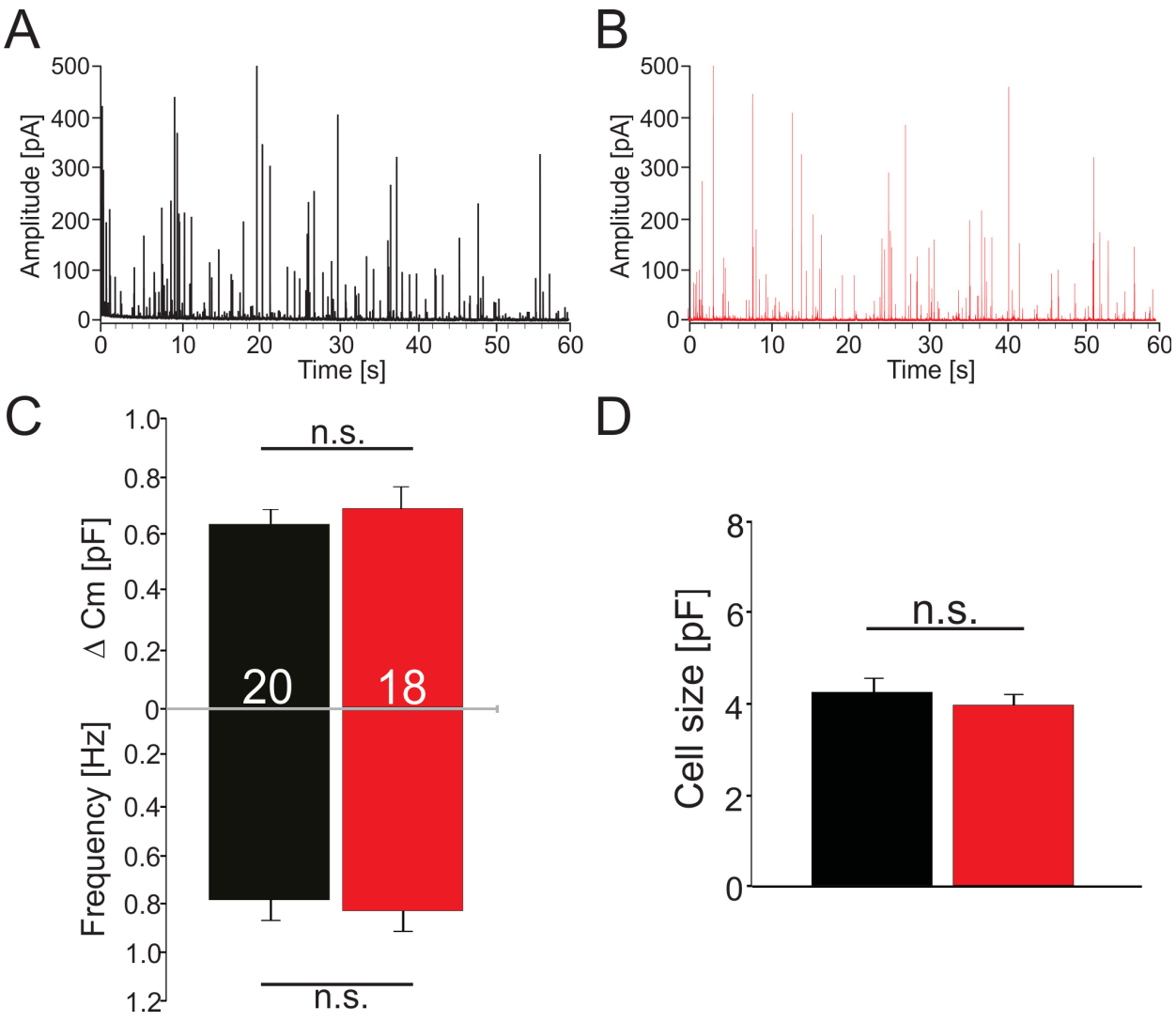

FIGURE 3.1: **Exocytosis is not impaired in WT vs KO condition at saturating calcium concentration (in P0 mice).** The representative recordings (WT in black and *Clcn3*$^{-/-}$ in red, Fig. **A** and **B** respectively) show no apparent significant difference, in terms of spike amplitude and frequency. Fig. **C** plots spike frequency versus Δ cell membrane capacitance. Fig. **D** shows the averaged initial cell size for both WT and KO cells. Error bars indicate means ± S.E.(standard error).

the majority of LDCV events share the same characteristics for a certain given parameter. In order to elucidate the fusion process occurring during exocytosis, spike kinetic properties are characterized in terms of rise time, half width and decay time (**Fig. 3.3**). In particular, rise time (**Fig. 3.3 A**) and decay time (**Fig. 3.3 C**) represent the velocity of the vesicle fusion, while half width (**Fig. 3.3 B**) reflects the event duration.

In the above graphs (**Fig. 3.3**), the frequency distribution of the three different kinetic parameters describes spike characteristics (**Fig. 3.3 D, E, F**). WT and *Clcn3*$^{-/-}$ do not differ in terms of vesicle fusion kinetics. This indicates that properties of release events are

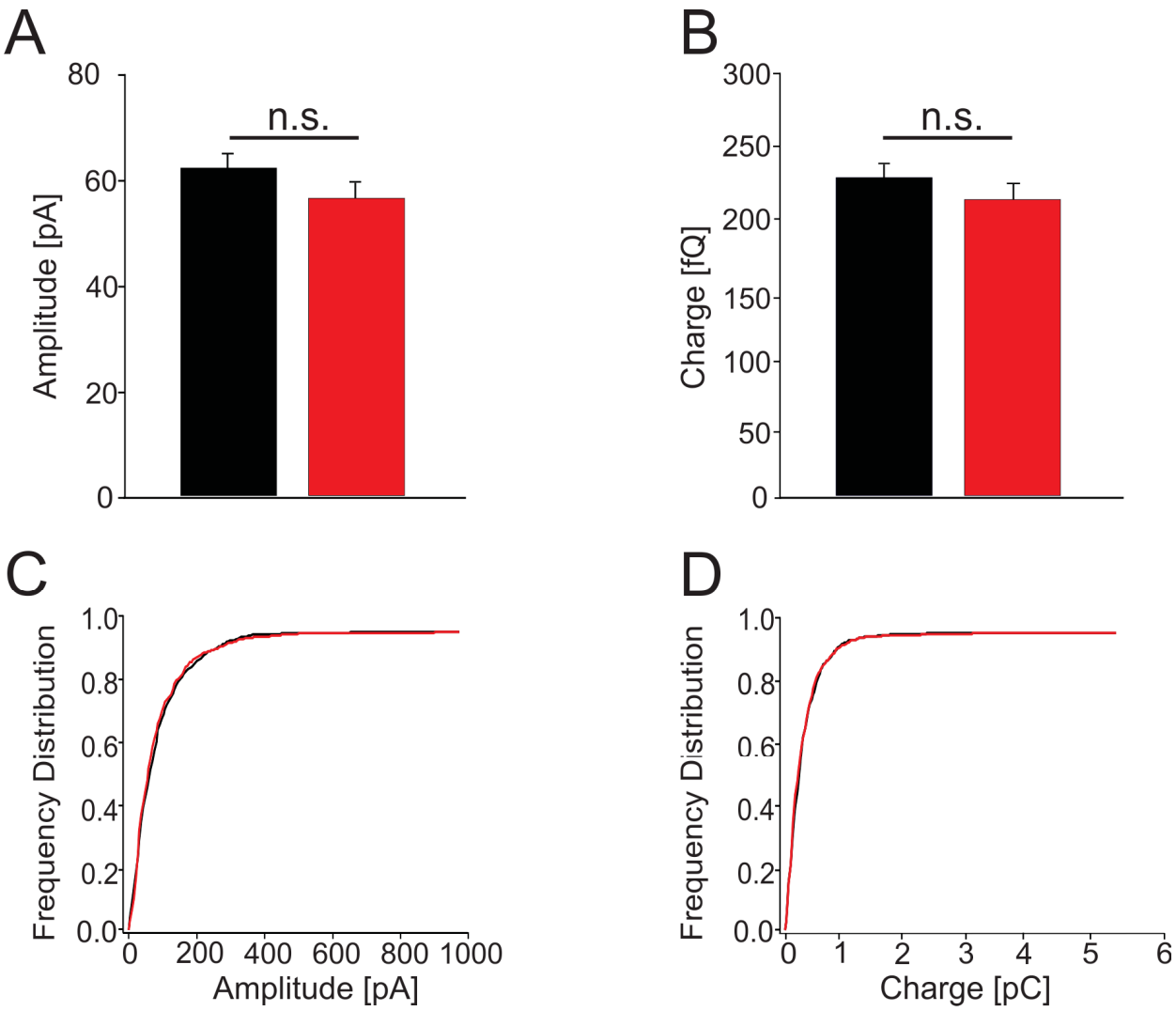

FIGURE 3.2: **Spike Amplitude and Charge and relative frequency distribution graphs (in P0 mice).** WT (black) and KO (red) response show no difference in terms of spike amplitude and relative charge, or released catecholamine amount.

not altered in the absence of ClC-3. The same experimental conditions were performed in different post-natal stages, *e.g.*, in adult mice (P60). As previously described, exocytosis is triggered by intracellular infusion of 20 μM of $[Ca^{2+}]_i$. Similarly, no significant effects were observed in *Clcn3*$^{-/-}$ chromaffin cells.

In conclusion, LDCV biogenesis as well as catecholamine loading are not regulated by ClC-3 in adrenal chromaffin cells of new-born mice (P0).

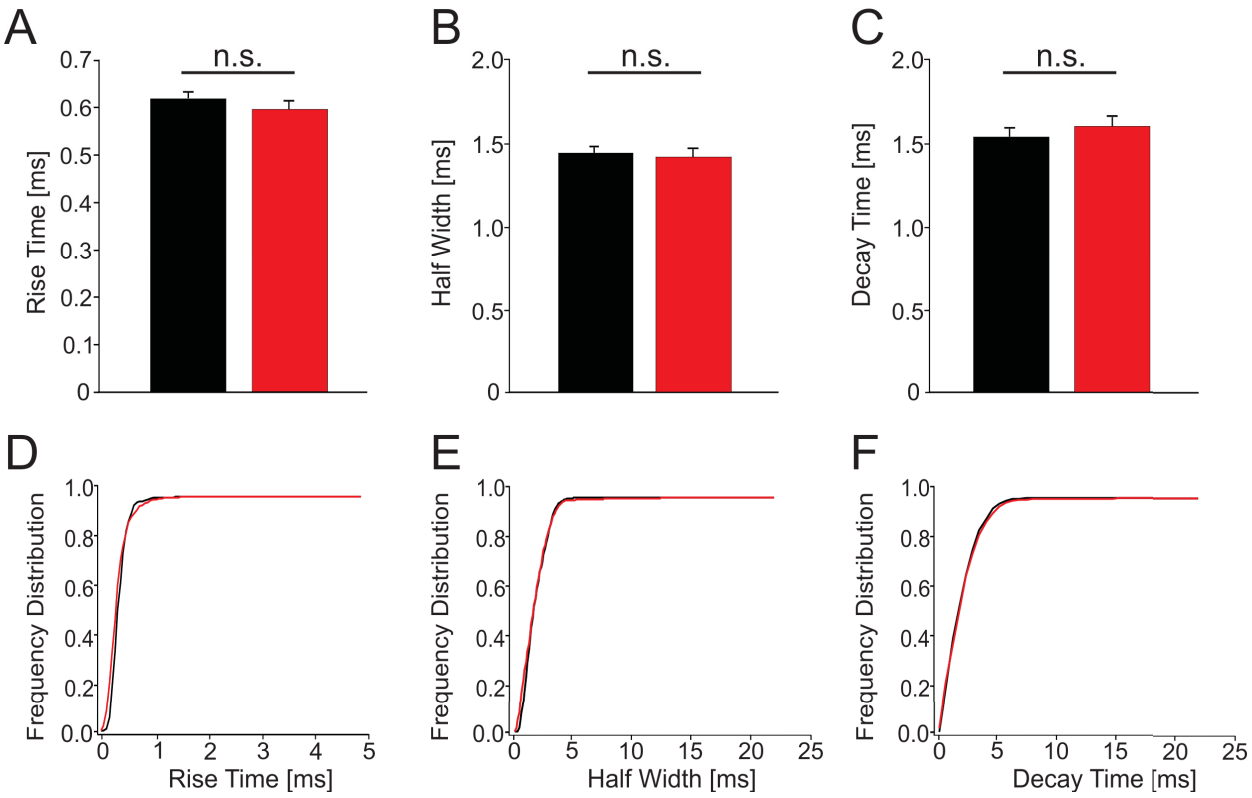

FIGURE 3.3: **Kinetic parameters and relative frequency distribution graphs (in P0 mice).** Kinetic properties which characterize the fusion process are not affected by the absence of ClC-3.

3.1.2 Exocytosis is not impaired in absence of ClC-3 in late post-natal stages at high calcium concentration (20μM)

The same experiments were performed in chromaffin cells culture derived from adult mice (P60). Indeed, it is known from previous studies[5] that adult mice lacking of ClC-3 showed an impaired exocytosis. In particular, spike frequency and C_m increase were both reduced in absence of ClC-3. As we did in previous experiments, we dialyzed adult chromaffin cells with saturating calcium concentration.

Correlation between rate of membrane capacitance increase and mean event frequency are showed in **Fig. 3.4 C**. Interestingly, increase of membrane capacitance as

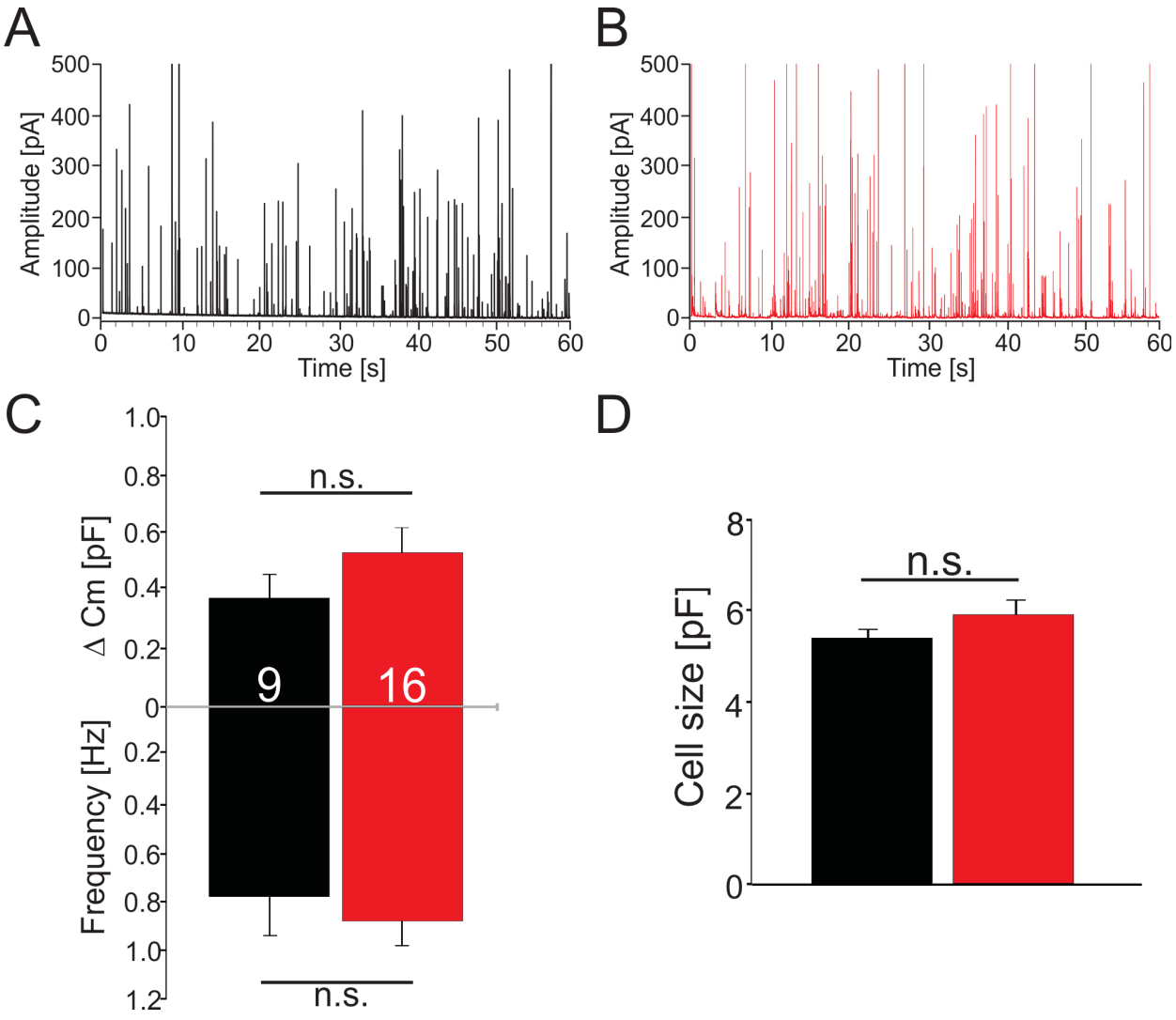

FIGURE 3.4: **Exocytosis is not impaired in WT vs KO condition at saturating Ca^{2+} concentration (in P60 mice).** The two representative recordings (WT in black and *Clcn3*$^{-/-}$ in red) show no apparent significant difference, considering spike amplitude and frequency (**A, B**). Amperometric spike events versus C_m increase are reported in **Fig. C**. Averaged cell size for both conditions is reported in **Fig. D**.

well as spike occurrence are not affected in adult *Clcn3*$^{-/-}$ chromaffin cells at saturating $[Ca^{2+}]_i$. The mean cell size is reported for both conditions in **Fig. 3.4 D** and is similar.

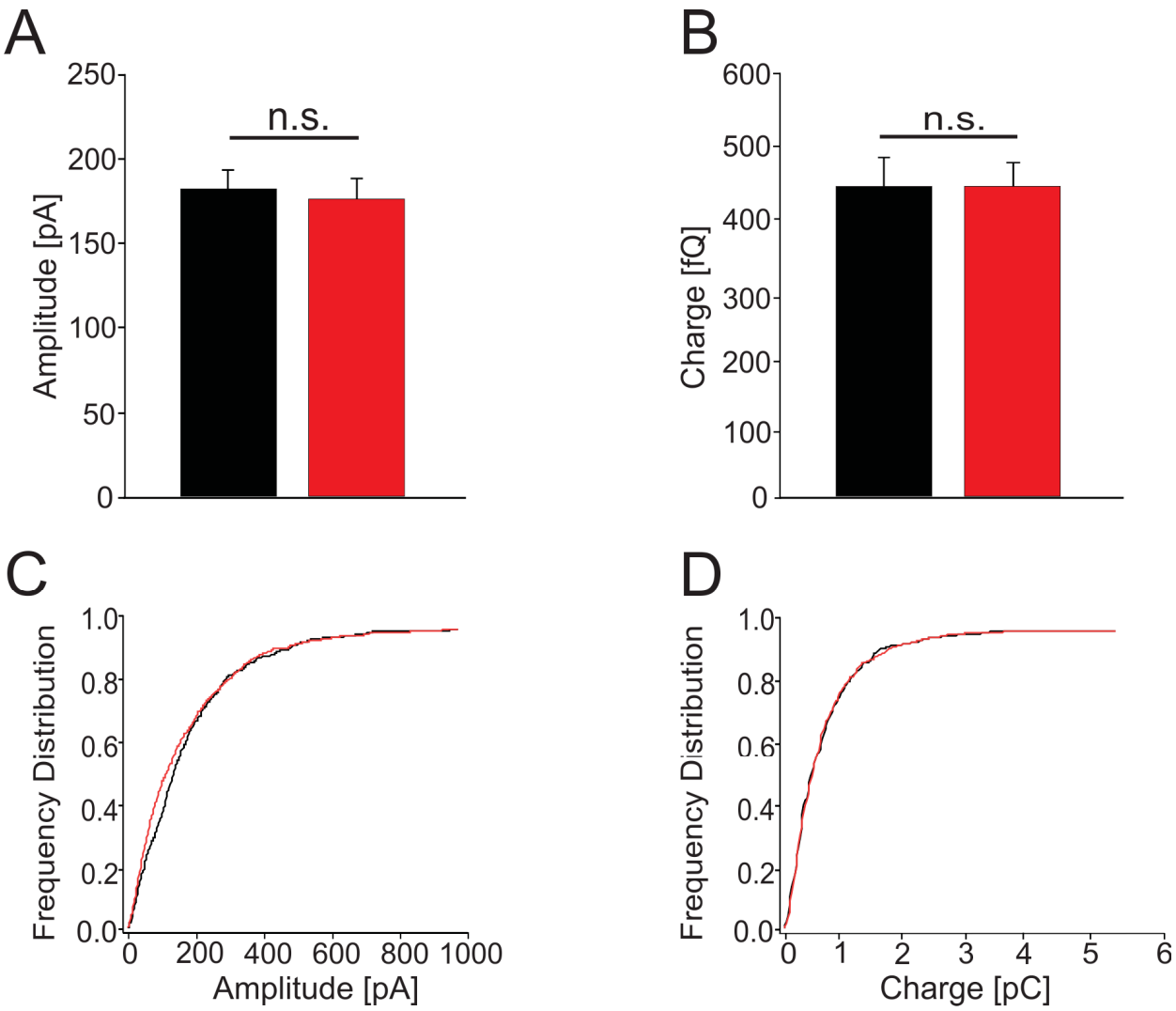

FIGURE 3.5: **Spikes Amplitude and Charge and relative frequency distribution (in P60 mice).** Amplitude and charge are reported in **Fig. A, B** for WT (in black) and KO (in red) cells and their relative cumulative frequency distribution is shown **Fig. C, D**.

Surprisingly, neither spike amplitude nor charge are reduced in *Clcn3*$^{-/-}$ cells (**Fig. 3.5 A, B**). Their relative cumulative frequency distribution graphs, reported in **Fig. 3.5 C, D**, confirm that large-dense core vesicle fusion events share the same characteristics. This result points out that catecholamine loading/uptake process is probably not regulated by ClC-3, as proposed by other works[5], which reported a reduced charge and amplitude measured in absence of ClC-3. It should also be mentioned, that Maritzen and colleagues performed amperometry by perfusing chromaffin cells with high-K^+-containing extracellular solution. This substantial different protocol in stimulating exocytosis might explain, at least partially, the discrepancy between our results and previously reported data[5].

In **Fig. 3.6 A, B, C**, kinetic parameters, which characterize LDCV fusion, are

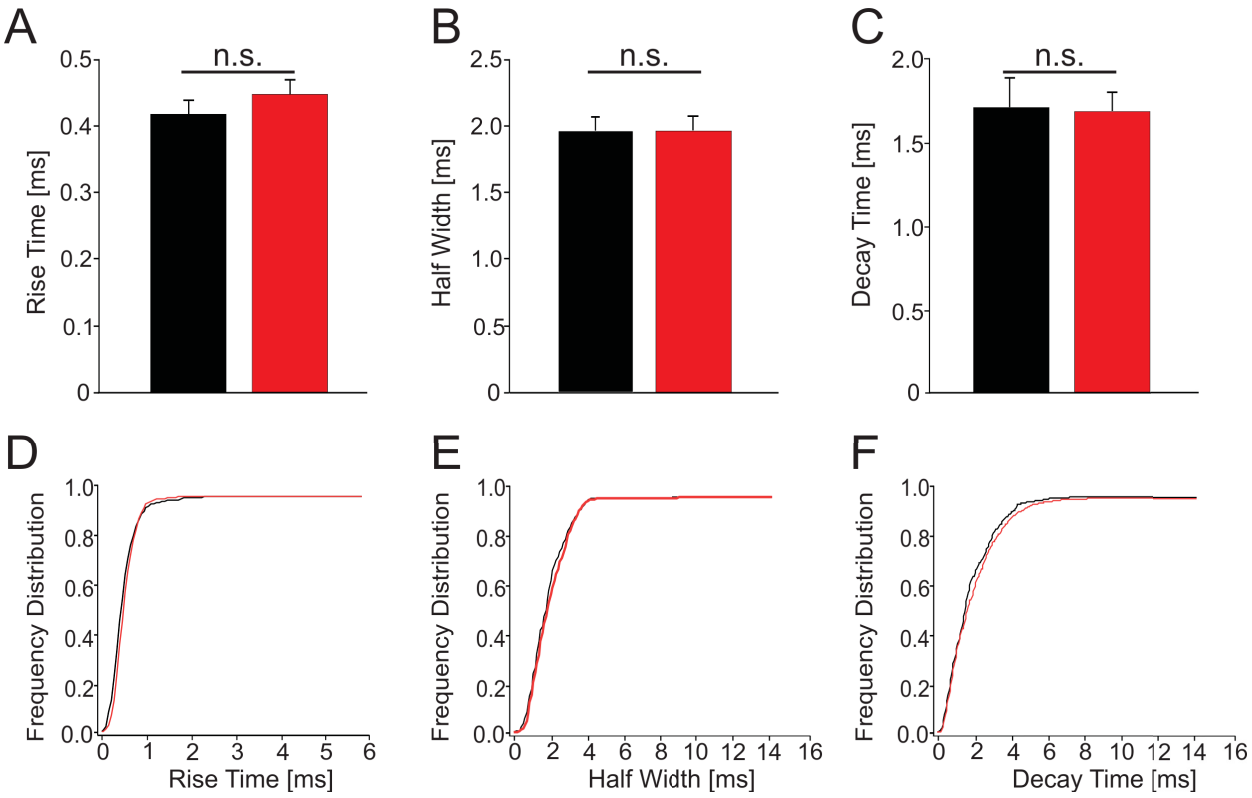

FIGURE 3.6: **Kinetic parameters and relative frequency distribution graphs (in P60 mice).** Kinetic properties are not affected in adult mice lacking of ClC-3.

unaltered in the *Clcn3*$^{-/-}$ mouse model. Coherently, frequency distribution graphs depicted in **Fig. 3.6 D, E, F** well represent the substantial similar LDCV event distribution in WT (black) and KO (red) condition.

In conclusion, we could not observe any effect in any of the measured parameters in *Clcn3*$^{-/-}$ condition. Astonishingly, the whole exocytosis appeared not be regulated by ClC-3. Since those results were very unexpected, we performed the same kind of experiments by dialyzing the cells with lower calcium concentration. Indeed, such saturating $[Ca^{2+}]_i$ might possibly mask any effect on exocytosis in *Clcn3*$^{-/-}$ cells.

3.2 ClC-5 but not ClC-3 undergoes an age-dependent regulation in adrenal glands

cDNA samples were obtained as previously described. In brief, adrenal glands were isolated from 5 WT P0 mice and 3 WT P60 mice for each cDNA samples, to obtain in total three different cDNA samples for each condition. The qRT-PCR experiments were then

run in triplicate, using specific primers to detect 18S and β-Actin (used as reference genes) and ClC-3 and ClC-5 (genes of interest).
The expression level of the two reference genes is unchanged in adult stages (**Fig. 3.7**), which confirms the appropriate choice of 18S and β-Actin as inner controls. Quantitative RT-PCR experiments were performed at INM-4 (Fzj), in collaboration with Verena Graf and Dr. Antje Willuweit.

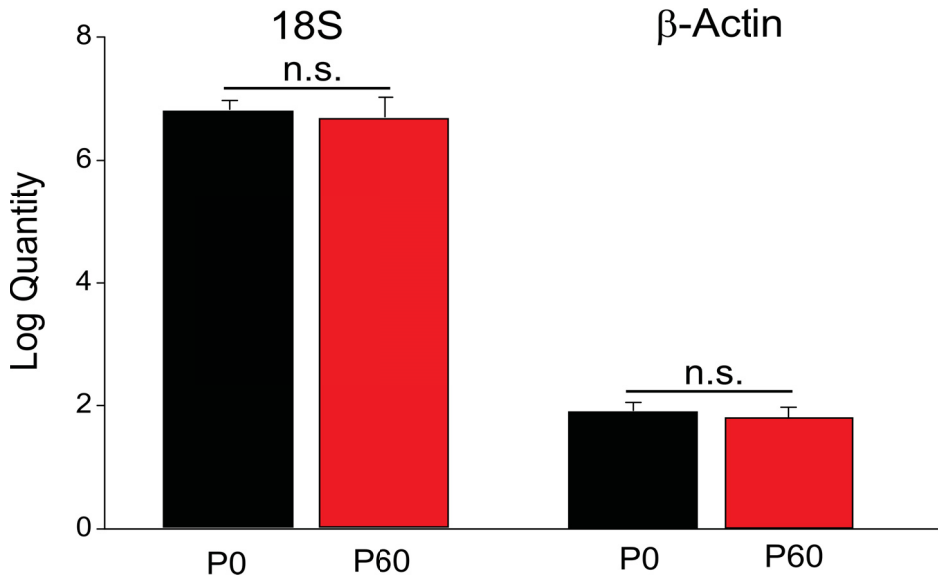

FIGURE 3.7: **qRT-PCR (in P0-P60 WT mice).** 18S and β-Actin were used as housekeeping (or reference) genes. The expression level of both genes is stably expressed in the two different post-natal stages (P0 and P60 WT mice).

The two reference genes were used as control. It was important to find housekeeping genes whose expression level was stable along the post-natal development and 18S and β-Actin turned out to be suitable as control genes.

The mRNA expression level of ClC-3 and ClC-5 was tested in P0 and P60 WT mice. While ClC-3 is similarly expressed in both post-natal stages, ClC-5 is down-regulated in adult stages (P60), as shown in **Fig. 3.8**.

Interestingly, ClC-5 is up-regulated in *Clcn3*$^{-/-}$ P0 mice (**Fig. 3.9**). This result indicates that, in absence of ClC-3, ClC-5 is up-regulated in order to compensate for the absence of the other protein. To conclude, not only ClC-5 undergoes a developmental age-dependent regulation, but it is also up-regulated in *Clcn3*$^{-/-}$ P0 mice.

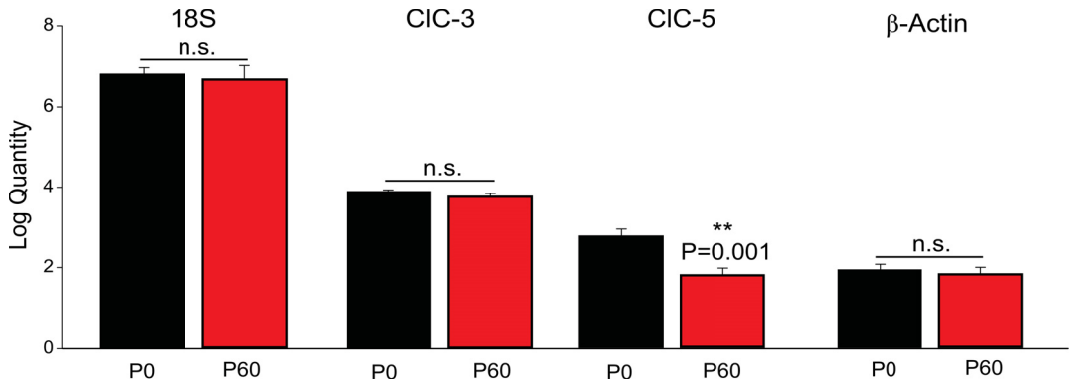

FIGURE 3.8: **qRT-PCR experiments reveal the expression level of ClC-3 and ClC-5 in different post-natal stages.** While ClC-3 is stably expressed in the two different developmental phases(P0 vs P60), ClC-5 is down-regulated in adult stages (P60).

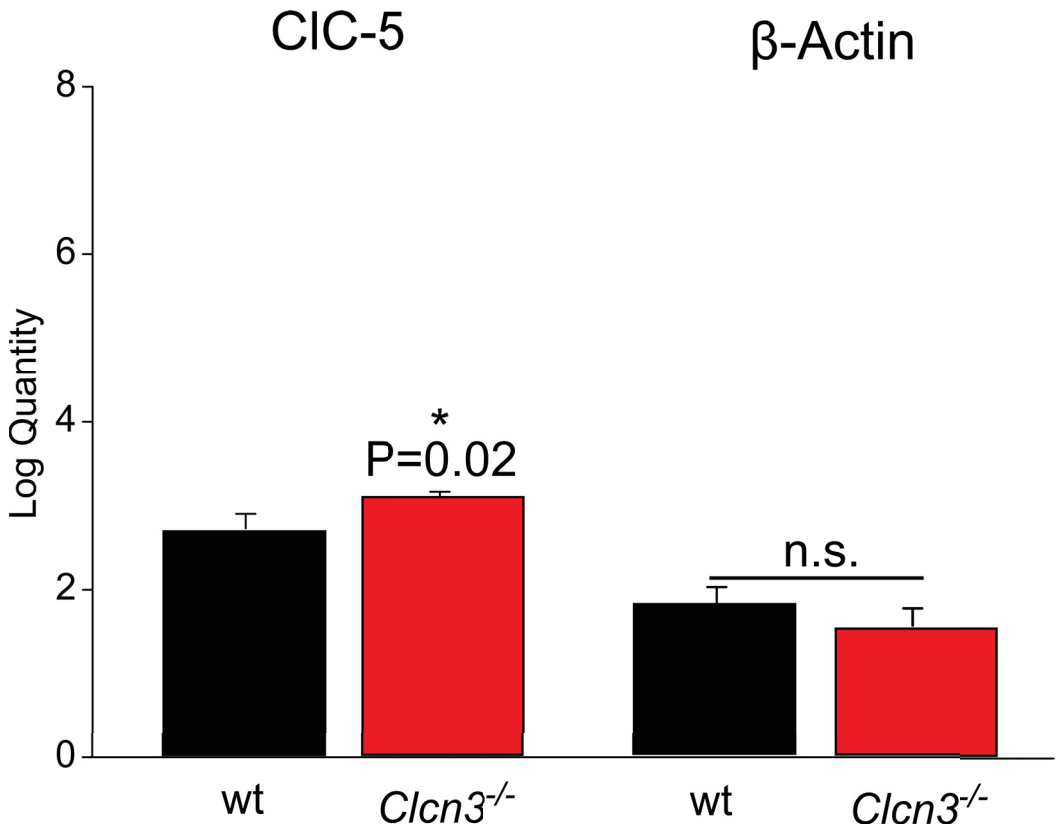

FIGURE 3.9: **qRT-PCR (in WT vs KO P0 mice)** The expression level of ClC-5 was checked in absence of ClC-3.

3.2.1 Catecholamine release is not affected by the absence of ClC-3 nor ClC-5 in early post-natal stages at saturating calcium concentration (20μM)

The so-called DKOs condition was generated through the lenti-viral strategy. In brief, *Clcn3*$^{-/-}$ chromaffin cells were transfected with shRNA (in the short hairpin vector) designed to silence (via knock-down strategy) the target gene, in this case ClC-5, by therefore generating the double KOs condition. WT cells were similarly transfected with non specific shRNA to obtain the scrambled condition, used as control. The same strategy was also applied to knock-down ClC-5 in WT chromaffin cells, to generate the so-called ClC-5 knock-down condition. In order to stimulate exocytosis, cells were dialyzed with saturating $[Ca^{2+}]_i$ (approximately 20 μM).

Three different conditions were measured in P0 mice and representative recordings did not show any obvious reduction in absence of only ClC-5 or of both proteins (ClC-3 and ClC-5), as reported in **Fig. 3.10 A, B, C**. Indeed, membrane capacitance increase and spike frequency are not affected in any of the three measured conditions: (Scr)WT in blue (n=18), ClC-5kd in orange (n=18) and double KOs in green (n=10) (**Fig. 3.10 D**). Accordingly, the initial cell size of the three different conditions is comparable (**Fig. 3.10 E**). The aim of this set of experiments is to test whether ClC-3 or ClC-5 might be implicated in regulating exocytosis.

Amplitude (I_{max}) and charge (Q) reported in **Fig. 3.11 A, B** reflect no significant impairment in the amount of released catecholamines in DKOs. The frequency distribution graphs **Fig. 3.11 C, D** depict charge and amplitude parameters and represent the event distribution per cell, measured in different conditions: (Scr)WT, ClC-5kd and DKO.

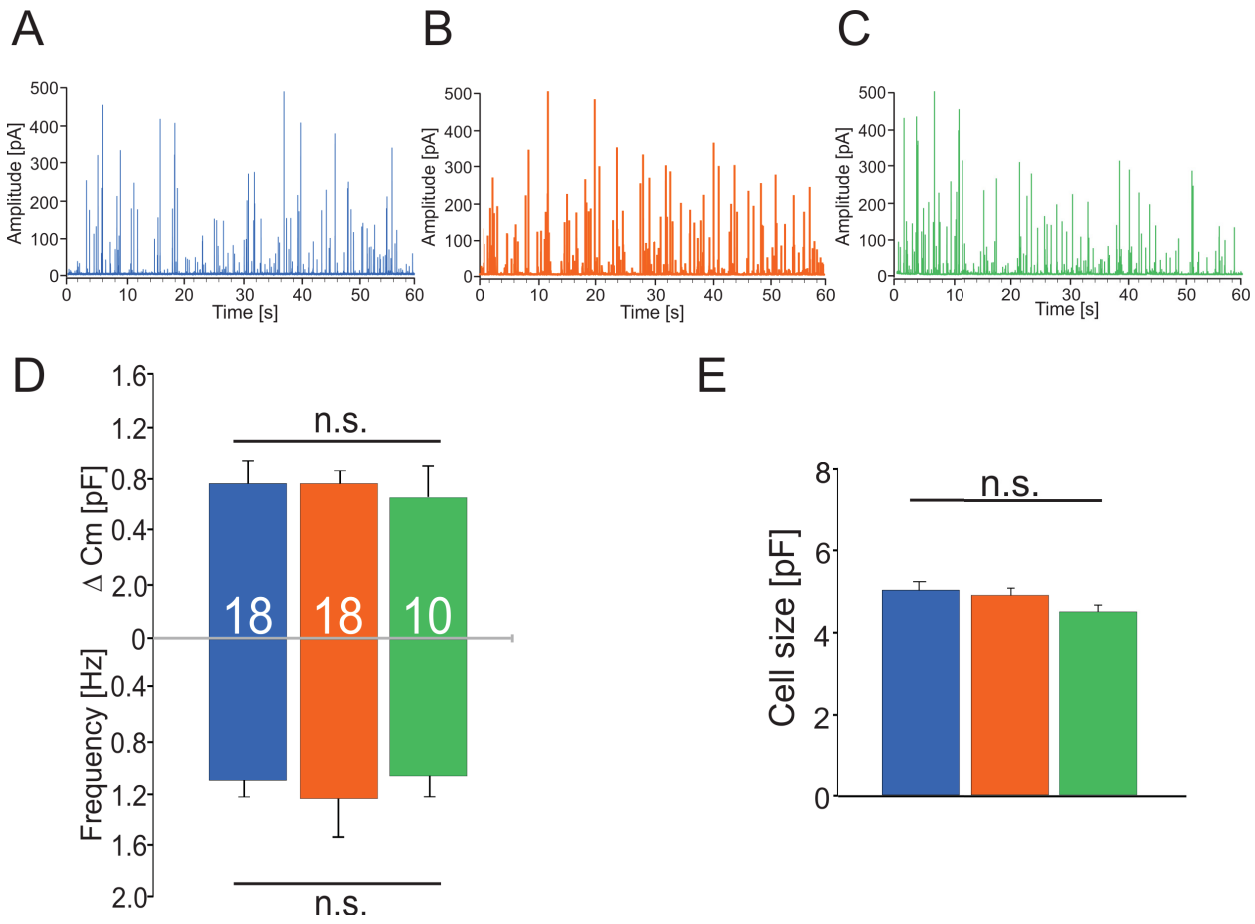

FIGURE 3.10: **Exocytotic response is not affected in absence of ClC-3 or ClC-5 in saturating calcium concentration.** Representative recordings show (Scrambled) WT (in blue), ClC-5 knock-down (in orange) and double KOs conditions (in green) measured in P0 mice in **Fig. A, B, C**, respectively. All the three representative recordings show no apparent significant difference, considering spike amplitude and frequency. Spike occurrence (**Fig. D**) and initial cell size (**Fig. E**) are comparable for all three conditions.

Kinetic parameters (rise time, half width and decay time) reveal no impairment in the dynamic properties which characterize vesicle fusion upon stimulation (**Fig. 3.12 A, B, C**). Similarly, cumulative frequency distribution graphs (**Fig. 3.12 D, E, F**, respectively) confirm that large-dense core vesicle (LDCV) fusion events are unaltered in DKOs at early post-natal stages (P0). ClC-3 was proposed as regulator of intracellular acidification in synaptic vesicles and secretory granules, and thus in catecholamine loading. On the other hand, ClC-5 is known to be implicated in endocytosis. The aim of the previously described set of experiments was to test whether ClC-3 or ClC-5 might be implicated in catecholamine loading and therefore we focused on amplitude and charge analysis of exocytotic events. In presence of saturating $[Ca^{2+}]_i$, we could not observe any impairment

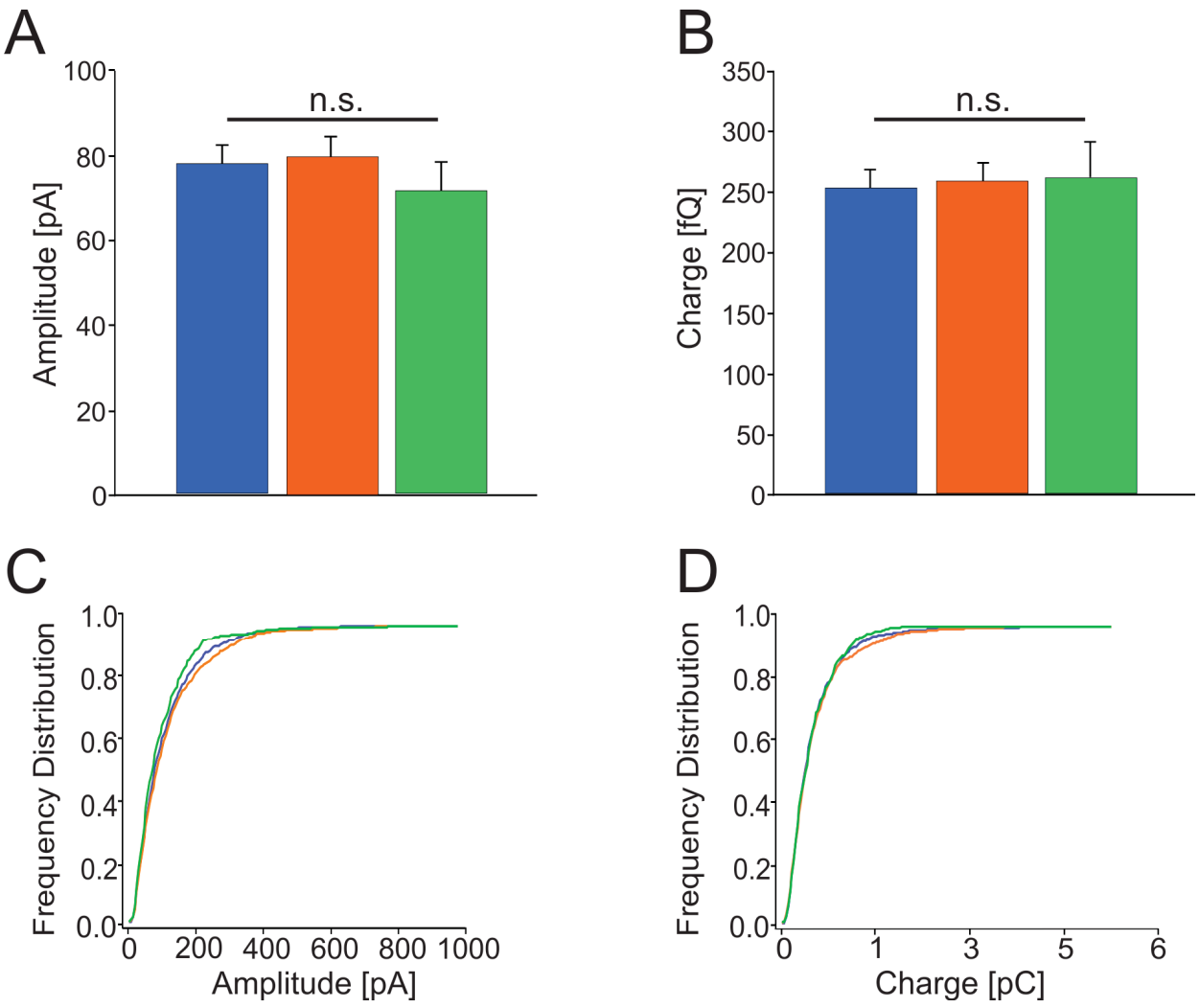

FIGURE 3.11: **Spikes Amplitude and Charge and relative frequency distribution (in P0 mice) in absence of ClC-3/ClC-5.** Amplitude and charge (**A, B** respectively) reflect an unaltered release of catecholamine amount after deletion of ClC-5 as well as in absence of both ClC-3 and ClC-5. The relative event distributions (**C, D** respectively) show similar LDCV events occurring during exocytosis.

in catecholamine loading as shown in C_m increase (**Fig. 3.10 D**) and confirmed in amplitude/charge analysis (**Fig. 3.11**) nor in the fusion process (**Fig. 3.12**) in absence of ClC-3, ClC-5 or both. Intriguingly, LDCV biogenesis is apparently not regulated by ClC-3/ClC-5, since the frequency of exocytotic event is not affected (**Fig. 3.10 D**).

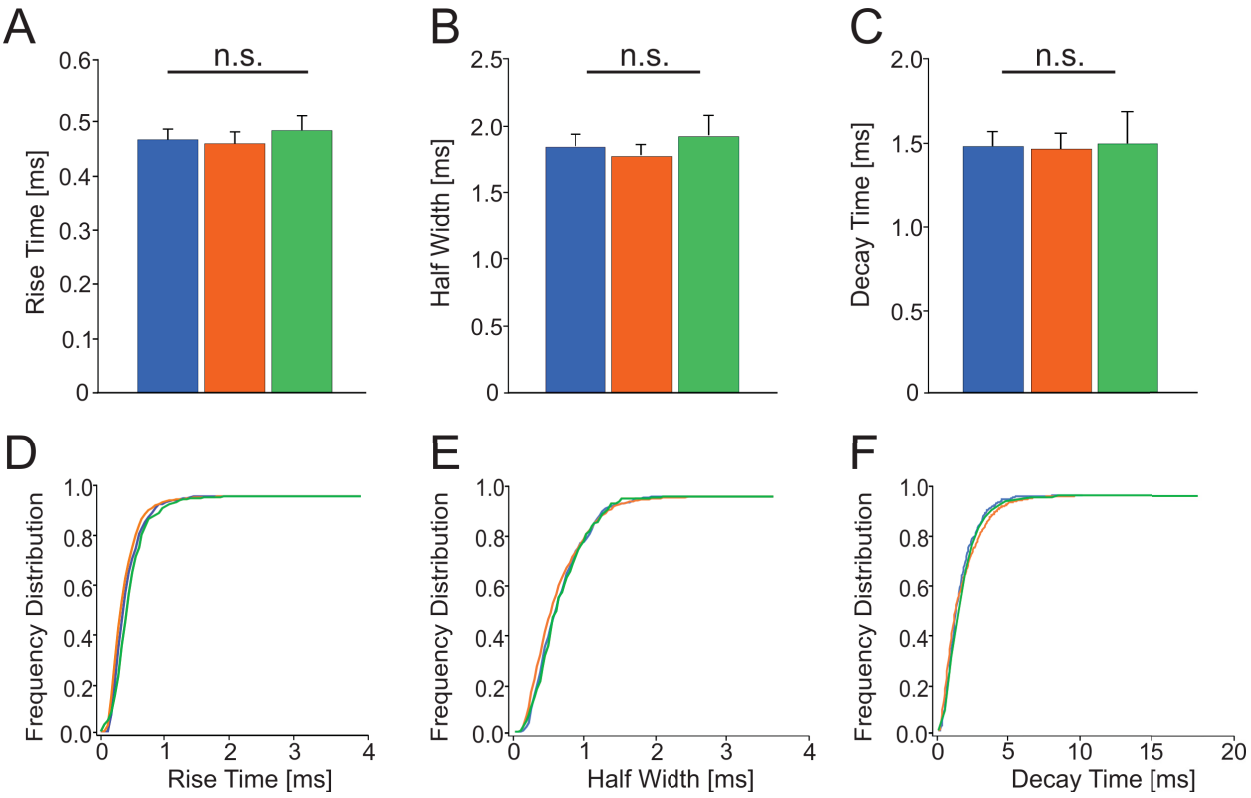

FIGURE 3.12: **Kinetic parameters and relative frequency distribution graphs (in P0 mice) in absence of ClC-3/ClC-5.** Bar graphs of kinetic parameters (A, B, C) and respective cumulative events (D, E, F) reflect the exocytotic fusion process measured in P0 mice.

3.2.2 Spikes frequency is significantly reduced in the absence of ClC-3 in adult stages at low intracellular calcium (3μM)

In the previous experiments, exocytosis was triggered by an intracellular infusion of 20 μM of $[Ca^{2+}]_i$. Such calcium concentration is well above physiological conditions, where calcium normally rises up to 5-10 μM. Hence, we reduced the free $[Ca^{2+}]_i$ to 3μM. Interestingly, we could detect a significant reduction in spike frequency when ClC-3 is lacking in adult mice, while in new born mice no impairment was detectable. Representative measurements of KO condition clearly show a reduced spike occurrence. Thus, ClC-3 can affect the number of exocytotic events (**Fig. 3.13**).

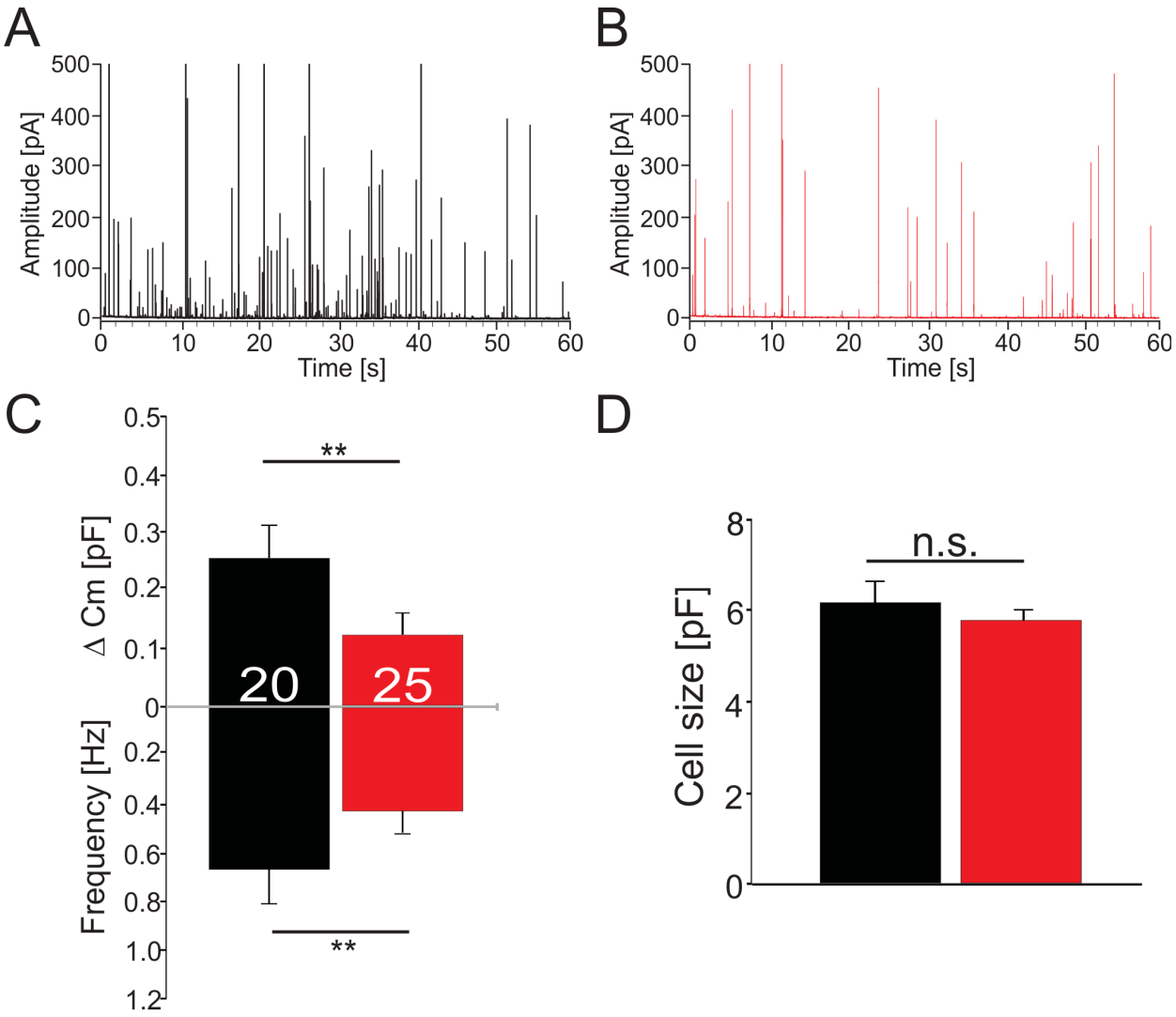

FIGURE 3.13: **Exocytosis is impaired in WT vs KO (P60 mice) at 3 μM of calcium.** The KO recording shows a spikes frequency which is dramatically reduced compared to the WT.

Both C_m increase and spike frequency are severely reduced in the KO response (in red) compared to WT (in black), while their cell size is comparable (**Fig. 3.13 D**). A reduced spike occurrence in KO condition indicates that ClC-3 is able to affect the number of vesicles fusing during exocytosis. Therefore, ClC-3 might be implicated in one of the multiple steps which render the secretory granules able to fuse (or fusion-competent). The strong correlation between ΔC_m and amperometric event frequency indicates that changes in membrane capacitance are directly caused by alterations in granule exocytosis (and not by endocytosis). This correlation is well in agreement with the close relationship between the two types of measurements.

Amplitude and charge showed in **Fig. 3.14 A, B** and their frequency distribution graphs (**Fig. 3.14 C, D**) prove that ClC-3 does not regulate catecholamine loading in

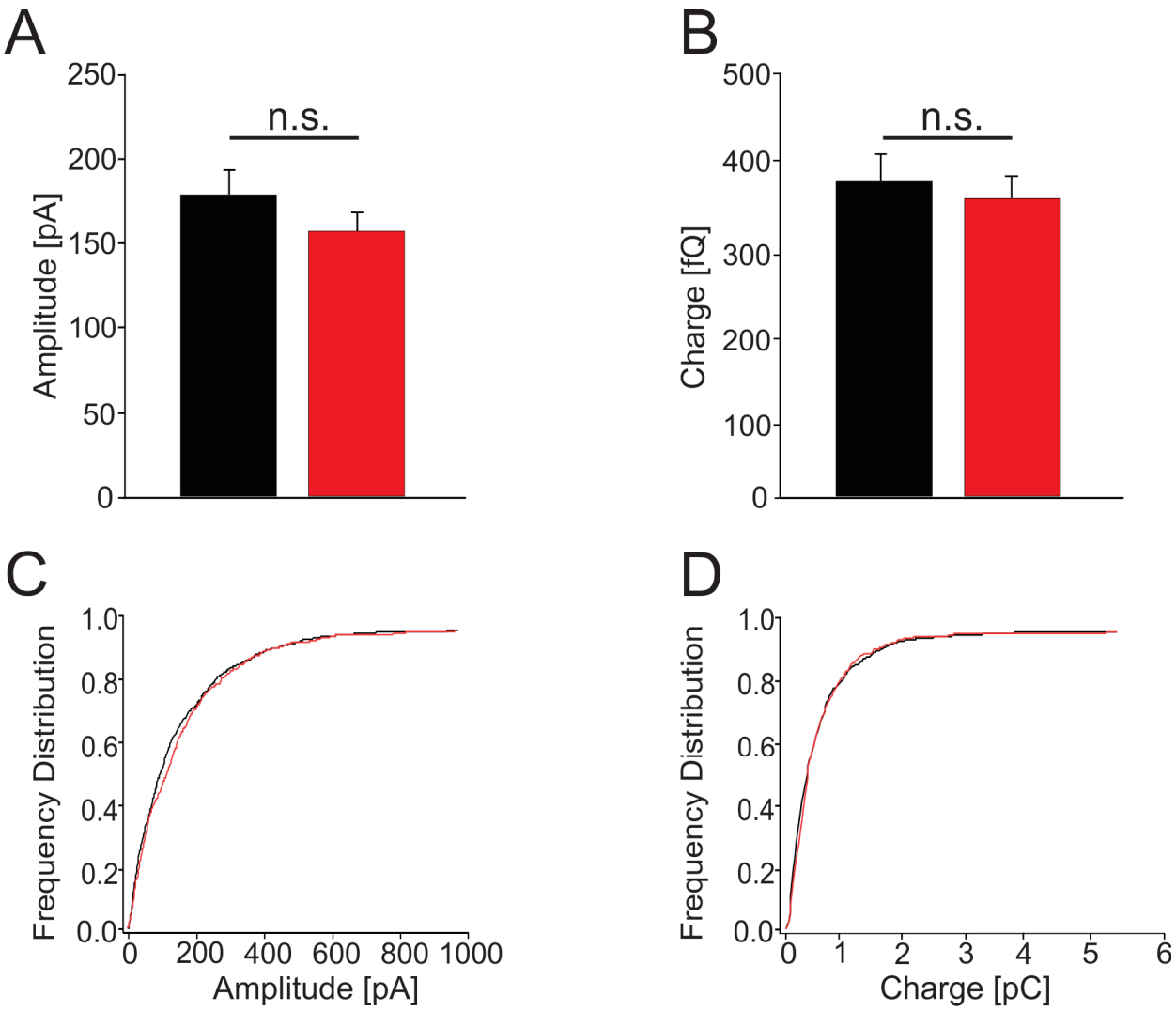

FIGURE 3.14: **Spikes charge and amplitude, measured in adult mice.** Catecholamines concentration and spike amplitude are not affected in absence of ClC-3.

LDCVs. Similarly, one might expect that neurotransmitter uptake in synaptic vesicles (SVs) would not be controlled by ClC-3.

In addition, the fusion process itself was analyzed to check whether ClC-3 might be possibly implicated in regulating vesicle fusion **Fig. 3.15**. In conclusion, loss of ClC-3 does not change the mode of exocytosis. The fusion process in not affected in terms of kinetics in KO condition.

Taken together, these results support the hypothesis that ClC-3 can influence the number of vesicles which can reach a fusion-competent state in adult chromaffin cells. This might also explain the involvement of ClC-3 in exocytosis. On the contrary,

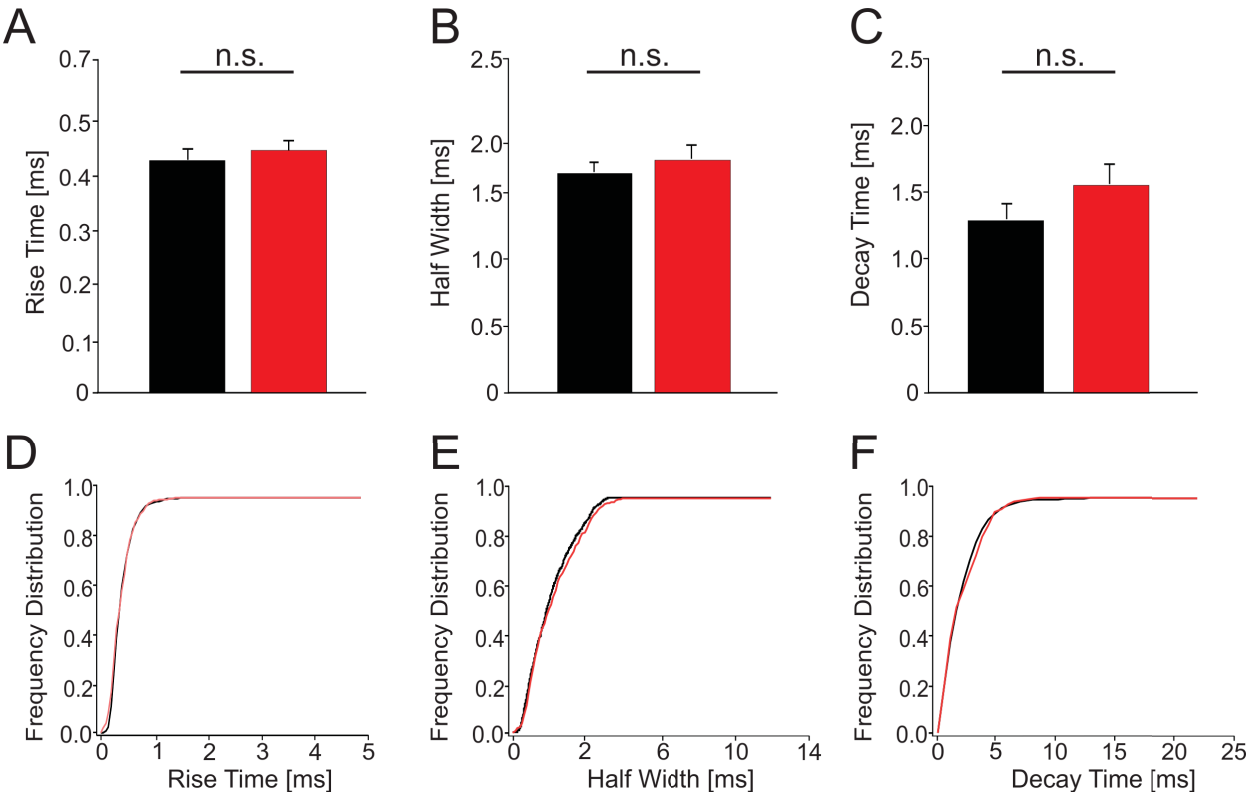

FIGURE 3.15: **Bar graphs of kinetic properties measured in P60 WT (black) and KO (red) mice.** None of the kinetic properties is affected in absence of ClC-3.

catecholamine loading into LDCVs as well as single vesicle fusion kinetics are not affected by ClC-3 in comparison to WT cells.

3.2.3 Spikes frequency is significantly reduced in the DKO condition in early post-natal stages at low intracellular calcium (3μM)

Representative amperometric measurements of (Scrambled)WT in blue, (Scrambled)KO in purple, ClC-5 knock-down in orange and double-knock outs in green are depicted below. No obvious phenotype was observed in absence of only ClC-3 or ClC-5. Interestingly, spike occurrence appears to be strongly reduced in the DKOs condition. Exocytosis was triggered by dialyzing the cells with 3 μM of $[Ca^{2+}]_i$.

As control, WT and KO chromaffin cells were transfected with non specific shRNA using the Lentiviral Expression System. Thus, (Scr)WT and (Scr)KO conditions were generated. ClC-5 knock-down and double KOs are measured in order to study a possible implication of ClC-3 or ClC-5 in exocytosis. A significant reduction in ΔC_m was

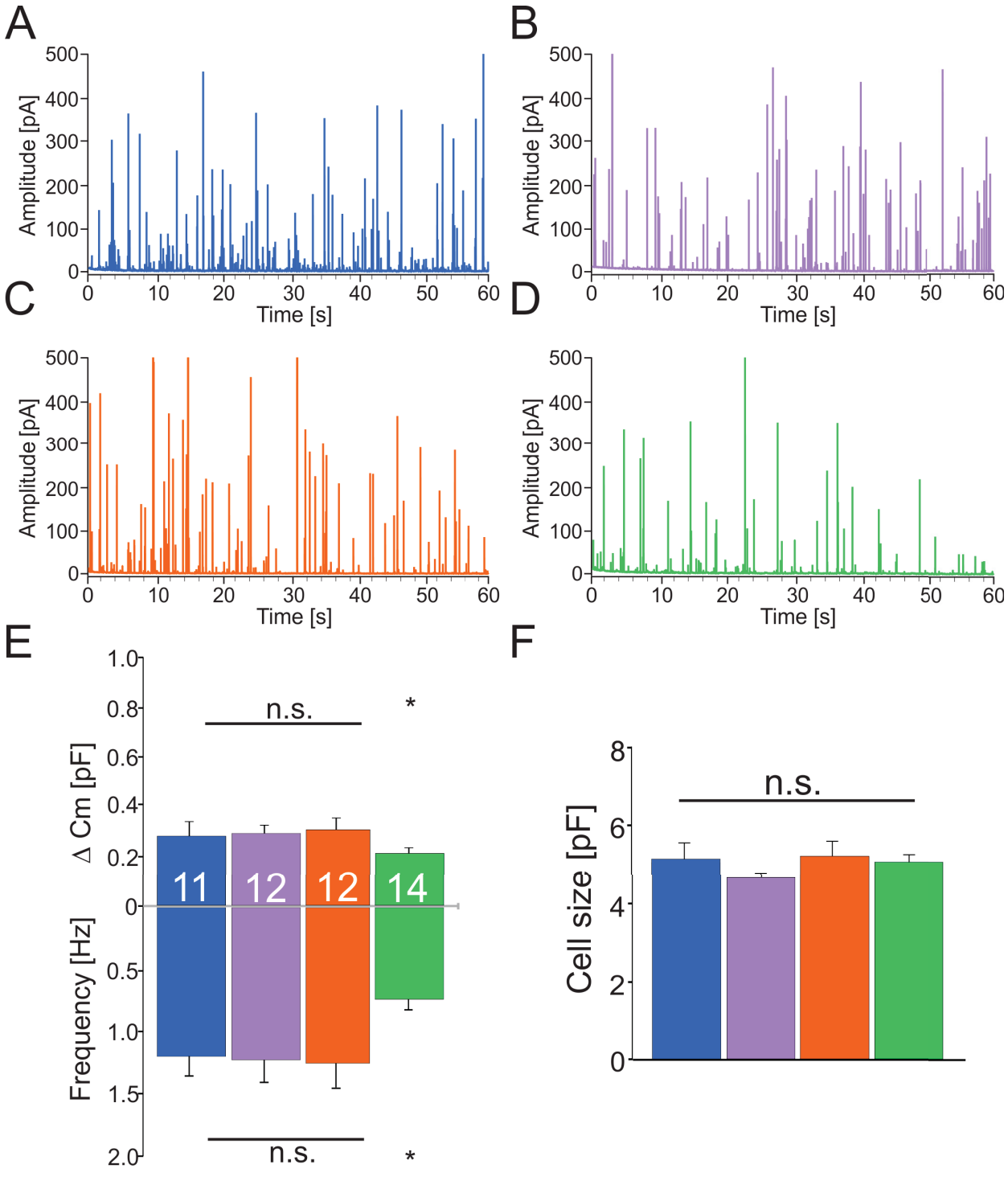

FIGURE 3.16: **Exocytosis is impaired in absence of ClC-3/ClC-5 (P0 mice) at 3 μM of calcium.** Representative Measurements of shRNA-Scrambled WT (in blue), Scrambled KO (in purple), ClC-5 knock-down (in orange) and DKOs (in green) measured in P0 chromaffin cells. The occurrence of exocytotic events is significantly decreased in DKOs response.

detected in absence of both chloride/proton exchangers. Consistently, spikes occurrence was reduced as well (**Fig. 3.16 C**). This impairment was not observed in the solely absence of ClC-3 or ClC-5. No significant variations in cell size was observed in any of the four conditions. This indicates that it is necessary to silence both ClC-3 and ClC-5 to produce a similar reduction in spike frequency in P0 mice as that observed in P60 mice in absence of only ClC-3. Double KOs condition did not reveal any impairment in charge nor amplitude parameters.

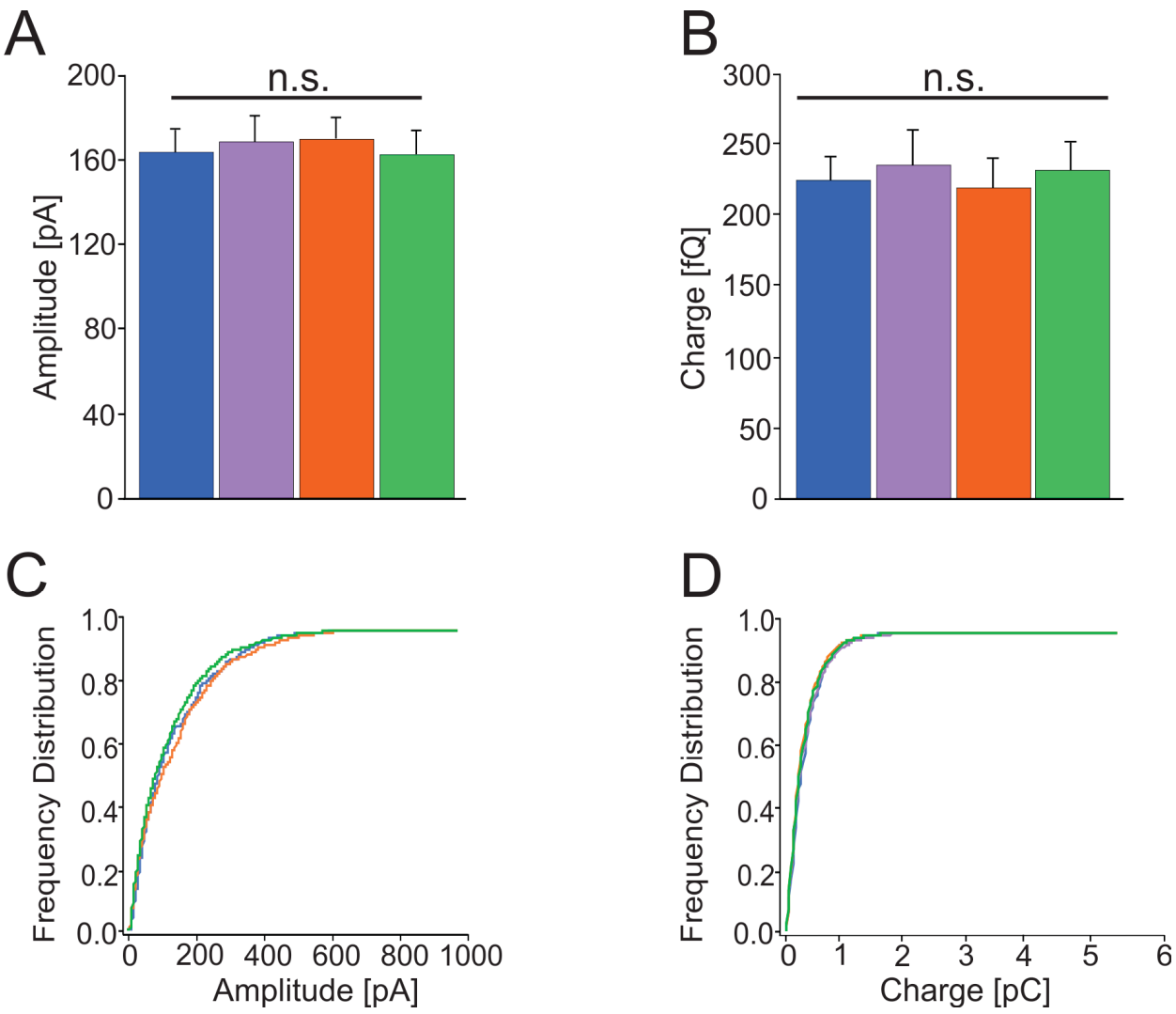

FIGURE 3.17: **Spikes Amplitude and Charge and relative frequency distribution (in P0 mice) in absence of ClC-3/ClC-5.** Catecholamine amount as well as spike amplitude are not affected in the DKO condition.

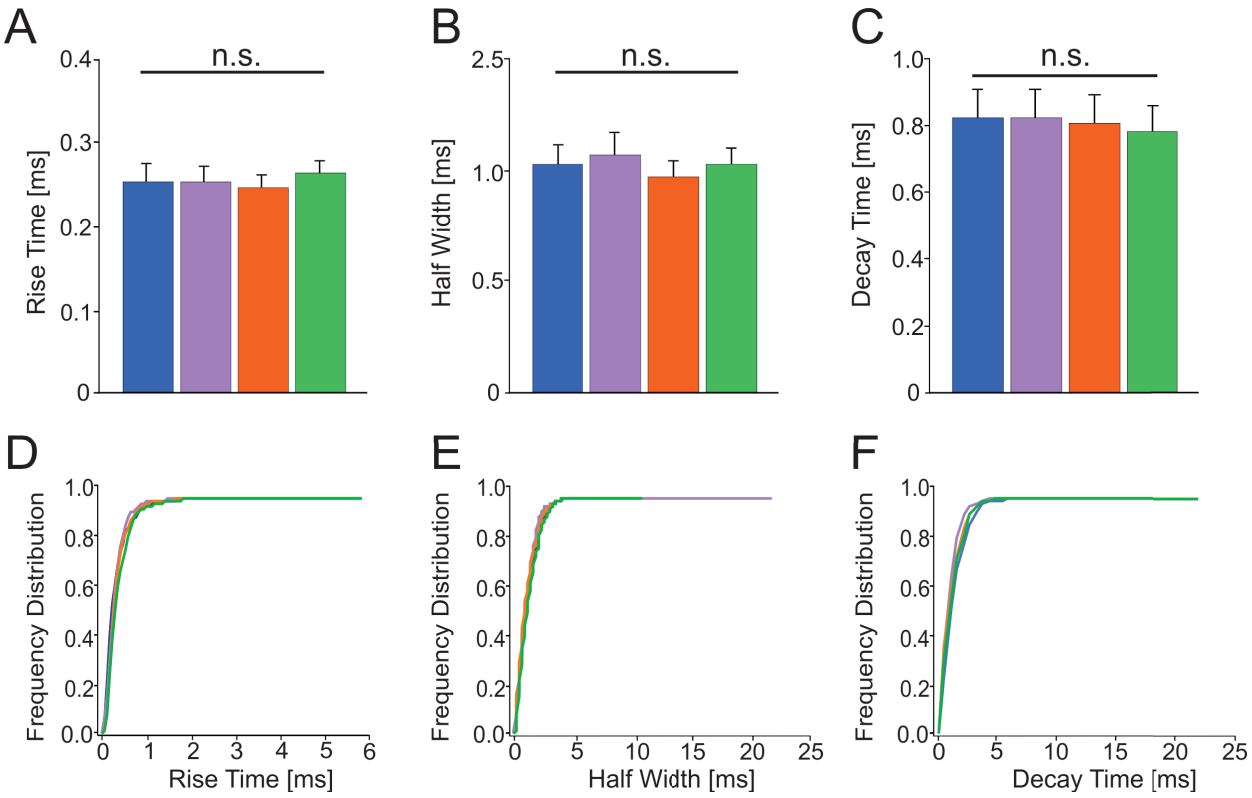

FIGURE 3.18: **Kinetic parameters and relative frequency distribution graphs (in P0 mice) in absence of ClC-3/ClC-5.** $Rise_{time}$, half-width and $decay_{time}$ are substantially invariant in (Scr)WT, (Scr)KO, ClC-5kd and DKO conditions.

Spikes characteristics, such as $Rise_{time}$, spike Half-width and $Decay_{time}$, are not affected in DKOs chromaffin cells of new born mice. Coherently, frequency distribution graphs reflect unchanged kinetic properties **Fig. 3.18**. In conclusion, the number of vesicles fusing during exocytosis is reduced in DKO condition (P0). A decreased spike occurrence can be due to an impaired vesicle mobilization during the priming process or decreased LDCV biogenesis. This reduction is similar to that observed in P60 mice, in absence of ClC-3. This suggest that, in early post-natal stages (P0), ClC-5 might compensate for the absence of ClC-3.

3.3 LDCV priming is impaired in *Clcn3*$^{-/-}$ adult mice (P60), but not in new-born (P0)

Capacitance measurements were made in the whole-cell patch-clamp configuration by applying trains of depolarizing stimuli, as previously described (see **Fig. 2.5**). In brief, exocytosis was monitored as changes in membrane capacitance (C_m) using the Lindau-Neher technique.

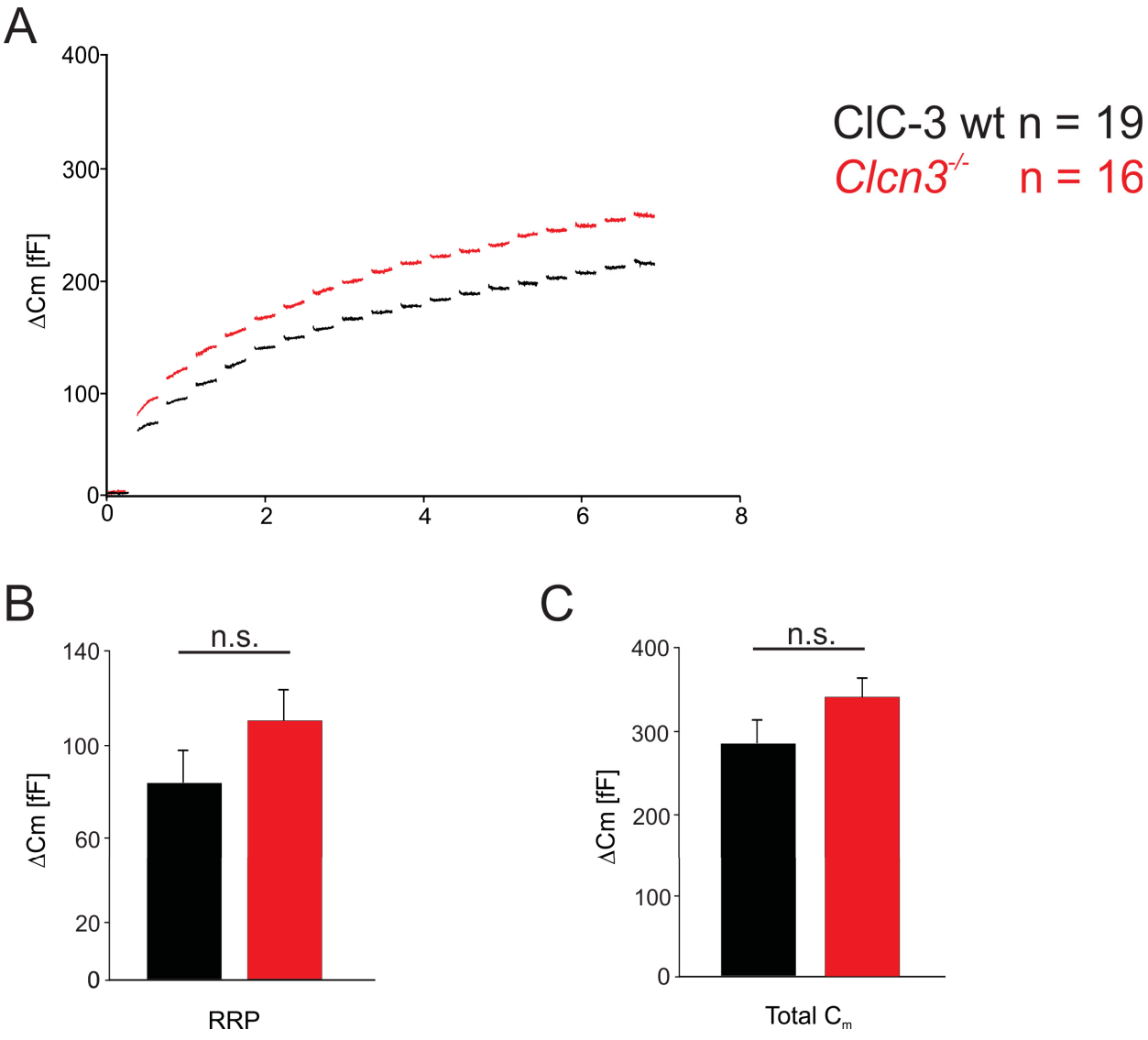

FIGURE 3.19: **Membrane capacitance measurements are monitored in WT (black) and KO (red) conditions in new born mice (P0).** No relevant impairment was observed in absence of ClC-3 by applying a depolarization protocol.

Applying this specific protocol, it is possible to evaluate the priming process measured in the very first C_m step-like increase. Interestingly, the priming process is not

affected in *Clcn3*$^{-/-}$ cells, in early post-natal stages. In contrast, an increase (even though not statistically significant) was observed in absence of ClC-3 which might be explained as a compensatory effect provided by ClC-5.

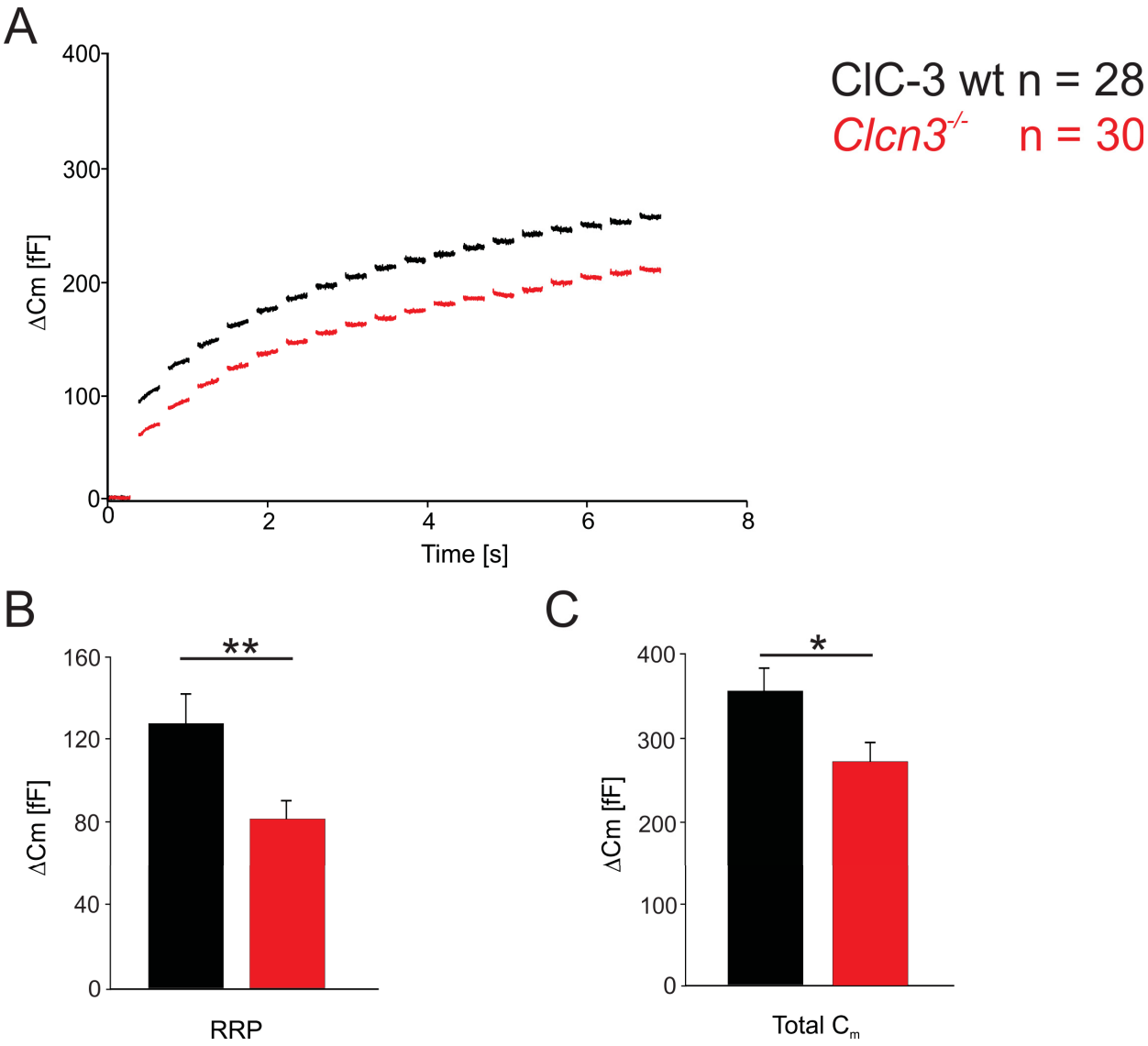

FIGURE 3.20: **Membrane capacitance measurement recorded in P60 mice.** WT (black) and ClC-3 knock-out (red) adult chromaffin cells reveal an impairment in the exocytotic process. Interestingly, the first capacitance increase

Such a compensation would not be observed in late post-natal stages, as ClC-5 (according to our qRT-PCR data) is down-regulated in adult stages (P60) and its expression level would not be sufficient to counter-balance the absence of ClC-3. Indeed, exocytosis was severely reduced in adult *Clcn3*$^{-/-}$chromaffin cells. Experiments were performed with the contribution of Juan Sierra, Dr. Antonio Yarzagaray and Dr. Raul E. Guzman (ICS-4, Fzj). The readily releasable pool (RRP) of vesicles is ready to get fused to the plasma

membrane and undergo exocytosis. This vesicle pool is indeed quickly depleted after the first train of depolarization. As reported in the bar graphs, neither the RRP fraction nor the total membrane capacitance increase are affected by the absence of ClC-3 **Fig. 3.19**. On the contrary, a significant reduction was observed in *Clcn3*$^{-/-}$ adult mice (P60), measured in the same experimental condition (**Fig. 3.19 B, C**, respectively). On the contrary, in adult mice the whole exocytotic process (total C_m) is significantly reduced in *Clcn3*$^{-/-}$, but this impairment mainly derives from a defective priming step. The physiological relevance of this effect indicates that ClC-3 plays an important role in the vesicle priming process and can thus control the whole exocytosis in late post-natal stages.

3.4 LDCV priming is impaired in the DKOs condition in new born mice (P0)

Capacitance measurements were made in the whole-cell patch-clamp configuration by applying a depolarization protocol.

Four different conditions are here compared, where (Scr)WT (in blue) and (Scr)KO (in purple) are used as reference and compared to ClC-5 knock-down (in orange) and double KOs (in green). The initial cell surface was similar for each condition. Membrane capacitance recordings revealed that vesicle priming (which reflects the RRP fusion) is strongly decreased when both ClC-3 and ClC-5 are absent in new born mice (**Fig. 3.21**). It is interesting to point out that such impairment measured in DKO is even more dramatic compared to the reduced RRP observed in adult *Clcn3*$^{-/-}$ cells **Fig. 3.20**. The total C_m of DKOs is reduced of one third compared to the control, while the RRP fusion, that reflects the priming process, is decreased to one third **Fig. 3.21**.

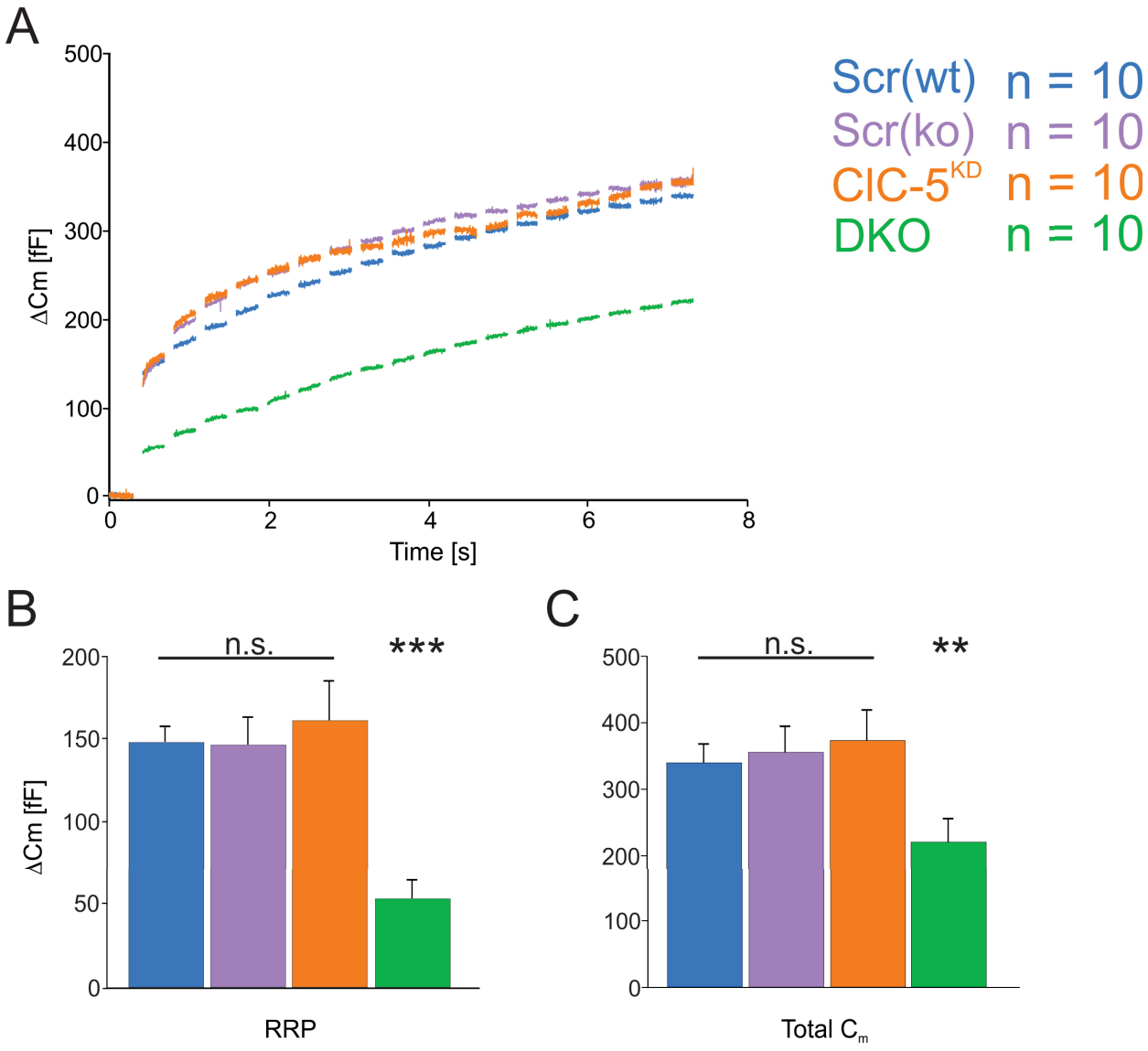

FIGURE 3.21: **Membrane capacitance recordings were performed in P0 chromaffin cells.** No significant effect was observed in (Scr)WT, (Scr)KO or ClC-5kd. In the DKOs condition instead, the RRP (**B**) is reduced to ≈ 50 fF ± 11 fF, while (Scr)WT is ≈ 150 fF ± 9 fF. The total C_m (**C**) in control condition is 339 fF ± 27 fF, while in DKOs is 220 fF ± 33 fF.

3.5 Subcellular localization of ClC-3 and ClC-5 in neuroendocrine cells

The intracellular localization of the chloride/proton exchangers ClC-3 and ClC-5 has been so far only partially characterized in the neuroendocrinal system (*e.g.*, in secretory granules[4],[5]). It is therefore still missing a clear subcellular characterization of the different splice variants of ClC-3 and ClC-5 as well. While it is known that both ClC-3 and ClC-5 are located along the endosomal pathway when over-expressed in a heterologous

expression system[68], their compartmental distribution in neuroendocrine cells needs to be further addressed. At the beginning of this work, we over-expressed the three different splice variants of ClC-3 in PC-12 cells, derived from pheochromocytoma of the rat adrenal medulla. PC-12 cells are conventionally used as a model for neurosecretion and neuronal studies. Like other types of neuroendocrine cells, they store and release catecholamines (mainly Dopamine and Norepinephrine)[162]. Because of their relative versatility and convenient availability (*e.g.*, ease of culture), PC-12 cells were initially used to characterize the subcellular distribution of ClC-3.

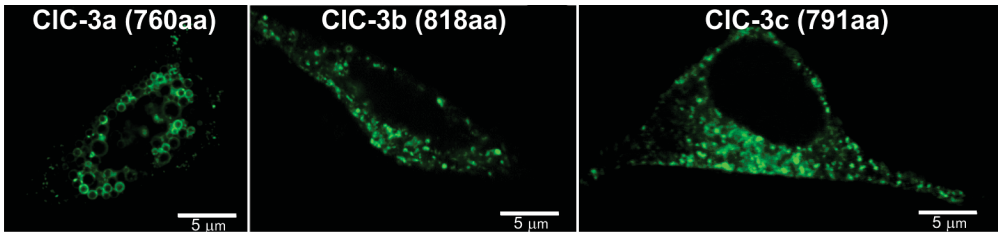

FIGURE 3.22: **Subcellular distribution of three different splice variants of ClC-3 in PC-12 neuroendocrine cells.** ClC-3a and b shows a highly similar localization, which appears distinct from that of ClC-3c.

While ClC-3a and ClC-3b show a high similarity in their intracellular distribution (which coincides with lisosomal-like structures, as shown in **Fig. 3.22**), ClC-3c appears to be mainly expressed in a peri-nuclear region and along the plasma membrane.

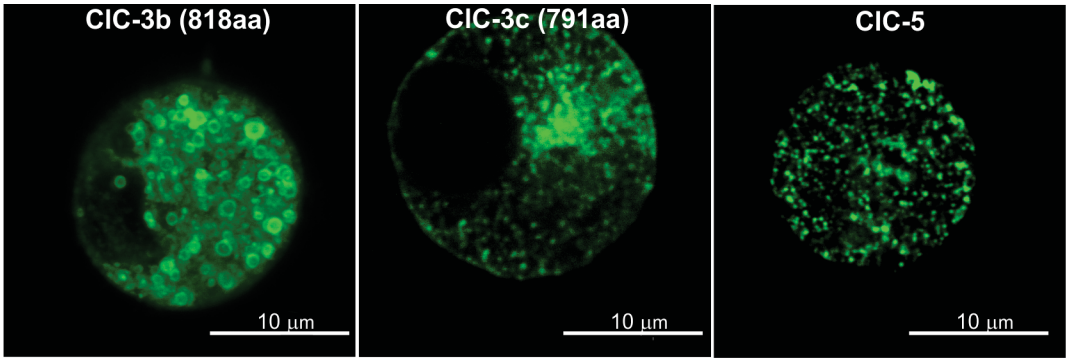

FIGURE 3.23: **Subcellular distribution of ClC-3 and ClC-5 in adrenal chromaffin cells.**

In order to address their intracellular distribution in the native system, we over-expressed ClC-3 and ClC-5 in chromaffin cells as well. ClC-3b shows a very peculiar distribution which closely resembles that of lysosomal-like structures, coherently with what we previously observed in PC-12 cells. On the other hand, ClC-3c appears to be enriched in a peri-nuclear area and partially along the plasma membrane as well, consistently with what we observed in MDCKII cells[68] and PC-12 cells. ClC-5 shows a slightly

different punctiform subcellular distribution in specific intracellular compartments (**Fig. 3.23**).

3.5.1 ClC-3 splice variants are located in different subcellular compartments in adrenal chromaffin cells

As previously described[68], ClC-3 exists in different splice variants which are located in diverse subcellular compartments. In this set of experiments, ClC-3b/c are co-expressed together with marker proteins specific for different endosomal compartments.

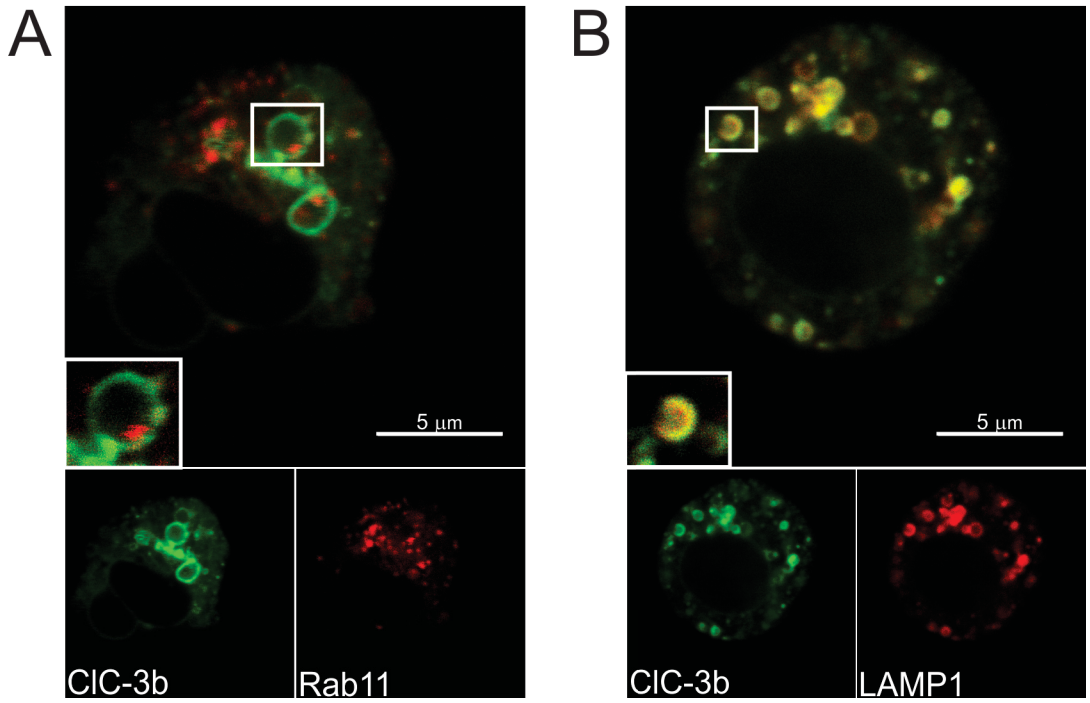

FIGURE 3.24: **Subcellular distribution of ClC-3b in chromaffin cells.** ClC-3b was co-expressed with two different subcellular markers, Rab11 (**A**) and LAMP1 (**B**).

Rab11 is a well-characterized marker for recycling endosomes[137], while LAMP1 is mainly located in lysosomes[163]. To test whether ClC-3b (818aa) is located together with one of the two markers, we co-expressed it with Rab11 or LAMP1 using Lipofectamine2000 Reagent®, as previously described. The protein of interest is GFP-tagged, while the marker is mRFP-tagged. Therefore, the two fluorescent proteins can be precisely detected by using different excitation and emission wavelengths and the appropriate detection filter. We observed a highly degree of co-localization of ClC-3b and LAMP1 **Fig. 3.24 B**, while hardly any co-localization was observed for ClC-3b and Rab11 **Fig. 3.24 A**.

This result is well in agreement with our previous work and with the subcellular localization characterized in HEK293 and TSA cells[68].

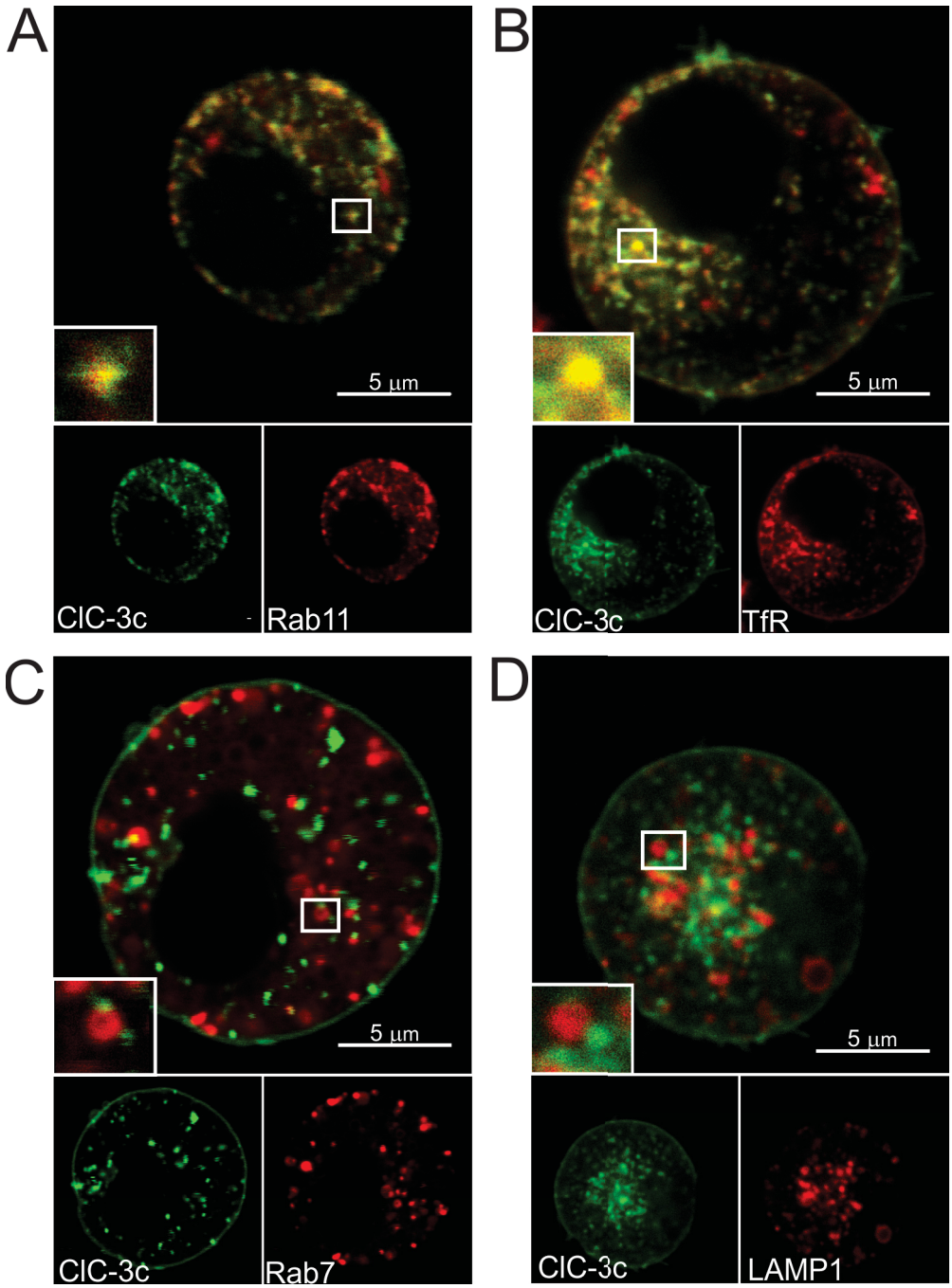

FIGURE 3.25: **Subcellular distribution of ClC-3c in chromaffin cells.** ClC-3c was co-expressed with Rab7 (**C**) and Rab11 (**A**), different endosomal markers belonging to the Rab protein family, LAMP1 (**D**), marker for lysosomes, and the transferrin-receptor marker (TfR) (**B**), located in recycling endosomes.

ClC-3c (791aa) was previously found in Rab11-positive recycling endosomes in HEK293 cells[68]. Similarly, here we tested the localization of ClC-3c together with Rab7

(**Fig. 3.25 C**) marker for late endosomes[130], LAMP1 (**Fig. 3.25 D**), Rab11 and transferrin-receptor marker (TfR) (both present in recycling endosomes[137],[164]) (**Fig. 3.25 A, B**). Coherently with previous studies, ClC-3c does not co-localize with Rab7 (**Fig. 3.25 C**) nor with LAMP1 (**Fig. 3.25 D**), but was rather found together with Rab11 and TfR markers (**Fig. 3.25 A, B**, respectively). The role of recycling endosomes is to guarantee a proper intracellular trafficking. In particular, proteins expressed on the plasma membrane, such as t-SNARE proteins, undergo a significant recycling process since only a small percentage is synthesized *ex novo*[165]. This suggests that ClC-3c, which is located in such type of compartments, might perform its function by controlling a proper acidification of recycling endosomes and therefore supervising the whole intracellular trafficking pathway.

3.5.2 ClC-5 is located in a specific sub-population of recycling vesicles in adrenal chromaffin cells

To our knowledge, the intracellular localization of ClC-5 has never been described in the neuroendocrinal system via confocal laser-scan microscopy. In order to confirm whether ClC-3 and ClC-5 might perform a similar biological role, we would expect to observe a comparable subcellular distribution of these proteins. When over-expressed in chromaffin cells, ClC-5 was found located in TfR-positive organelles (**Fig. 3.26 A**), while no substantial co-localization was observed with Rab11, as shown in **Fig. 3.26 B**. This reveals that, while ClC-3c was found in both types of recycling endosomes, ClC-5 would be predominantly expressed in a subpopulation of those. These results are not surprising, if we consider that ClC-3 and ClC-5 might share a similar distribution (and function) only in a specific type of endosomes, where they can regulate the intracellular recycling pathway.

We analyzed the signal distribution measured in the two different fluorescence microscopy channels (green and red) in order to determine whether the two fluorescent probes were co-localized with one another. This kind of analysis is important if we assume that the different subcellular distributions of the proteins is related to their functional compartmentalization. However, such co-localization analysis does not reveal any possible interaction between the two proteins, but rather indicate their presence in the same intracellular compartments.

To quantitatively estimate the degree of co-localization between the protein of interest and its marker, we performed co-localization analysis using JACoP, a plug-in

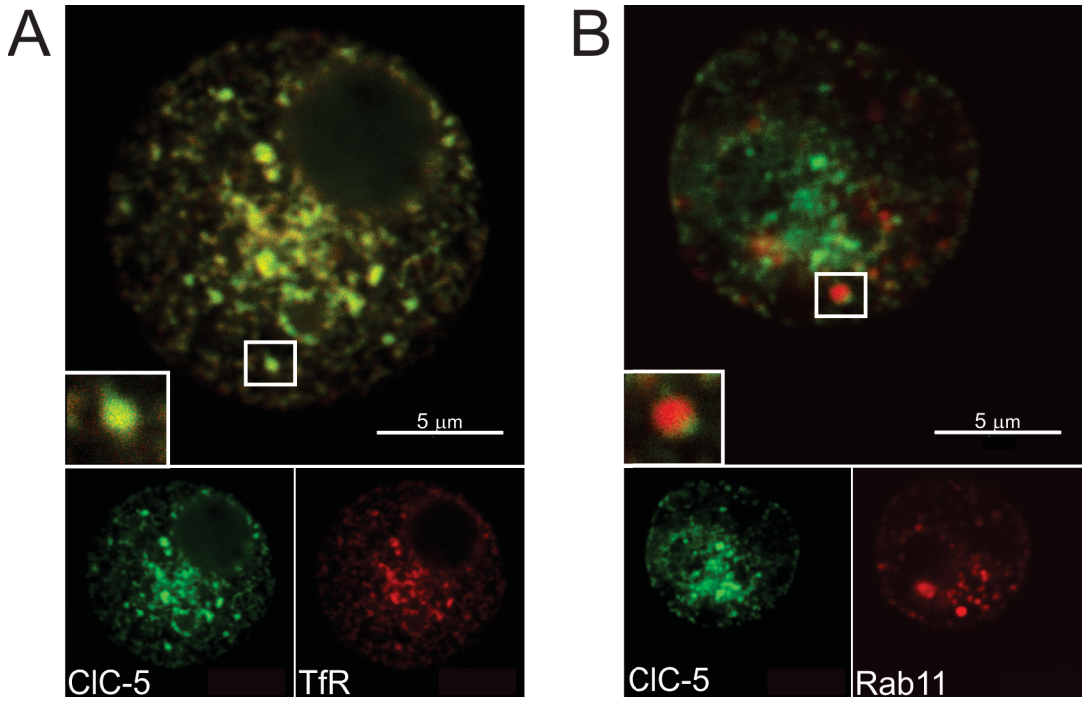

FIGURE 3.26: **Subcellular distribution of ClC-5 in chromaffin cells.** ClC-5 was co-expressed with two different recycling endosomes markers, TfR (**A**) and Rab11 (**B**).

available in ImageJ software (National Health Institute, Bethesda). In brief, it permits to calculate the Mander's correlation coefficient which can vary from 0 to 1, where 0 corresponds to non-overlapping images, while 1 reflects 100% co-localization[166]. This parameter indicates the degree of fluorescence of the co-localizing pixels in each channel (green and red) and is based on the Pearson's correlation coefficient with average intensity values not considered in the mathematical formula[167]. In this study, M1 represents the percentage of EGFP signal (which correspond to ClC-3/ClC-5 fluorescence) overlapping with the respective endosomal marker. For each condition, at least 10 cells were measured from two or more chromaffin cell cultures. When multi-stacks images were used, at least 10 different stacks (1 μm maximum width each) were measured.

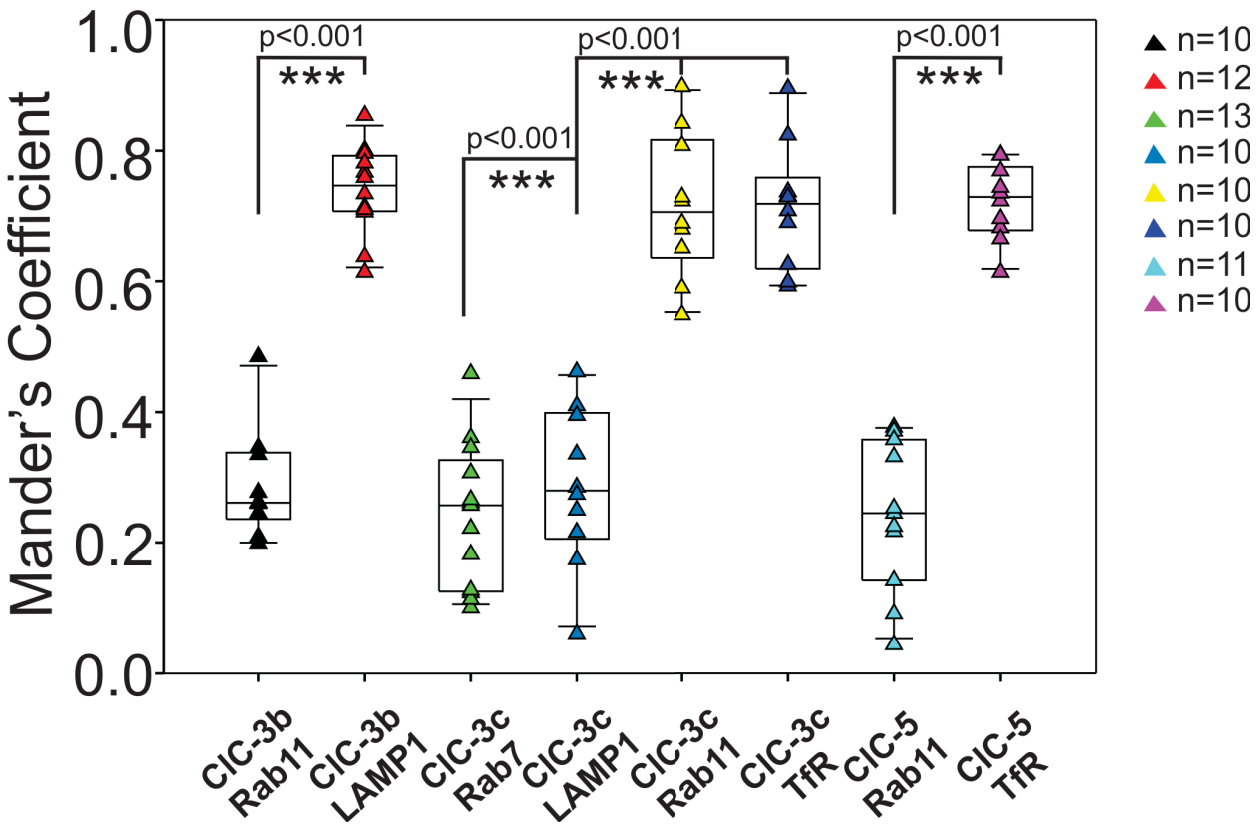

FIGURE 3.27: **Co-localization analysis of ClC-3 and ClC-5 and their respective markers.** The Mander's coefficient was analyzed by using JACoP, a plug-in embedded in ImageJ software (NIH).

3.5.3 Localization of ClC-3 and ClC-5 in large dense core vesicles (LDCVs)

Since ClC-3 and ClC-5 are involved in the exocytotic response, in order to get a new insight about their direct or indirect implication in neurosecretion, we checked their presence in secretory granules (LDCVs) via immunocytochemistry. ClC-3 splice variant c was the only one which shares a high degree of co-localization with Synaptobrevin II (SybII), a vesicle-associated membrane protein highly expressed in LDCVs in neuroendocrine cells[168].

ClC-3c is present in LDCVs where it shows high degree of co-localization with SybII in PC-12 cells (**Fig. 3.28**). We then addressed the question whether a similar localization could be observed in chromaffin cells as well. Unlike ClC-3b and ClC-5, the subcellular distribution of ClC-3c confirmed a high degree of co-localization with SybII (**Fig. 3.29 A**) with a Mander's Correlation Coefficient value close to 1 (M1 = 0.70 ± 0.031) (**Fig. 3.29 B**) in an average of 10 cells. Conversely, ClC-3b was not found in such type of

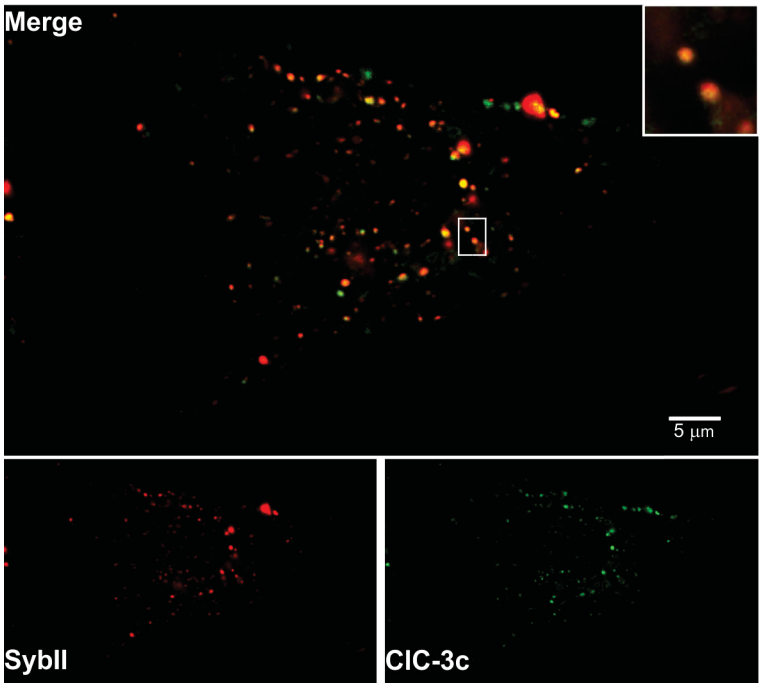

FIGURE 3.28: **Localization of ClC-3c (green channel) and Synaptobrevin II (red channel) in PC-12 cells.** PC-12 cells were transfected with ClC-3c GFP-tagged and Synaptobrevin II mRFP-tagged. The substantial co-localization of ClC-3c and SybII reveals that indeed this splice variant is located in LDCVs.

secretory granules, coherently with previous studies[5]. Interestingly, ClC-5 seemed not to be present in LDCVs as well (**Fig. 3.29 B**), revealing a prominent localization along the endosomal pathway where it can most probably regulate endocytosis[76],[169] and possibly endosomal trafficking and recycling processes. Thus, ClC-3c and ClC-5 might mutually, yet in a different manner, govern vesicle mobilization during the priming process.

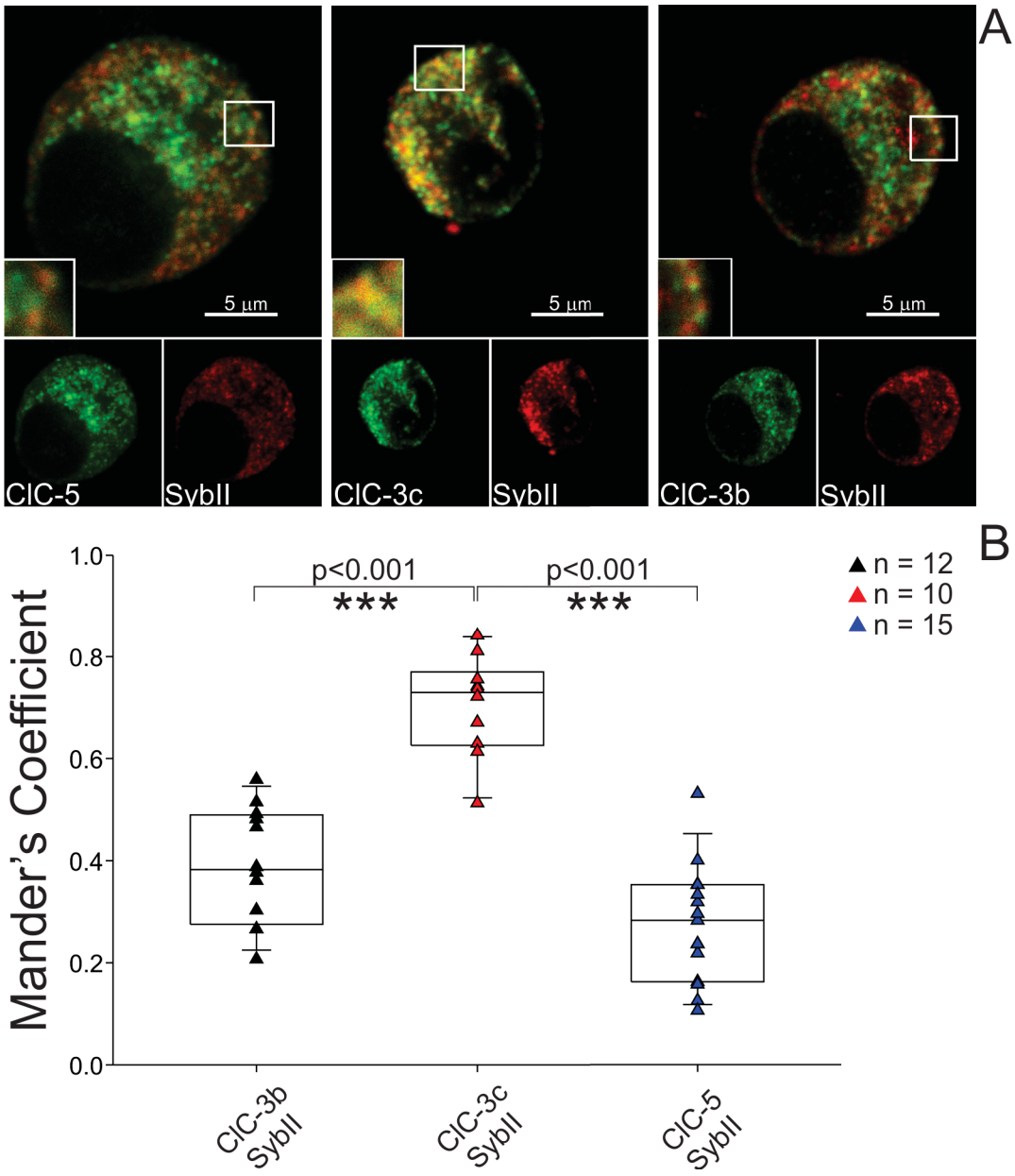

FIGURE 3.29: **Localization of ClC-3c, ClC-3b and ClC-5 in secretory granules of chromaffin cells.** Chromaffin cells were transfected with ClC-3c/b/ClC-5 GFP-tagged and counter-stained using an antibody against Synaptobrevin II (**A**). Mander's Coefficient analysis is reported in the panel below (**B**).

Chapter 4

Discussion

Exocytosis is a process necessary for cell communication and environmental adaptation. Thus, it is not surprising that it has been extensively studied and characterized over the last decades. The basis of intracellular communication is the release of neurotransmitters (*e.g.* glutamate and GABA), hormones (such as catecholamines), as well as neuropeptides and digestive enzymes. Importantly, these molecules are stored and protected into membrane-bound compartments which are synaptic vesicles (SVs) in neurons and large-dense core or synaptic-like (micro)vesicles (SLMVs and LDCVs, respectively) in neuroendocrine cells. This precious cargo needs to be released in response to specific stimuli and is tightly regulated. Calcium has been studied as one of the major exocytosis-triggering stimulus. The vesicle fusion process strongly depends on the assembly of the fusion machinery which relies on the SNARE proteins activity. However, several regulatory steps are interwoven with each other and their interaction is fundamental for exocytosis to occur. This present work delineates a new role for the chloride/proton exchangers ClC-3 and ClC-5 which resulted to be among regulating factors of exocytosis. The experiments prove that ClC-3 and ClC-5 are able to regulate the LDCV priming process. Furthermore, this thesis gives a new insight about a compensating and mutual role performed by ClC-3 and ClC-5. In particular, in early developmental stages both proteins are able to regulate vesicle priming, while in adult stages ClC-3 plays a prominent role in neurosecretion.

4.1 Membrane capacitance measurements correlated with amperometric recordings permit to monitor exocytosis in real time with high temporal resolution

Exocytosis was monitored by applying the "sine wave + DC" mode in the lock-in amplifier configuration, as previously described. Membrane capacitance measurements were performed in parallel with amperometric recordings. Amperometry allows detection of released LDCVs products (such as catecholamines) and permits single exocytotic events analysis, as described (**Fig. 2.6**). The nature of information gained by combining these two techniques permits to correlate the vesicle fusion process with the amount of catecholamines released during neurosecretion. Indeed, amperometry (but not capacitance) can detect catecholamines released only from a limited cell surface (around 20% of the entire cell area), while capacitance (but not amperometry) can monitor exocytosis occurring in the whole cell. This renders the combination of these techniques surprisingly powerful and highly attractive.

4.1.1 Analysis of amperometric spike's shape reveals information about the cargo content and its release dynamics

It was still an open debate whether ClC-3 might counterbalance the electrogenic force provided by the V-ATPase, and therefore actively regulate the intracellular acidification of synaptic vesicles or other secretory granules (*e.g.* LDCVs). Amperometric detection permits us to rule this possibility out and check if catecholamine concentration is affected in absence of ClC-3. Indeed, we observed that both spike amplitude and charge are not reduced in ClC-3 KO (**Fig. 3.14**) and DKO (**Fig. 3.17**) chromaffin cells. This result leads to the conclusion that ClC-3 (and ClC-5) does not regulate the loading and the uptake of catecholamines, at least in the neuroendocrinal system. Similar conclusions might also be hypothesized at neuronal level, where the role of ClC-3 in neurotransmitters uptake remains obscure[62],[65]. Furthermore, analysis of kinetic properties (rise time, half-width and decay time) reveal unaltered dynamics during the fusion process in both responses (**Fig. 3.15**, **Fig. 3.18**). These findings indicate that neither ClC-3 nor ClC-5 regulate the transient fusion pore formation, when the secretory vesicle is merging with the plasma membrane, as well as the release process itself. This was also confirmed by analysis of the foot signal in both conditions (data not shown). Unaltered rise and decay time also

reveal that the time-course of the fusion process is unaffected and that the release mode is not controlled by these exchangers.

4.2 Putative role of ClC-3 and ClC-5 in exocytosis

Previous studies tried to elucidate the role of ClC-3 in the central nervous system due to its significant effect on hippocampal neuronal degeneration[1]. Several hypothesis have been postulated to explain such a strong effect, but so far its underlying mechanism remains obscure. For instance, the neurotransmitters loading was proposed as limiting factor in exocytosis of *Clcn3*$^{-/-}$ cells. The presence of ClC-3 itself in synaptic vesicles and LDCVs has been however questioned, since lack of a specific antibody has prevented its clear intracellular localization. Now, if we assume that ClC-3 is located in synaptic vesicles, one might speculate that it is also implicated in synaptic acidification thus regulating neurotransmitter loading (*e.g.*, glutamate/GABA and catecholamines).

More recently, the role of ClC-3 in the neuroendocrinal system has been investigated by several groups. In 2008 Maritzen and colleagues observed that the number of amperometric spikes as well as the whole exocytosis was reduced in *Clcn3*$^{-/-}$ adult mice. Amperometric detection revealed a reduction in the charge as well as amplitude parameters, which indicate a defect in the loading of catecholamines, stored and released by LDCVs in chromaffin cells[5]. Astonishingly, they could not observe the presence of the protein in such type of secretory granules in β-pancreatic and chromaffin cells, but rather only in synaptic-like microvesicles (SLMVs) which release acetylcholine but not catecholamines. Nonetheless, another group previously reported conflicting data, in which they observe the presence of ClC-3 in secretory granules of β-pancreatic cells[4]. In our experiments, we could not observe any reduction in terms of charge and amplitude when we performed amperometry in both P0 (**Fig. 3.17**) and P60 *Clcn3*$^{-/-}$ (**Fig. 3.14**) mice at saturating $[Ca^{2+}]_i$. However, at low $[Ca^{2+}]_i$, we also observed a significant reduction in the number of vesicles fusing during exocytosis in both P0 and P60 *Clcn3*$^{-/-}$ mice, but again with no effect on catecholamine amount and kinetic fusion properties. This finding well fits with a defect in the priming process, that is the process necessary to render the vesicles fusion-competent. Indeed, our capacitance measurements showed a decreased response to the first voltage pulse as well as in the total capacitance increase in *Clcn3*$^{-/-}$ adult mice (**Fig. 3.20**). A further reduction in the first pulse-increase and whole exocytosis was observed in absence of both ClC-3 and ClC-5 in new-born mice (**Fig. 3.21**). Depolarization-induced exocytosis relies on the raise of intracellular calcium through

voltage-gated Ca^{2+} channels. Interestingly, no significant decrease in Ca^{2+} currents was measured in absence of ClC-3 (data not shown).
We here propose that ClC-3 and ClC-5 can affect LDCV priming. This process is known to be dependent on the proper vesicle acidification[4],[170]. During mobilization towards the plasma membrane, vesicles need to be primed via an ATP-dependent process that renders the vesicles able (competent) to respond to a calcium signal[141]. Another possible function of ClC-3 and ClC-5 antiporters might be the regulation of the recycling process, which is also controlled in an acidification-dependent manner. In this perspective, SNAP25 appears a promising candidate. Indeed, SNAP25 is a *t*-SNARE protein which plays a key role in determining the number of primed vesicles. The availability of this protein mainly relies on its recycling, since only a small fraction of the protein is synthesized *de novo*[165]. Now, since the intracellular membrane trafficking depends on the proper endosomal acidification, the whole recycling process would be impaired after disruption of both ClC-3 and ClC-5. This would finally decrease the availability of SNAP25 and might therefore prevent the SNARE complex formation.

4.3 ClC-3 regulates the priming process of LDCVs in adult mice

The role of ClC-3 in the neuroendocrinal system has been addressed in this study. We used a combination of patch clamp and amperometric technique to elucidate vesicle fusion. Our results revealed that ClC-3 regulates one specific step of the whole exocytotic process, which is vesicle priming (**Fig. 3.19**).

1. ClC-3 might play a direct effect on the priming step. Exocytosis depends on luminal acidification[170],[171]. Neurotransmitter and catecholamine loading is also affected by the intracellular vesicle acidification. Previous experiments showed that bafilomycin A1 can inhibit catecholamine uptake by blocking the V-ATPase of chromaffin granules in PC-12 cells[170]. In addition, bafilomycin can dramatically impair the whole exocytosis[4]. As demonstrated by our amperometric results (**Fig. 3.14**), neither amplitude nor charge are significantly affected in *Clcn3*$^{-/-}$ response. This reflects an unaltered catecholamine loading into LDCVs, which indicates that ClC-3 does not play a role in granule acidification (and that probably does not work as a counterpart of the V-ATPase). This is also consistent with

the unaffected hormone concentration measured in *Clcn3*$^{-/-}$ β-pancreatic cells by Maritzen and colleagues[5].

The pH gradient is also a crucial factor for the formation of LDCVs, since it affects the aggregation and proper sorting of Chromogranin A (CgA), a regulated secretory protein in neuroendocrine cells[170]. The use of bafilomycin A1 revealed indeed an impaired sorting of CgA to LDCVs for exocytosis as well as a a reduced release probability and a significant decrease in the number of LDCVs[170]. If ClC-3 (and ClC-5) can play a role in the pH gradient regulation, this might explain why we also observed a strong reduction in LDCV fusion frequency in *Clcn3*$^{-/-}$ and DKO cells (**Fig. 3.13 C**, **Fig. 3.16 C**). However, it seems to be unlikely that impaired granular acidification has effects on LDCV biogenesis but not on catecholamine uptake.

On the other hand, the fusogenicity of SNARE proteins regulates the assembly of the SNARE machinery. Indeed, the lipidic composition of vesicle membrane has also been proposed as a regulating factor of the priming step[174]. The fusion process implicates rearrangements of the lipid matrix, in particular energy is required to bring the apposed membranes into contact[175]. The matrix lipid mixing is favored by the induced membrane curvature, which is controlled, among others, by SNARE proteins[176]. However, other factors such as the electric membrane potential, might be implicated in curving the lipid bilayer of the membrane[177]. In this perspective, the possible impact of ClC-3 on vesicle fusogenicity process needs to be further addressed.

2. ClC-3 might play an indirect effect on the priming step. Apart from granular acidification, membrane potential and ATP-hydrolysis, a proper vesicle priming relies on the stable assembly and formation of the SNARE complex. The most important SNARE proteins involved are the *t*-SNARE proteins SNAP25 and Syntaxin I, and the *v*-SNARE Synaptobrevin (VAMP) II and Synaptotagmin I (the main calcium sensor). The priming process, which permits to stabilize the vesicle fusion with the plasma membrane, mainly depends on the stable interaction between SNAP25 and Synaptotagmin[180]. It is known from previous work that SNAP25 is mainly recycled through recycling endosomes[181]. Our subcellular localization experiments reveal that ClC-3 and ClC-5 are both present in a subset of recycling endosomes (TfR-positive, **Fig. 3.27**). An intriguing hypothesis would be that in absence of such exchangers, the whole recycling process might be impaired. Indeed, the intracellular trafficking is regulated in a pH-dependent manner, which is likely dependent on the proper function of ClC-3 and/or ClC-5. If the intracellular trafficking

is affected in their absence, the SNAP25 recycling process, occurring through recycling endosomes, would be subsequently impaired. This would reduce the availability of SNAP25 and ultimately would affect the stability of the SNARE complex. One might thus speculate that a primary consequence would be a reduced priming process. For instance, a reduction in availability of dynamin results in impaired exocytosis of synaptic vesicles[182]. This hypothesis seems to be consistent with previous data[5]. Disruption of ClC-5 leads to impaired endosomal acidification in the proximal renal tubule[74] together with defective endocytosis[76],[77]. ClC-3, which is a close relative of ClC-5, might be implicated in endocytosis as well, since exo- and endocytosis are tightly interwoven processes. An impaired endocytosis is also consistent with a reduced membrane protein recycling.

4.4 ClC-3 and ClC-5 regulate the priming process in newborn mice

In order to address the question whether the chloride/proton exchangers ClC-3 and ClC-5 might play a mutual role in early developmental stages (P0), we checked their subcellular distribution. ClC-3 is mainly located in intracellular organelles, in particular the splice variant b (and a, data not shown) is located in lysosomal-like structures (**Fig. 3.24**), while ClC-3c is predominantly expressed in recycling endosomes, in particular in a subset of endosomes containing Rab11 and transferrin receptor (TfR) (**Fig. 3.25 A, B**). ClC-5 in mainly expressed in TfR-positive endosomes (**Fig. 3.26 A**), which are recycled in a clathrin-dependent manner or, in other words, in a fast-recycling way[183]. Vesicles which express Rab11 on the other hand are recycled in a clathrin-independent fashion (*e.g.*, through recycling endosomes) and undergo a slow recycling process[137]. That is, they need to enter in contact with adaptor proteins, before they can be internally recycled along the endosomal recycling pathway. ClC-3 and ClC-5 are both localized in TfR-positive recycling endosomes, coherently with previous data[5], where they might regulate the endosomal acidification process and therefore control protein recycling.
In this scenario, the recycling process might have a secondary effect on the availability of proteins implicated in the assembly of the SNARE machinery. A possible indirect implication would therefore be an impaired vesicle priming. There are two possible ways, one direct and one indirect, through which ClC-3 (together with ClC-5, in early developmental phases) can govern the priming process, as previously described.

Interestingly, we found that the priming process is not affected by the absence of ClC-3 in new-born mice (**Fig. 3.19**), while it is in *Clcn3*$^{-/-}$ adult mice (**Fig. 3.20**). This means that, while ClC-3 plays a prominent role in late post-natal stages, in early developmental stages there is another protein capable of compensating the function of ClC-3. Our quantitative real-time PCR experiments performed in adrenal glands indicate that ClC-5 is a good candidate to compensate for the absence of ClC-3 (**Fig. 3.9**). Our data show that ClC-5 is up-regulated in P0 *Clcn3*$^{-/-}$-deficient mice. Intriguingly, this compensation would not be possible in other tissues and organs, such as the brain, where ClC-3 most probably plays a more prominent role compared to that of ClC-5. On the other hand, our results suggest that the role of ClC-5 is less dominant in adult P60 stages, where it is strongly down-regulated (**Fig. 3.8**). The down-regulation of ClC-5 was also previously observed in the enteric nervous system (ENS), measured at different embryonic stages[184].

4.5 ClC-3 is located in LDCVs, while ClC-5 is mostly expressed in recycling endosomes

In 2008 Maritzen and colleagues could not observe the presence of ClC-3 in LDCVs[5]. This finding was quite surprising and made difficult a clear correlation between the impairment observed in exocytosis in ClC-3 KO cells and the actual presence of ClC-3 in secretory granules. Importantly, another group could instead detect ClC-3 in such type of organelles[4]. It has to be stated that in none of the previously mentioned works a specific ClC-3 splice variant was tested. Therefore, a major point of our study was to check whether a specific splice variant might be indeed responsible for neurosecretion. Interestingly, we could not detect the presence of ClC-3b in large dense core vesicles, where it shows a poor co-localization with Synaptobrevin II (**Fig. 3.29**), a vesicle-associated membrane protein highly expressed in LDCVs in neuroendocrine cells[168][186]. On the contrary, ClC-3c was found in secretory granules where it has a high degree of co-localization with Synaptobrevin II (**Fig. 3.29**). Astonishingly, unlike ClC-3c, ClC-5 was not found in secretory granules, coherently with a previous work[5]. This results seem to confirm a major role played by ClC-3 in exocytosis, whose absence can be compensated by ClC-5 only in early developmental stages. In this perspective, while ClC-3c might directly affect neurosecretion by governing the priming process of LDCVs, where is located, ClC-5 would rather compensate neurosecretion by regulating the endocytotic process and possibly the membrane protein trafficking and recycling of SNARE proteins.

4.6 Concluding remarks

Our work provides new insights about the role of chloride/proton exchangers in exocytosis. In particular, our data suggest that ClC-3 and ClC-5 can govern LDCV priming (**Fig. 3.21**) during neurosecretion in a developmental-regulated manner. Indeed, ClC-3 plays a prominent role in catecholamine release in late adult stages, as revealed by patch clamp and amperometry recordings. Interestingly, one specific splice variant of ClC-3, which is ClC-3c, appears to be located in secretory granules (LDCVs), while ClC-3b and ClC-5 could not be detected in such organelles. Thus, ClC-3c might directly regulate the priming step of LDCV exocytosis, while ClC-3b would play its major role in the lysosomal system and protein degradation. On the other hand, ClC-5 might be implicated in regulating the endosomal acidification and therefore the vesicle recycling and refilling process. Indeed, subcellular co-localization analysis and immunocytochemistry experiments showed that ClC-3b is mainly located in lysosomal-like structures, while ClC-5 was detected in a subset of recycling endosomes (TfR-positive), together with ClC-3c (**Fig. 3.27**). In addition, ClC-3c was also abundantly expressed in secretory granules (**Fig. 3.29**). In this perspective, ClC-3c and ClC-5 might together regulate exocytosis via controlling exocytosis in a direct and indirect manner, respectively.

To conclude, our data provide evidence that ClC-3 and ClC-5 are crucial for neurosecretion where mutually regulate the vesicle priming process in an age-dependent manner, probably mediating two different, yet linked, pathways.

Bibliography

[1] S. M. Stobrawa, *et al.*, *Neuron* **29**, 185 (2001).

[2] R. E. Guzman, A. K. Alekov, M. Filippov, J. Hegermann, C. Fahlke, *Frontiers in Cellular Neuroscience* **8** (2014).

[3] V. Riazanski, *et al.*, *Nature Neuroscience* **14**, 487 (2011).

[4] S. Barg, *et al.*, *Journal of cell science* **114**, 2145 (2001).

[5] T. Maritzen, D. J. Keating, I. Neagoe, A. A. Zdebik, T. J. Jentsch, *Journal of Neuroscience* **28**, 10587 (2008).

[6] L. V. Deriy, *et al.*, *Cell Metabolism* **10**, 316 (2009).

[7] D.-Q. Li, *et al.*, *Cell Metabolism* **10**, 309 (2009).

[8] O. Scheel, A. A. Zdebik, S. Lourdel, T. J. Jentsch, *Nature* **436**, 424 (2005).

[9] A. Picollo, M. Pusch, *Nature* **436**, 420 (2005).

[10] R. E. Guzman, M. Grieschat, C. Fahlke, A. K. Alekov, *ACS Chemical Neuroscience* **4**, 994 (2013).

[11] I. Neagoe, T. Stauber, P. Fidzinski, E.-Y. Bergsdorf, T. J. Jentsch, *Journal of Biological Chemistry* **285**, 21689 (2010).

[12] A. R. Graves, P. K. Curran, C. L. Smith, J. A. Mindell, *Nature* **453**, 788 (2008).

[13] P. Schulz, J. Werner, T. Stauber, K. Henriksen, K. Fendler, *PLoS ONE* **5**, e12585 (2010).

[14] L. Leisle, C. F. Ludwig, F. A. Wagner, T. J. Jentsch, T. Stauber, *The EMBO Journal* **30**, 2140 (2011).

[15] W. Günther, A. Lchow, F. Cluzeaud, A. Vandewalle, T. J. Jentsch, *Cell Biology* **95**, 8075 (1998).

[16] H. Sakamoto, *et al.*, *American Journal of Physiology - Renal Physiology* **277** (1999).

[17] C. Miller, *Philosophical transactions of the Royal Society of London. Series B, Biological sciences* **299**, 401 (1982).

[18] C. Miller, M. M. White, *Biophysics* **81**, 2772 (1984).

[19] T. J. Jentsch, K. Steinmeyer, G. Schwarz, *Nature* **348**, 510 (1990).

[20] R. Dutzler, E. B. Campbell, M. Cadene, B. T. Chait, R. MacKinnon, *Nature* **415**, 287 (2002).

[21] S. Meyer, R. Dutzler, *Structure* **14**, 299 (2006).

[22] J. W. Scott, *et al.*, *Journal of Clinical Investigation* **113**, 274 (2004).

[23] B. Schwappach, S. Stobrawa, M. Hechenberger, K. Steinmeyer, T. J. Jentsch, *Journal of Biological Chemistry* **273**, 15110 (1998).

[24] G. Carr, N. Simmons, J. Sayer, *Biochemical and Biophysical Research Communications* **310**, 600 (2003).

[25] T. Schmidt-Rose, T. J. Jentsch, *The Journal of biological chemistry* **272**, 20515 (1997).

[26] M. Maduke, C. Williams, C. Miller, *Biochemistry* **37**, 1315 (1998).

[27] S. Hebeisen, C. Fahlke, *Biophysical Journal* **89**, 1710 (2005).

[28] S. Hebeisen, *et al.*, *Journal of Biological Chemistry* **279**, 13140 (2004).

[29] R. Estévez, M. Pusch, C. Ferrer-Costa, M. Orozco, T. J. Jentsch, *The Journal of Physiology* **557**, 363 (2004).

[30] R. E. Guzman, S. Bungert-Plümke, A. Franzen, C. Fahlke, *Journal of Biological Chemistry* **292**, 19055 (2017).

[31] M. Matsuzaki, *et al.*, *Nature* **428**, 653 (2004).

[32] L. Feng, E. B. Campbell, Y. Hsiung, R. MacKinnon, *Science* **330**, 635 (2010).

[33] A. Bateman, *Trends in Biochemical Sciences* **22**, 12 (1997).

[34] C. Lorenz, M. Pusch, T. J. Jentsch, *Proceedings of the National Academy of Sciences* **93**, 13362 (1996).

[35] G. Stölting, M. Fischer, C. Fahlke, *Frontiers in Physiology* **5** (2014).

[36] R. Mohammad-Panah, *et al.*, *Journal of Biological Chemistry* **278**, 29267 (2003).

[37] T. Suzuki, *et al.*, *Journal of Cellular Physiology* **206**, 792 (2006).

[38] F. Weinreich, T. J. Jentsch, *Journal of Biological Chemistry* **276**, 2347 (2001).

[39] A. Accardi, C. Miller, *Nature* **427**, 803 (2004).

[40] H. Jayaram, A. Accardi, F. Wu, C. Williams, C. Miller, *PNAS* **105**, 11194 (2008).

[41] C. Fahlke, H. T. Yu, C. L. Beck, T. H. Rhodes, A. L. George, *Nature* **390**, 529 (1997).

[42] R. Dutzler, *Science* **300**, 108 (2003).

[43] A. Accardi, *et al.*, *The Journal of General Physiology* **126**, 563 (2005).

[44] A. Accardi, S. Lobet, C. Williams, C. Miller, R. Dutzler, *Journal of Molecular Biology* **362**, 691 (2006).

[45] C. Saviane, F. Conti, M. Pusch, *The Journal of General Physiology* **113**, 457 (1999).

[46] G. Stölting, *et al.*, *Pflügers Archiv - European Journal of Physiology* **465**, 1423 (2013).

[47] M. I. Niemeyer, L. P. Cid, L. Zúñiga, M. Catalán, F. V. Sepúlveda, *The Journal of Physiology* **553**, 873 (2003).

[48] A. Accardi, M. Pusch, *The Journal of General Physiology* **116**, 433 (2000).

[49] L. Zúñiga, *et al.*, *The Journal of Physiology* **555**, 671 (2004).

[50] M. Koch, *et al.*, *Science* **257**, 797 (1992).

[51] K. Steinmeyer, *et al.*, *Nature* **354**, 304 (1991).

[52] D. B. Simon, *et al.*, *Nature Genetics* **17**, 171 (1997).

[53] E. Rugarli, *Nature Genetics* **10**, 466 (1995).

[54] M. Poet, *et al.*, *Proceedings of the National Academy of Sciences* **103**, 13854 (2006).

[55] U. Kornak, *et al.*, *Cell* **104**, 205 (2001).

[56] E. Cleiren, *et al.*, *Human molecular genetics* **10**, 2861 (2001).

[57] D. Kasper, *et al.*, *The EMBO Journal* **24**, 1079 (2005).

[58] M. Kawasaki, *et al.*, *Neuron* **12**, 597 (1994).

[59] G. Borsani, E. I. Rugarli, M. Taglialatela, C. Wong, A. Ballabio, *Genomics* **27**, 131 (1995).

[60] L. W. Dickerson, *et al.*, *Brain Research* **958**, 227 (2002).

[61] M. Yoshikawa, *et al.*, *Genes to cells : devoted to molecular & cellular mechanisms* **7**, 597 (2002).

[62] D. Duan, C. Winter, S. Cowley, J. R. Hume, B. Horowitz, *Nature* **390**, 417 (1997).

[63] X. Q. Wang, *et al.*, *Neuron* **52**, 321 (2006).

[64] T. C. Südhof, *Neuron* **28**, 317 (2000).

[65] G. Ahnert-Hilger, R. Jahn, *Nature Neuroscience* **14**, 405 (2011).

[66] M. Hara-Chikuma, Y. Wang, S. E. Guggino, W. B. Guggino, A. Verkman, *Biochemical and Biophysical Research Communications* **329**, 941 (2005).

[67] T. Stauber, T. J. Jentsch, *Annual Review of Physiology* **75**, 453 (2013).

[68] R. E. Guzman, E. Miranda-Laferte, A. Franzen, C. Fahlke, *Journal of Biological Chemistry* **290**, 25851 (2015).

[69] T. Okada, T. Akita, K. Sato-Numata, M. R. Islam, Y. Okada, *Cellular Physiology and Biochemistry* **33**, 539 (2014).

[70] T. Ogura, *et al.*, *The FASEB Journal* **16**, 863 (2002).

[71] M. Gentzsch, *et al.*, *Journal of Biological Chemistry* **278**, 6440 (2003).

[72] S. E. Fisher, *et al.*, *GENOMICS* **29**, 598 (1995).

[73] T. Stauber, S. Weinert, T. J. Jentsch, *Comprehensive Physiology* (John Wiley & Sons, Inc., Hoboken, NJ, USA, 2012).

[74] W. Günther, N. Piwon, T. J. Jentsch, *Pflügers Archiv - European Journal of Physiology* **445**, 456 (2003).

[75] O. Devuyst, P. T. Christie, P. J. Courtoy, R. Beauwens, R. V. Thakker, *Human molecular genetics* **8**, 247 (1999).

[76] N. Piwon, W. Günther, M. Schwake, M. R. Bösl, T. J. Jentsch, *Nature* **408**, 369 (2000).

[77] S. S. Wang, *et al.*, *Human molecular genetics* **9**, 2937 (2000).

[78] M. Hara-Chikuma, *et al.*, *Journal of Biological Chemistry* **280**, 1241 (2005).

[79] T. Friedrich, T. Breiderhoff, T. J. Jentsch, *The Journal of biological chemistry* **274**, 896 (1999).

[80] J. D. Lippiat, A. J. Smith, *Frontiers in Physiology* **3** (2012).

[81] N. Satoh, *et al.*, *Pflügers Archiv - European Journal of Physiology* **468**, 1183 (2016).

[82] D. Tyteca, *European Journal of Cell Biology* **80**, 466 (2001).

[83] E. T. Kavalali, *The Journal of Physiology* **585**, 669 (2007).

[84] F. Aniento, F. Gu, R. G. Parton, J. Gruenberg, *The Journal of cell biology* **133**, 29 (1996).

[85] E. I. Christensen, *et al.*, *Proceedings of the National Academy of Sciences* **100**, 8472 (2003).

[86] G. T. H. van Kempen, H. VanderLeest, R. van den Berg, P. Eilers, R. Westerink, *Biophysical Journal* **100**, 968 (2011).

[87] T. Martin, R. Grishanin, *Methods Cell Biol.* (Methods Cell Biol., 2003), pp. 267–286.

[88] G. Kilic, *Biophysical Journal* **83**, 849 (2002).

[89] R. D. Burgoyne, A. Morgan, *Cell Calcium* **24**, 367 (1998).

[90] J. W. Barclay, A. Morgan, R. D. Burgoyne, *Cell Calcium* **38**, 343 (2005).

[91] B. Jena, *Protein & Peptide Letters* **16**, 712 (2009).

[92] J. Di Giovanni, *et al.*, *Journal of Biological Chemistry* **285**, 23665 (2010).

[93] T. Söllner, M. K. Bennett, S. W. Whiteheart, R. H. Scheller, J. E. Rothman, *Cell* **75**, 409 (1993).

[94] J. Rizo, C. Rosenmund, *Nature structural & molecular biology* **15**, 665 (2008).

[95] P. I. Hanson, R. Roth, H. Morisaki, R. Jahn, J. E. Heuser, *Cell* **90**, 523 (1997).

[96] R. B. Sutton, D. Fasshauer, R. Jahn, A. T. Brunger, *Nature* **395**, 347 (1998).

[97] T. C. Südhof, J. Rizo, *Neuron* **17**, 379 (1996).

[98] R. B. Kelly, *Current Biology* **5**, 257 (1995).

[99] M. Yoshihara, J. T. Littleton, *Neuron* **36**, 897 (2002).

[100] Y. Lai, X. Lou, C. Wang, T. Xia, J. Tong, *Scientific Reports* **4**, 4575 (2015).

[101] E. Hui, C. P. Johnson, J. Yao, F. M. Dunning, E. R. Chapman, *Cell* **138**, 709 (2009).

[102] S. Martens, M. M. Kozlov, H. T. McMahon, *Science* **316**, 1205 (2007).

[103] L. V. Chernomordik, M. M. Kozlov, *Annual Review of Biochemistry* **72**, 175 (2003).

[104] D. A. Archer, M. E. Graham, R. D. Burgoyne, *Journal of Biological Chemistry* **277**, 18249 (2002).

[105] X. Chen, *et al.*, *Neuron* **33**, 397 (2002).

[106] K. E. Marz, P. I. Hanson, *Trends in neurosciences* **25**, 381 (2002).

[107] J. Rettig, *Science* **298**, 781 (2002).

[108] J. Sørensen, *Pflgers Archiv - European Journal of Physiology* **448** (2004).

[109] T. Voets, *et al.*, *Neuron* **31**, 581 (2001).

[110] J. Kesavan, M. Borisovska, D. Bruns, *Cell* **131**, 351 (2007).

[111] S. Watanabe, *et al.*, *Nature* **504**, 242 (2013).

[112] D. R. Stevens, C. Schirra, U. Becherer, J. Rettig, *Frontiers in Synaptic Neuroscience* **3** (2011).

[113] J. B. Sørensen, *et al.*, *The EMBO Journal* **25**, 955 (2006).

[114] D. Elmqvist, D. M. Quastel, *The Journal of physiology* **178**, 505 (1965).

[115] M. A. Bittners, R. W. Holz, *The Journal of biological chemistry* **267**, 16219 (1992).

[116] L. von Rüden, E. Neher, *Science (New York, N.Y.)* **262**, 1061 (1993).

[117] T. Xu, T. Binz, H. Niemann, E. Neher, *Nature Neuroscience* **1**, 192 (1998).

[118] T. Voets, *et al.*, *Proceedings of the National Academy of Sciences* **98**, 11680 (2001).

[119] S. Yamamori, *et al.*, *The Journal of Comparative Neurology* **519**, 916 (2011).

[120] L.-G. Wu, E. Hamid, W. Shin, H.-C. Chiang, *Annual Review of Physiology* **76**, 301 (2014).

[121] N. Wang, *et al.*, *Canadian Journal of Physiology and Pharmacology* **90**, 791 (2012).

[122] X.-S. Wu, *et al.*, *Nature Neuroscience* **12**, 1003 (2009).

[123] W. W. Douglas, R. P. Rubin, *The Journal of physiology* **167**, 288 (1963).

[124] K. S. Vogel, *Medical Intelligence Unit* (Springer Nature, 1996), pp. 99–118.

[125] D. Bruns, *Methods* **33**, 312 (2004).

[126] D. Laifenfeld, *et al.*, *Journal of Neuroscience* **27**, 7141 (2007).

[127] Y.-B. Hu, E. B. Dammer, R.-J. Ren, G. Wang, *Translational Neurodegeneration* **4**, 18 (2015).

[128] O. M. Schlüter, M. Khvotchev, R. Jahn, T. C. Südhof, *Journal of Biological Chemistry* **277**, 40919 (2002).

[129] G. Fischer von Mollard, *et al.*, *European journal of cell biology* **65**, 319 (1994).

[130] P. A. Vanlandingham, B. P. Ceresa, *Journal of Biological Chemistry* **284**, 12110 (2009).

[131] M. V. Khvotchev, M. Ren, S. Takamori, R. Jahn, T. C. Südhof, *The Journal of neuroscience : the official journal of the Society for Neuroscience* **23**, 10531 (2003).

[132] E. D. Gundelfinger, C. Reissner, C. C. Garner, *Frontiers in Synaptic Neuroscience* **7** (2016).

[133] G. Di Paolo, P. De Camilli, *Nature* **443**, 651 (2006).

[134] S. O. Rizzoli, W. J. Betz, *The Journal of neuroscience : the official journal of the Society for Neuroscience* **22**, 10680 (2002).

[135] K. Sakurada, *et al.*, *Biochemical and biophysical research communications* **177**, 1224 (1991).

[136] F. Lai, *Genomics* **22**, 610 (1994).

[137] S. Takahashi, *et al.*, *Journal of Cell Science* **125**, 4049 (2012).

[138] G. A. de Toledo, R. Fernández-Chacón, J. M. Fernández, *Nature* **363**, 554 (1993).

[139] S. O. Rizzoli, *The EMBO Journal* **33**, 788 (2014).

[140] O. P. Gross, H. von Gersdorff, *eLife* **5** (2016).

[141] T. C. Sudhof, J. Rizo, *Cold Spring Harbor Perspectives in Biology* **3**, a005637 (2011).

[142] A. A. Rodal, J. T. Littleton, *Current Biology* **18**, R259 (2008).

[143] T. Nolan, J. Hugget, E. Sanchez, *Lgc* p. 103 (2013).

[144] J. B. Sørensen, *et al.*, *Cell* **114**, 75 (2003).

[145] R. E. Guzman, Y. N. Schwarz, J. Rettig, D. Bruns, *Journal of Neuroscience* **30**, 10272 (2010).

[146] K. S. K. S. Cole, *Membranes, ions, and impulses : a chapter of classical biophysics* (University of California Press, 1968).

[147] E. Neher, A. Marty, *Proceedings of the National Academy of Sciences of the United States of America* **79**, 6712 (1982).

[148] M. Lindau, E. Neher, *Pflugers Archiv : European journal of physiology* **411**, 137 (1988).

[149] A. Hodgkin, A.F. Huxley, *Current* pp. 500–544 (1952).

[150] A. F. Huxley, *Current* pp. 424–448 (1951).

[151] Heka, *Heka Elektronick* pp. 1–259 (2013).

[152] T. Moser, E. Neher, *Proceedings of the National Academy of Sciences of the United States of America* **94**, 6735 (1997).

[153] D. Bruns, D. Riedel, J. Klingauf, R. Jahn, *Neuron* **28**, 205 (2000).

[154] T. J. Schroeder, *et al.*, *Analytical chemistry* **64**, 3077 (1992).

[155] G. Gerhardt, R. N. Adams, *Analytical Chemistry* **54**, 2618 (1982).

[156] A. Schulte, R. H. Chow, *Analytical Chemistry* **68**, 3054 (1996).

[157] R. M. Wightman, *et al.*, *Proceedings of the National Academy of Sciences of the United States of America* **88**, 10754 (1991).

[158] E. V. Mosharov, D. Sulzer, *Nature Methods* **2**, 651 (2005).

[159] E. V. Mosharov, *Exocytosis and Endocytosis* (Humana Press, 2008), pp. 315–327.

[160] R. H. Chow, L. von Rüden, E. Neher, *Nature* **356**, 60 (1992).

[161] M. Lindau, *et al.*, *Nature* **389**, 509 (1997).

[162] R. H. S. Westerink, A. G. Ewing, *Acta Physiologica* **192**, 273 (2007).

[163] N. Cella, R. R. Cornejo-Uribe, G. S. Montes, N. E. Hynes, R. Chammas, *Differentiation* **61**, 113 (1996).

[164] H. Kobayashi, M. Fukuda, *Communicative & Integrative Biology* **6**, e25036 (2013).

[165] N. L. Kononenko, V. Haucke, *Neuron* **85**, 484 (2015).

[166] S. Bolte, F. P. Cordelièrs, *Journal of Microscopy* **224**, 213 (2006).

[167] E. M. Manders, J. Stap, G. J. Brakenhoff, R. van Driel, J. A. Aten, *Journal of cell science* **103 (Pt 3**, 857 (1992).

[168] E. Papini, O. Rossetto, D. F. Cutler, *Journal of Biological Chemistry* **270**, 1332 (1995).

[169] Y. Wang, *et al.*, *American Journal of Physiology-Renal Physiology* **289**, F850 (2005).

[170] L. Taupenot, K. L. Harper, D. T. O'Connor, *Journal of Biological Chemistry* **280**, 3885 (2005).

[171] M. Camacho, J. D. Machado, M. S. Montesinos, M. Criado, R. Borges, *Journal of Neurochemistry* **96**, 324 (2006).

[172] J. Brown, *Frontiers in Synaptic Neuroscience* (2010).

[173] R. Khanin, H. Parnas, L. Segel, *Biophysical journal* **72**, 507 (1997).

[174] C. Salaün, D. J. James, L. H. Chamberlain, *Traffic* **5**, 255 (2004).

[175] J. A. Szule, J. R. Coorssen, *Biochimica et Biophysica Acta (BBA) - Molecular Cell Research* **1641**, 121 (2003).

[176] H. T. McMahon, M. M. Kozlov, S. Martens, *Cell* **140**, 601 (2010).

[177] D. S. Bruhn, M. A. Lomholt, H. Khandelia, *The Journal of Physical Chemistry B* **120**, 4812 (2016).

[178] J. J. Feher, *Quantitative Human Physiology* (Elsevier, 2012).

[179] T. Hori, T. Takahashi, *Neuron* **76**, 511 (2012).

[180] R. Mohrmann, *et al.*, *Journal of Neuroscience* **33**, 14417 (2013).

[181] X. X. Aikawa, Y., M. T. F.J., *Molecular Biology of the Cell* **17**, 711 (2006).

[182] F. Kawasaki, M. Hazen, R. W. Ordway, *Nature Neuroscience* **3**, 859 (2000).

[183] B. D. Grant, J. G. Donaldson, *Nature Reviews Molecular Cell Biology* **10**, 597 (2009).

[184] C. S. Hirst, *et al.*, *PLOS ONE* **10**, e0123436 (2015).

[185] G. Salazar, *et al.*, *Journal of Biological Chemistry* **279**, 25430 (2004).

[186] A. Gümürdü, *et al.*, *Scientific Reports* **7**, 45661 (2017).